PERFORMANCE IMPROVEMENT OF COMPOSITE MATERIALS USED AS HYDROGEN STORAGE TANKS BY MICROSTRUCTURAL MODIFICATIONS

A Thesis Submitted to
the Graduate School of Engineering and Science of
İzmir Institute of Technology
in Partial Fulfillment of the Requirements for the Degree of

DOCTOR OF PHILOSOPHY

in Mechanical Engineering

by
Zeynep AY

December 2020
İZMİR

Dedicated to my grandfather Mehmet;

ACKNOWLEDGEMENTS

First of all, I would like to thank my advisor Prof. Dr. Metin TANOĞLU for his mentorship, patience, valuable suggestions, and guidance in my dissertation during my Ph.D. I would also like to thank my Ph.D. thesis committee members Assoc. Prof. Dr. Sevgi KILIÇ ÖZDEMİR and Assoc. Prof. Dr. Sinan KANDEMİR for their support and valuable suggestions. I should also thank Assoc. Prof. Dr. H. Seçil ARTEM, staff in the Mechanical Engineering Department and IYTE MAM.

Thanks to my lab mates and friends, who helped and supported throughout my Ph.D. study, Mehmet Deniz GÜNEŞ, Ceren TÜRKDOĞAN, Gözde ESENOĞLU, Mustafa AYDIN, Osman KARTAV, Sinan ÜSTÜN, Yusuf Can UZ, Hatice SANDALLI, Assist. Prof. Dr. Bertan BEYLERGİL, Seçkin MARTİN and Ece MERİÇ MIZRAK.

I am so grateful to my sister Assoc. Prof. Başak AY SAYLAM, who is my mentor and idol in my life, and her family. Thank you for giving me motivations, suggestions, and everlasting supports and being my side all the time. Thank you, my sister, for being my mentor, idol, and best friend.

I would also like to thank my father, Süreyya AY, and my mother, Vesile AY, who raised me and have always supported and encouraged me. Thank you for being my mom and dad. I would never be where I find myself today without your everlasting love and supports.

Finally, I would like to thank SOLAK family and especially many thanks to my intended husband Ertan SOLAK for his everlasting supports, motivation, helps, and understandings while writing my thesis.

I also gratefully acknowledge that my funding was provided by the Scientific and Technological Research Council of Turkey (TÜBİTAK) (2211/C National Ph.D. Scholarship Program in the Priority Fields in Science and Technology) and 100/2000 YÖK Doctoral Scholarship. Also, my thesis title was supported by TÜBİTAK via project number 215M182.

ABSTRACT

PERFORMANCE IMPROVEMENT OF COMPOSITE MATERIALS USED AS HYDROGEN STORAGE TANKS BY MICROSTRUCTURAL MODIFICATIONS

The goal of this Ph.D. thesis is to improve the performance of the cylindrical composites manufactured by filament winding method by using the toughened matrix resin with nano-sized filler (noncovalently functionalized with ethoxylated alcohol chemical-vapor-deposition-grown SWCNTs). The effect of SWCNT concentration on the mechanical performance of these composites was investigated and discussed. One of the main focus of this thesis is to examine the effect of nano-sized filler type and filler concentration on the performance of the epoxy-based composites. For this purpose, epoxy-based nanocomposites with different nano-sized filler types (SWCNT, TEGO, and HNT) at varying concentrations were developed by a calendaring (3-roll-mill) method. A series of mechanical tests were performed for reference composite and developed nanocomposites. The scanning electron microscopy (SEM) was used to reveal the morphology and toughening mechanisms by examining the fractured surface of nanocomposites. The rheological behaviors and contact angle measurements with glass fiber of the selected filler (SWCNT) incorporated epoxy suspensions were investigated to determine the suitability of suspensions for the filament winding process. The reference and SWCNT modified glass fiber (GF)-based cylindrical fiber-reinforced polymeric composites (CFRPCs) with an inner diameter of 60 and 275 mm were manufactured by the filament winding method. The split-disk and three-point bending tests were performed for GF-based CFRPCs. The double cantilever beam (DCB) test was also carried out for the reference and SWCNT modified GF-based CFRPCs to investigate the effect of SWCNT existence on the interlaminar fracture toughness of CFRPCs. The fractured surfaces after the DCB test were analyzed under the SEM to comprehend the toughening mechanisms, and micro-and nano-sized filler morphologies. Consequently, it was revealed that blending and hence toughening the epoxy resin with SWCNT improves the interlaminar properties of the GF-based composites.

ÖZET

HİDROJEN DEPOLAMAYA YÖNELİK KOMPOZİT TANK MALZEMELERİNİN PERFORMANSININ MİKROYAPI MODİFİKASYONU İLE İYİLEŞTİRİLMESİ

Bu doktora tezinin amacı; nano-boyutlu dolgu (etoksilenmiş alkol ile kovalent olmayarak fonksiyonlandırılmış kimyasal-buhar-biriktirme-ile-üretilen SWCNT'ler) ile toklaştırılmış matris reçinesi kullanarak filament sarma yöntemi ile imal edilmiş silindirik kompozitlerin performansını arttırmaktır. SWCNT konsantrasyonun bu kompozitlerin mekanik performansı üzerindeki etkisi araştırılmış ve tartışılmıştır. Bu tezin önemli odaklarından biri; nano-boyutlu dolgu tipi ve dolgu konsantrasyonunun epoksi-bazlı kompozitlerin performansına etkisini incelemektir. Bu nedenle, değişen konsantrasyonlarda farklı nano-boyutlu dolgu tiplerine sahip (SWCNT, TEGO ve HNT) epoksi-bazlı nanokompozitler kalenderleme (3-silindirli-değirmen) yöntemi ile geliştirilmiştir. Referans kompozit ve geliştirilmiş nanokompozitler için bir dizi mekanik test gerçekleştirilmiştir. Nanokompozitlerin kırılma yüzeyi inceleme yolu ile morfolojiyi ve toklaştırma mekanizmalarını anlamak için taramalı elektron mikroskobu kullanılmıştır. Seçilen dolgu (SWCNT) içeren epoksi süspansiyonlarının filament sarma işlemine uygunluğunu belirlemek için reolojik davranışları ve cam elyaf ile temas açısı ölçümleri incelenmiştir. İç çapı 60 ve 275 mm olan referans ve SWCNT modifiye edilmiş cam elyaf bazlı silindirik elyaf ile kuvvetlendirilmiş polimerik kompozitler filament sarma yöntemi ile üretilmiştir. Silindirik elyaf ile kuvvetlendirilmiş polimerik kompozitler için bölünmüş-disk ve üç nokta eğme testleri yapılmıştır. SWCNT içeriğinin silindirik elyaf ile kuvvetlendirilmiş polimerik kompozitlerin laminalar arası kırılma tokluğu üzerindeki etkisini araştırmak için de Çift Ankastre Kiriş (DCB) testi referans ve SWCNT modifiye edilmiş kompozitler için gerçekleştirilmiştir. Çift Ankastre Kiriş testinden sonra kırılan yüzey, toklaştırma mekanizmalarını ve mikro-ve nano-boyutlu dolgu morfolojilerini anlamak için taramalı mikroskop ile analiz edilmiştir. Sonuç olarak, epoksinin SWCNT ile karıştırılması ve neticesinde toklaştırılmasının, GF-bazlı kompozitlerin laminar arası özelliklerini iyileştirdiği belirlenmiştir.

TABLE OF CONTENTS

LIST OF TABLES

Table **Page**

LIST OF FIGURES

Figure **Page**

Figure **Page**

Figure **Page**

Figure **Page**

Figure **Page**

CHAPTER 1

INTRODUCTION

1.1. Background

Hydrogen is the first and the lightest element in the periodic table. Besides, it is the most common element in the Universe, so it can be produced from almost all energy sources. Hydrogen can be in the form of gas or cryogenic liquid. However, hydrogen remains a gas at atmospheric temperatures and extremely high pressure. According to lightness, storability, and no pollutants or greenhouse gas emissions, hydrogen has been increasingly used as an alternative energy source since 1975. Moreover, as seen in Figure 1.1 demand for hydrogen usage has been growing and it is also going to show an increasing consumption trend in the future [1,2].

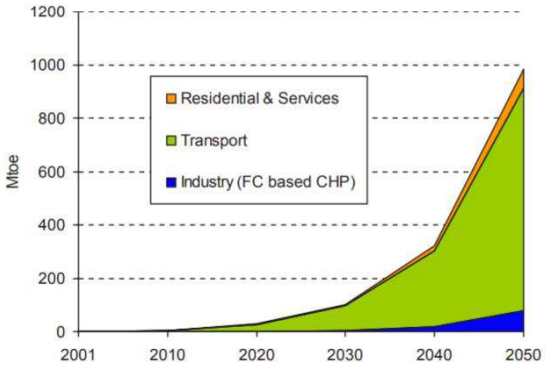

Figure 1.1 “World final hydrogen consumption by sector (H_2 case)” (Source: WETO-H_2, 2006)

Figure 1.2 shows the CO_2 emission caused by transportation. In the way that, according to the World Resource Institute (WRI), transportation (road, rail, air, and marine) caused 24% of CO_2 emission in 2016, and CO_2 emissions from transportation increase at a higher rate than other sectors. Also, 75% of the transportation emission

comes from road vehicles, which can be seen in Figure 1.3 [1,3]. In other words, transportation -including road, rail, air, and marine transportations- has a great effect on climate change. Additionally, one-quarter of the CO_2 emission is caused by the burning of fossil sources is from transportation.

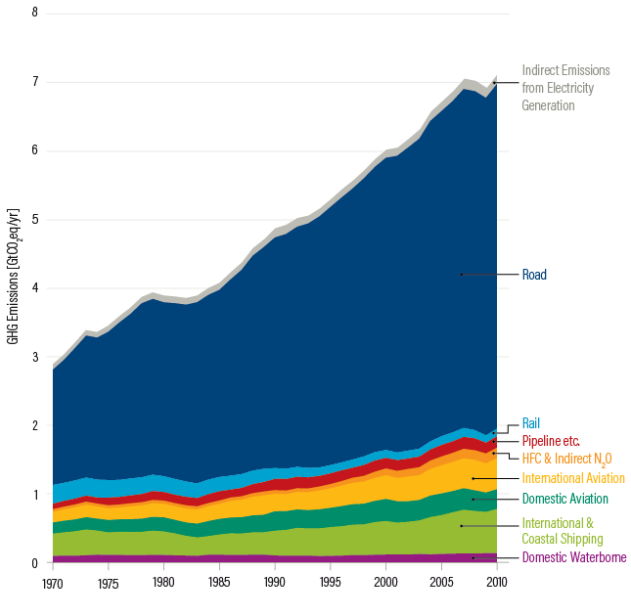

Figure 1.2 CO_2 emission caused by transportation (Source: IPCC World resource institute)

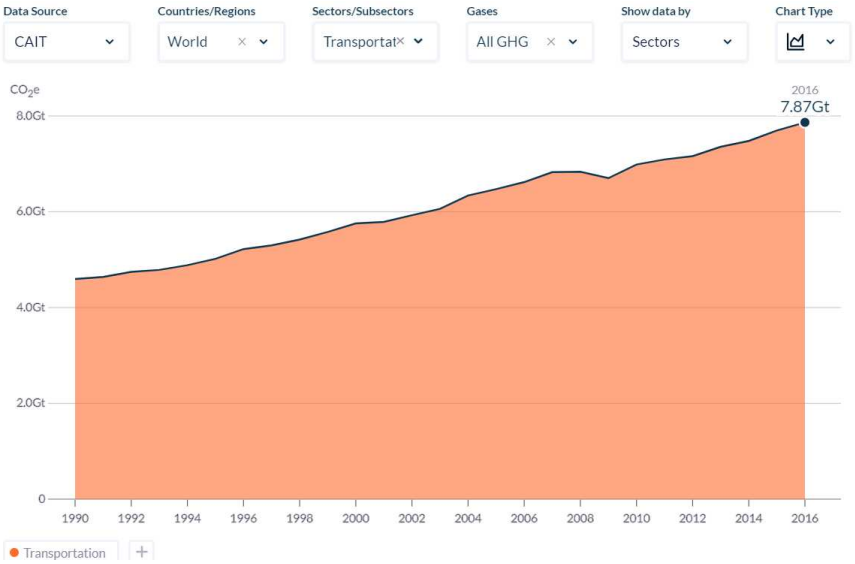

Figure 1.3 CO_2 emission rate depending on the year for transportation (Source: IPCC World resource institute)

On account of the vast majority of environmental pollution that comes from transportation, the common objectives of the Automobile sectors, which focus on alternative fuels, are [4];

- Converting the Internal Combustion engine with hydrogen fuel,
- Establishing storage techniques of hydrogen onboard vehicles.

Internal combustion engines powered by fuels like gasoline or diesel fuel, derived from fossil fuels [4]. Toxic gas (hydrocarbons, nitrogen oxide, etc.) and particles (carbon soot), carbon dioxide (CO_2), methane (CH_4) and, other gaseous that come out from the pipeline are greenhouse gases that contribute to global warming and cause serious environmental pollution [5]. For this reason, the European Union and other developed countries are making intensive efforts to prevent environmental pollution and avoid fossil fuel dependence. At present, scientists research replacing fossil fuels with natural compressed gasses both to increase vehicle performance and prevent environmental pollution. Because of zero greenhouse gas emissions, high energy efficiency, and unlimited nature, hydrogen is considered the new energy carrier of the next century. While purified hydrogen causes almost no carbon exhaust emissions, it also eliminates emissions such as hydrocarbon, carbon monoxide, and carbon dioxide [5].

The EU project "World energy technology outlook – 2050" (WETO-H_2) was created to seek feasible solutions for the critical constraints in the supply of oil and gas resources, due to the economic growth and world population together with energy demand, the future prices, and performances of energy technology. Based on a series of studies conducted so far, the current market behavior shows that access to the sources of fossil fuel to meet the increasing demand in the future will be difficult. The main purpose of WETO-H_2 is to foresee the improvement of long-term power generation and renewable technology due to the restrictions on resources and emissions. The scenarios of WETO-H_2 as followed [2];

- Production of hydrogen with chemical, thermo-chemical and electrical,
- Carbon capture and storage options in addition to fossil fuels to generate hydrogen and electricity,
- Production of electricity by fossil fuels, renewable energy or hydrogen,
- Lower the emission and improve the performance of vehicles.

Apart from climate change, the need for alternative resources has been increasing due to some cases like; increase in energy needs, an increase in oil and gas prices, limited

access to oil resources, etc. [1]. Therefore, policies targeting the usage of hydrogen technologies especially focused on transportation, and the number of countries supporting these policies have been increasing.

All energy chains must be evaluated from the production to the stage of consumption. Accordingly, production, storage, transportation, and distribution of hydrogen, which is an alternative renewable energy source, should be considered [6].

Hydrogen is an alternative renewable and sustainable transportation fuel, due to be an abundant element in the Universe. However, it does not exist alone on the planet. In the last decades, the production of hydrogen technologies has been developed by reducing the cost [5]. Commercial hydrogen is produced by two main processes;

- steam methane reforming of natural gas (NG),
- hydrolysis of water with renewable and conventional electricity (photovoltaic, wind, hydraulic).

According to many studies, converting primary energy to electricity is more economical and convenient environmentally. Besides, although it requires extra efficiency, it is more convenient to transfer electricity to the desired places. Production of hydrogen can be realized by using biomass and coal as well as using electricity [7].

Hydrogen is an alternative renewable and sustainable transportation fuel according to its light-weight and high energy density, and it can be stored in the form of gas, liquid, and via adsorption or absorption to the solids. Physical-and material-based storage of hydrogen is illustrated in Figure 1.4 [8]. However, it is challenged to store such a high dense for stationary and portable applications. The simple way to store hydrogen is as compressed gas because storing hydrogen at ambient temperature is possible, input and output for hydrogen gas are simple. The hydrogen gas filling system is shown in Figure 1.5 [9]. Because, while the storage of compressed hydrogen gas requires a high-pressure tank, which can stand to 350-700 bar, the storage of liquid hydrogen requires a cryogenic temperature.

Most especially, the scientists are making researches about compressed gasses to replace fossil fuels both increase vehicle performance and to prevent environmental pollution. Apart from meeting performance, cost requirements for hydrogen storage and delivery system are also essential [10]. Composite pressure vessels require permanent mandrels with a closed-end structure. According to the mandrel types, hydrogen gas can be stored in four types of pressure vessels as shown in Figure 1.4;

- Type I (metallic pressure vessels),

- Type II (hoop wrapped metal with fiber composite vessels),
- Type III (filament wound metallic liner wrapped with fiber embedded in a resin, also called composite material-based pressure vessels (COP)).
- Type IV (filament wound a plastic liner wrapped with fiber embedded in a resin) [11].

Type I pressure vessels have been widely used for a long while. However, in terms of cost and resistance to higher pressures, type I pressure vessels are challenged by composite pressure vessels [6]. For the automotive industry, light-weight is essential to improve the performance of the vehicle. Accordingly, engineers have recently focused on composite materials [12].

For transportation, fuels must be chemically stable, non-toxic, and safe. Hydrogen is a good choice due to considering as green energy. However, because hydrogen is lighter than the air, during the leak, hydrogen rises and expands in the air so quickly, leakage and spillage should be minimized during a possible accident. Also, since hydrogen is an odorless and colorless gas, filling stations must have sensors that can detect below 2-4% of hydrogen output [5]. Fuel systems of hydrogen vehicles must be carefully designed, and the fuel tank must be safe.

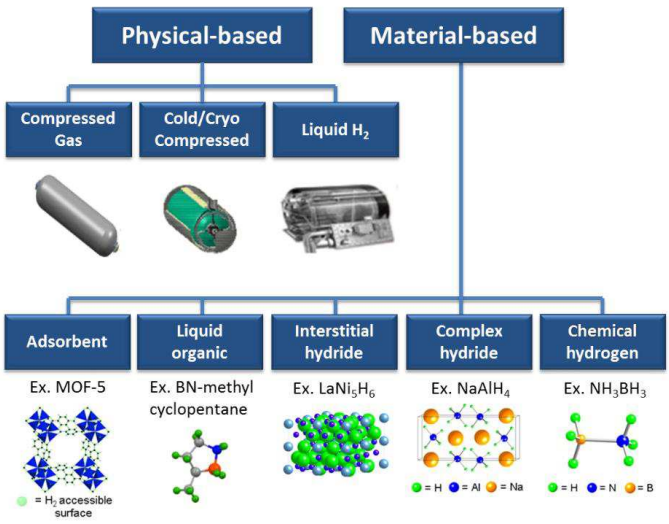

Figure 1.4 Hydrogen storage scheme (Source: Energy.gov)

Figure 1.5 Hydrogen gas filling system (Source: Laurent, 2020)

Vehicles powered by electricity and hydrogen generate near-zero pipeline emissions without the need for emission reduction equipment that results in any cost or weight increase [5]. Because the automotive industry light-weight is essential to improve the performance of the vehicle, engineers widely use composite materials for this purpose (Figure 1.6). Since 2000, the usage of hydrogen gas as a fuel has been increasing especially for transportation. Therefore, storing hydrogen gas in a light-weight tank is an important point for transportation [2,13].

Figure 1.6 Hydrogen gas storage vessels for hydrogen-powered vehicles (Source: Dorneanu, 2007)

1.2. Objectives

The main objective of this thesis is to characterize and improve the performance of the materials that are used for the manufacturing filament wound hydrogen storage composite vessels by microstructural modification. This study has one focus on the incorporation of the nano-sized fillers within the matrix, then adapts the nano-sized filled matrix to cylindrical composite structures produced with filament winding. The particular objectives are as follows;

- Dispersion of several nano-sized fillers within the epoxy matrix to produce nanocomposites.
- Characterize the structure and performance of the nanocomposites by several mechanical microstructural investigations and mechanical testings.
- Reveal the effect of the nano-sized fillers on the viscosity of the filled resin suspensions, which is used in the filament winding process.
- Determine an appropriate nano-sized filler type and its concentrations blended within the epoxy to be utilized for the manufacturing of filament wound hydrogen storage tanks or cylindrical structures.
- Adaptation of the nano-sized filled epoxy resin for filament wound (FW) cylindrical fiber-reinforced composite (CFRPC) production.
- Determine the mechanical and thermomechanical properties of the reference and nano-sized filler reinforced CFRPCs.
- Demonstrate the effect of the nano-sized filler existence on the interlaminar toughness of CFRPCs and analyze the toughening mechanisms and micro-and nano-sized filler morphology.
- Investigation and discussion of the nano-sized filler incorporation on the mechanical performance of CFRPCs.

1.3. Contributions

This thesis is based on the idea of increasing the performance of materials used in the production of filament-wound composite-based pressure vessels or cylindrical structures by incorporating nano-sized fillers within the epoxy matrix. Referring to this idea, the goal is taken to characterize and improve the performance of the filament-wound cylindrical glass fiber (GF)-based composites by the technique that toughening the epoxy matrix with SWCNT. Based on our knowledge, there are only a few studies reported in the literature on the investigation of the effect of the toughened epoxy matrix on the performance of CFRPCs. Although CNT-reinforced FRPCs have been extensively examined in the literature, the effect of CNT reinforcement on the mechanical-especially the Mode I interlaminar fracture toughness of CFRPCs has not been reported yet. This dissertation reveals the performance improvement of CFRPCs with CNT incorporation. And the Mode I interlaminar fracture toughness was remarkably improved, as its original contribution to the literature. Although CNTs have extraordinary mechanical performances, they are expensive. Therefore, CNTs at low concentrations without compromising their outstanding properties were used as the toughening filler in the present study, which is also an original contribution to the literature. The main highlights here are;

- Usage of the toughened epoxy matrix to enhance the delamination propagation behavior resulting from impact, etc.,
- Utilizing the toughened epoxy matrix at the outer layer of the composite cylindrical structures during the filament winding process.

For this reason, to investigate the effect of the contribution of SWCNT within the epoxy was examined by measuring the interlaminar fracture toughness for the GF-based CFRPCs under Mode I loading.

Since providing a satisfying performance of CFRPCs extremely depends on the interlaminar properties, the problem statement of this thesis is to obtain better interfacial interactions between all constituents of the produced composites. It is well known that the performance of CFRPCs is extremely related to the interlaminar properties. For the selection of the nano-sized fillers, the target was to select chemically compatible nano-sized fillers with the used epoxy matrix. In the study, epoxy-based nanocomposites were

characterized as a first stage, then a toughened epoxy matrix was adapted for the production of GF-based CFRPCs. Consequently, the performance of produced CFRPCs with selected nano-sized fillers (SWCNT) was evaluated.

1.4. Thesis Outline

Chapter 1 describes the background information about hydrogen, which is an alternative renewable energy source. Consequently, first hydrogen production, storage, transportation, and distribution are defined briefly. Then, the main objectives and the contributions of this thesis to the literature are discussed.

Chapter 2 starts with a definition, classification, and a brief overview of the composite materials. The importance of nanotechnology for the inclusion in the production of the composite materials is also mentioned and more details are given about micro-and nano-sized fillers for the contribution to the polymeric matrices. “Why to choose the nano-sized fillers?” was clarified based on the compression between nano-and micro-sized fillers. Additionally, the widely used carbonaceous and silica-based nanoparticles were expressed concisely. For the production of CFRPCs, the commonly used filament winding technique is also addressed. The importance of the nano-sized filler type, their chemical form, and their distribution within the thermoset resins to the nanocomposites and multi-functional fiber-reinforced polymeric composites were also mentioned here. Chemical router and physical methods for the preparation of nano-sized filler reinforced resin is also detailed. Since, while the laminated FRPCs have high strength in the in-plane direction, the strength is low through the thickness, several techniques to increase the strength throughout the thickness were mentioned. Among these techniques toughening the matrix material with micro/nano-sized fillers (alumina, silica, carbon black, graphene, carbon nanotubes) was detailed due to the scope of the thesis. Delamination and the toughening mechanisms were discussed circumstantially.

Chapter 3 presents the framework of this thesis. Referring to the literature review, the flowchart of this study was formed.

Chapter 4 describes the experimental method and instrumentation of the study. This chapter firstly describes the raw materials that are used for the production of nano-

sized filler incorporated NCs and CFRPCs. The morphology of the nano-sized fillers was determined by scanning electron microscopy (SEM). The description of the produced composites was also presented. Secondly, this chapter deals with experimental procedures and equipment. The relevant ASTM standard for the experimental procedures was also represented.

Chapter 5 introduces the experimental results for the produced NCs and CFRPCs. Herein, the effect of the nano-sized fillers on the mechanical performance of the epoxy matrix and CFRPCs is reported. The fractured surface of the composites was examined under SEM to comprehend the toughening mechanism in the NC and CFRPC systems. Dynamic mechanical analysis (DMA) was also conducted to determine the effect of SWCNT on the glass transition temperature (T_g) of CFRPCs. All the experimental results are discussed according to the results obtained from the literature.

Concluding remarks and future studies are described in Chapter 6. Also, a vita of the author is given at the end of the thesis.

CHAPTER 2

LITERATURE REVIEW AND FUNDAMENTAL CONCEPTS

2.1. Nanocomposites and Cylindrical Composite Structures

Composite materials consist of two or more physically distinct and mechanically separable parts, which are reinforcement (discontinuous phase) and matrix (continuous phase). These constituents can be combined in a controlled way to achieve optimum properties. Many materials in nature are composites, which exist in both animals and plants. For example, wood is made up of fibrous chains of cellulose molecules in a matrix of lignin while bone and teeth are both mostly composed of the hard inorganic crystal in a matrix of collagen [14].

The composite materials can be classified into three different categories, depending on the matrix materials;

- Ceramic Matrix Composites (CMCs),
- Metal Matrix Composites (MMCs), and
- Polymer Matrix Composites (PMCs).

In composite materials, polymer matrices are widely used in the industry due to their low cost, light-weight (alternative to metals), being less dense than metals and ceramics, and having high corrosion resistance. Further, polymers can be processed and manufactured with lower energy input than metals or ceramics. The matrix phase of PMCs can be classified as elastomers, thermoplastics, and thermosets. According to their structure of network polymer with a high cross-link density, thermosets are harder and stronger than elastomers and thermoplastics. Thermosets also have better dimensional stability, and higher mechanical properties than thermoplastics according to their chemical composition. The most used thermosets are; polyester, vinyl ester, and epoxy. While polyester and epoxy are almost linear in the elastic range, among them epoxy has the highest strength, as shown in Figure 2.1 [15]. Epoxy resins are the most preferred thermoset polymers used as coating and adhesives. Epoxy resins have advantages like

high stiffness and strength, creep resistance, chemical resistance, good adhesion properties, and minimal shrinkage during curing. Among the epoxy resins, the most widely used one is the diglycidyl ether of bisphenol-A (DGEBA) [16]. The chemical structure of DGEBA is illustrated in Figure 2.2.

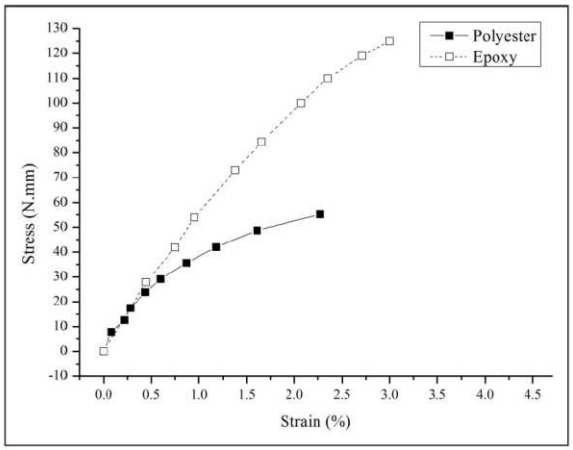

Figure 2.1 Stress-strain curves of epoxy and polyester (Source: Yu et al., 2017)

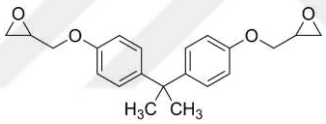

Figure 2.2 Chemical structure of the diglycidyl ether of bisphenol-A (DGEBA)

However, thermoset resins have a brittle structure and poor resistance to crack initiation and propagation, which cause a major problem for the engineering performance of the final structure. The incorporation of rigid micro-or nano-scale particles within the resin improves the fracture toughness of polymers [17]. In the last decades, fiber and/or micro-and nano-scale particle reinforced PMCs have been widely studied, according to their very high strength-to-weight and stiffness-to-weight ratios. These reinforcements provide design flexibility, high durability, and light-weight to polymer-based composites. Also, the resultant material can be adapted to many technological and industrial applications [18,19].

Mostly used conventional fiber types are carbon fiber (CF), glass fiber (GF), and aramid fibers. While CF has better mechanical properties, it is expensive, and it has a difficult adhesion with a polymer matrix. Among the micro-fiber reinforcements, GFs are

widely used for the manufacturing of FRPCs, due to their cheap price [15]. GF/epoxy composites were widely used in many applications such as piping systems and pressure vessels, according to their light-weight, high strength and stiffness, long fatigue life, low thermal expansion, corrosion resistance, chemical resistance, and structural flexibility [15,20,21]. GF-based FRPC presents a smooth internal interior, which ensures lower liquid loss than a typical piping system in an economical way [22]. Requirements for GF-based FRPC for piping and pressure vessel applications are to withstand the internal pressure as well as the combined loading [23–25]. When the internal pressure is applied to the cylindrical composites, it creates a hoop-to-axial-stress ratio of 2:1. According to the prediction of "netting analysis", which is an analytic method that assumes only the fibers carry the load, an optimum winding angle can be estimated as 54.7^0 for composite laminates [14,15,26,27]. As reported by Sulaiman et al., the optimum filament winding angle calculation for Tsai-Wu and Tasi-Hill was correlated with experimental results and "netting analysis". As shown in Figure 2.3, the maximum burst pressure was approved as a 55^0 filament winding angle, which is correlated with the "netting analysis" [26].

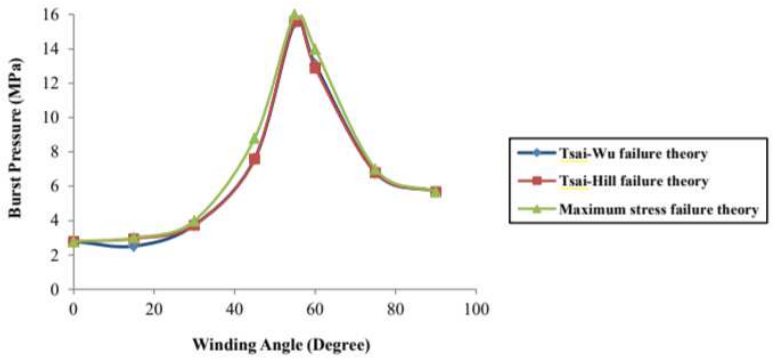

Figure 2.3 Burst pressure values at varying filament winding angles (Source: Sulaiman, 2013)

As described above, the composite materials are light as well as durable, and they provide design flexibility. However, the resistance of the polymers against impacts is generally low, which can be improved by the micro-and nano-sized filler addition. Although the resultant product is more efficient, the reinforcement materials are often expensive. But the cost can be lowered by using the minimum concentration of reinforcement with maximum resultant efficiency.

2.1.1. NC Materials

Nanotechnology is regarded as one of the most promising areas for technological development in the 21st century. In material research, the development of nanocomposite materials rapidly increasing these days. NCs are a class of materials whose one of the constitutes has dimensions on the nanoscale (<100nm). Even the addition of nano-sized materials between 0.5 and 5 percent by weight (wt.%), improve the properties like mechanical strength, toughness, and electrical or thermal conductivity.

For a maximum and optimal performance of the NCs, (1) type and concentration of nanofillers, (2) polymer matrix material, (3) fabrication of the NCs should be taken into account [28]. The polymeric matrices are usually filled with micro-scale fillers such as silica, alumina, etc. for obtaining outstanding mechanical strength [29,30]. However, by the reason of their low density, high specific surface area, and high mechanical properties, nano-scale fillers draw the most attention to produce NCs in recent studies. Figure 2.4 shows the three-dimensional (3D) distribution of micro-and nano-scale fillers in a polymeric matrix. According to the differences in dimension and geometry of micro-and nano-sized fillers, the number of fillers for a given filler volume fraction varies and it is higher for nano-sized fillers [30]. Spherical nanoparticles could form a hexagonal dense packed structure within the polymeric matrix. However, the maximum packing density is the face-centered cubic configuration with 74 vol. %. For the fiber-or rod-like nanostructures, the dense packing occurs when the tubes are arranged in periodic and aligned order [31].

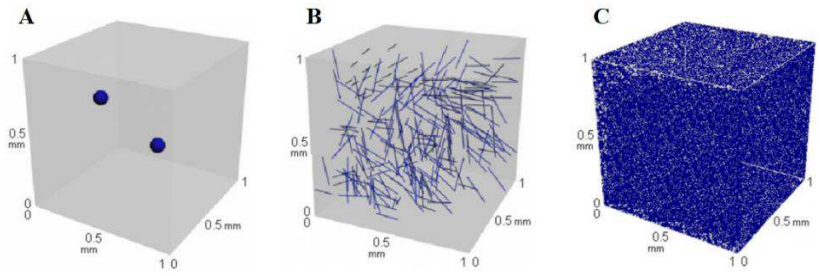

Figure 2.4 Distribution of micro-sized fillers (A: Al_3O_3 and B: Carbon fiber) and nano-sized filler (C: CNT) at 0.1 vol.% in a reference volume $1mm^3$ (Source: Ma et al., 2010)

The investigation of the question of "why to use nanomaterials?" has attracted great attention among researchers. One of the main reasons for this is the high surface interaction between the nano-sized filler and the polymer. According to the large number of particles and size effect of nano-scale fillers, their distribution in a polymer matrix is larger than for micro-scale fillers. The bulk density and the surface area of commonly used fillers are listed in Table 2.1.

The surface-to-volume ratio with different aspect ratios (length/diameter) as a function of the diameter of widely used micro-and nano-sized fillers -a variety CNTs, fumed silica (FS), carbon black (CB), and conventional fibers- are shown in Figure 2.5. The surface/volume ratio decreases with an increasing diameter, which increases the distributed amount of the filler within the polymeric matrix. The physical form of the nano-sized fillers (e.g., tubes, particles, plates) is directly linked to the specific area of interaction. Consequently, the shape of the nano-sized filler highly affects the desired property of polymer-based composites[31,32].

Table 2.1 The dimension, density, and the surface area of commonly used micro-and nano-sized fillers

Filler	Average dimensions of filler	Density (g/cm3)	The surface area of individual particles (S)
silica	20 nm in diameter	2.65	$S=\pi d^2$
halloysite	1-15 µm in length (l), 10-150 nm in diameter (d)	1.8-2.6	$S= S=\pi dl+\pi d^2/2$
clay	<0.002 mm in diameter	2.837	$S=\pi d^2$
carbon fibers	5 µm in length (l), 8 µm in diameter (d)	1.77	$S=\pi dl+\pi d^2/2$
glass fibers	5 µm in length (l), 11µm in diameter (d)	2.58	$S=\pi dl+\pi d^2/2$
GNP	45 µm in length (l), 7.5 nm in thickness (t)	2.2	$S=4l^2+2lt$
CNT	12 nm in diameter (d), 20 µm in length (l)	1.8	$S=\pi dl+\pi d^2/2$

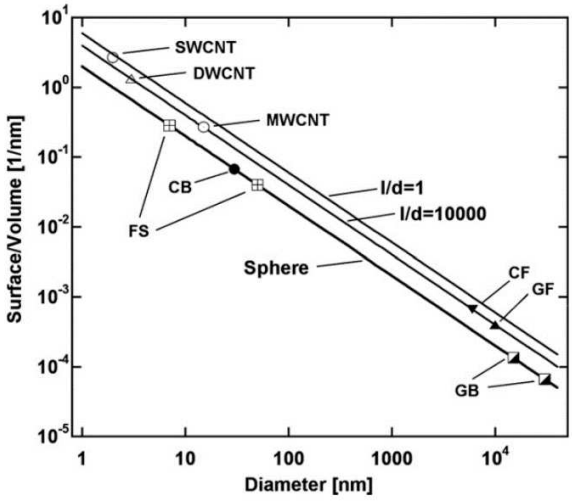

Figure 2.5 The ratio of particle surface and volume for spherical and fibrous particles as a function of the particle diameter (Source: Fiedler et al., 2006)

Polymeric NCs are widely used in many applications due to their superior properties like strength, toughness, durability, electrical properties, etc. Many nano-scale particles are used as reinforcement for NCs [33]. Figure 2.6 shows the fracture toughness of NCs based on widely used fillers as a function of filler content [34]. Among the nano-sized fillers, CNTs showed a good effect on the fracture toughness at low contributions 0.1-2.0 wt.%. Also, K_{Ic} showed a better improvement for graphene-based epoxy NCs at lower filler content varying from 0.01 to 1.0 wt. % [34,35].

For a maximum and optimal performance of the NCs, achieving a good dispersion and homogeneous distribution of the nano-sized fillers within the polymer matrix constructing interconnected networks between matrix and filler is essential. Once the homogeneous distribution of the nano-sized fillers is achieved for NCs, the performance of the NCs increases automatically according to the effective load transfer. Also, the high aspect ratio, alignment of the nano-sized particles, and the stress transfer affect the performance of the NCs. The other critical factor is the interfacial interaction between the nano-sized filler and polymer matrix for the improvement of mechanical and electrical properties of the polymer matrix material.

On behalf of improving the bonding and adhesion, surface modifications via covalent and non-covalent functionalization are implemented to the micro-and nano-sized fillers. The covalent functionalization forms a strong C-C bond between the filler and the modified material, while the non-covalent functionalization forms intermolecular forces.

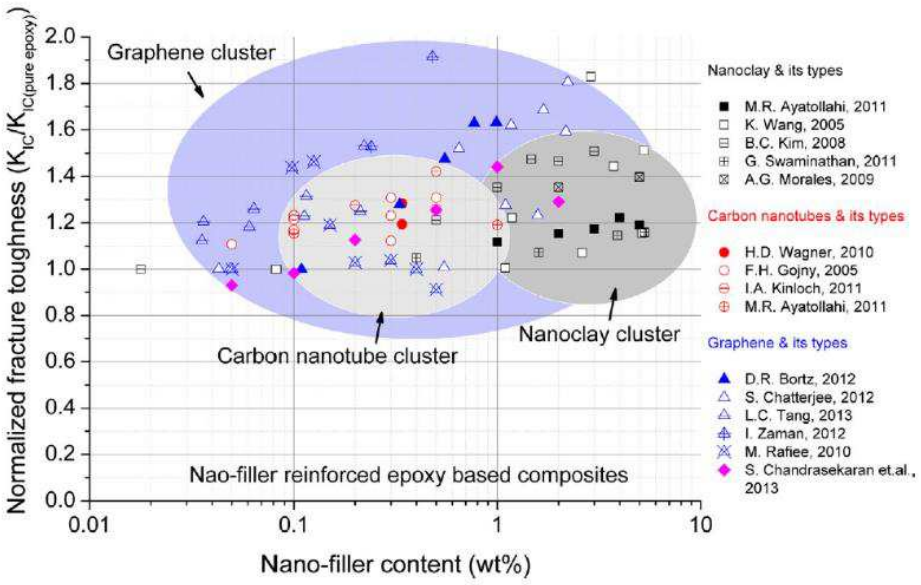

Figure 2.6 Normalized fracture toughness as a function of nano-sized filler content for different nano-scale particle reinforced epoxy NCs (Source: Chandrasekaran et al., 2014)

Both functionalization increase the mechanical properties of NCs, meanwhile, the non-covalent bonding can damage the morphology of the filler due to the harsh treatment [28,29]. Surface modifications of the fillers are usually assisted by the mechanical dispersion techniques of fillers within the polymer matrix. There are many mechanical methods for the dispersion of nano-sized fillers within the polymer matrix (thermoplastic, elastomeric, thermosetting). However, herein generally processing methods for thermosets will be mentioned. Widely used production techniques for nano-sized filler reinforced epoxy NCs are; ultra-sonication, spin casting, shearing, and milling [28–30].

2.1.1.1. Carbonaceous Filler Reinforced NC Materials

Carbonaceous nanofillers like carbon black (CB), carbon nanotubes (CNTs), and graphene nanoplates (GNPs), are widely used as reinforcements for improving the mechanical, and electrical properties of polymeric matrices.

Carbon black (CB)

CB is an amorphous form of carbon with a high conductive zero-dimensional (0D) metal powder. CB can be manufactured in five types with different manufacturing processes; (1) furnace black, (2) thermal black, (3) lampblack, (4) channel black, and (5) acetylene black. Among them, thermal black and furnace black are widely used as additives for plastic applications [36]. CB is a cheap carbon-based nano-sized filler that in particular is used for the production of conductive polymeric composites, due to their abundant availability, low density, high electrical conductivity, and chemical stability [28,37–40]. CB also improves the mechanical, electrical, optical, chemical, and surface properties of polymers. According to their good conductive properties and increasing mechanical properties of polymers, CB is commonly used in engineering applications, for instance automotive, electronics, packaging, aerospace, biomedical, sports goods, etc. [41,42]. A CB particle size range is generally 5-100 nm. However, CB particles tend to agglomerate due to the strong Van der Waals force and the size of CB agglomerates can be reached between 70-500 nm from 5-100 nm [43]. The clusters of the agglomerated CB particles result in defects within the polymer NCs, which leads to a decrease in the mechanical properties of polymer composites. For the improvement of the mechanical and electrical properties of polymer composites, improving the dispersion of CB particles within the polymer is essential. This can be achieved by chemical or physical modification of CB particles [28,41]. As wells as the chemical or physical modification of CB particles, the dispersion quality of CB particles within the polymer is also important for enhancing the performance of polymers.

Carbon nanotubes (CNT)

CNTs are an important type of carbonaceous material. Since they were discovered in 1991 [44], the usage of CNTs has been increasing in most areas of science and engineering. However, they were already used in the 6th century for coating [45–47]. Due to their unusual mechanical, thermal, and electrical properties, stability, and functionality make them ideal candidates for advanced filler materials in composites [48,49]. Especially, for the enhancement of mechanical improvement of plastics, using CNTs as reinforcing filler has dramatically increased in recent years. Depending on the process for CNTs, there are two types of them; (1) Single-walled carbon nanotube (SWCNT), and (2) Multi-walled carbon nanotubes (MWCNT). These CNTs have extraordinary high stiffness in tensile load, high strength, and low density [50]. SWCNT has the largest specific surface area (SSA) (~1300 m^2/g) then MWCNT (~600 m^2/g). SWCNT improves fracture toughness

as well as other mechanical properties of epoxy resins even at minimum concentrations, considering the large surface area and high mechanical properties of SWCNTs [31,51]. SWCNT has been shown to hinder the accumulation of stress in composites and increase the stress transfer mechanism through interaction with the epoxy resin [52]. Nevertheless, CNTs are able to agglomerate due to the Van der Wall force attraction. In addition to attractive forces, frictional contacts and elastic interlocking mechanisms are also responsible for flocculation [53]. These agglomerations exist between the tubes as a result of their significant surface areas and high aspect ratios. The larger the CNTs, the stronger the interacts and entanglements between the CNTs. However, in some cases, longer CNTs could lead to good mechanical properties to composites, even if the distribution is not good [54].

Graphene nanoparticle (GNP)

A single layer of graphene is considered the thinnest material in the world [55,56]. Due to the two-dimensional (2D) structure of graphene sheets, they have a relatively high specific surface area, outstanding mechanical and electrical properties, and low manufacturing cost [57]. The usage of graphene sheets as reinforcement within a polymer matrix improves the electrical and thermal properties, as well as mechanical properties of the matrix material by the reason of the superior features of graphene [56,58–60]. Graphite comprises many layers of graphene sheets that stand with the Van der Waals attraction. The attraction between the sheets makes graphene unstable and tends to stick together, which brings about dispersion and exfoliation of graphene sheets within the polymer matrix more challenging. Because the clusters of graphene sheets -called agglomeration- causes a slip between the sheets when a load is applied to the nanocomposite and lowers the efficiency of graphene sheets [61]. For the enhancement of mechanical properties of the matrix; the compatibility of the filler and the matrix, and the alignment of the graphene sheets within the polymer matrix are essential issues. Surface modification of graphene can lead to a good adhesion/interaction between the matrix and filler, resulting in an enhanced mechanical property of the matrix. The functionalization of graphene via chemical or physical approaches has been tried to be used to obtain a uniform dispersion of the graphene within the polymeric matrix [14,55]. For individual separation of carbon sheets by peeling off, the graphite has been studied since the beginning of the twentieth-century [62]. In literature, there are several techniques for the production of graphene sheets such as; (1) mechanical exfoliation [63], (2) chemical vapor deposition (CVD) and epitaxial

growth on silicon carbide and ruthenium [64,65], (3) solvothermal synthesis [66], (4) thermal exfoliation and reduction of graphene oxide (GO) [67] and, (5) liquid-phase exfoliation of graphite by sonication [68]. The conventional approaches are chemical and thermal exfoliations that have been widely used to produce the single-layered graphene nanosheets [69]. Thermally exfoliated/expanded graphene (TEGO) is synthesized by graphite oxidation and thermal expansion of the GO. In most studies, TEGO is used for improving the thermal, electrical, and mechanical properties of polymers due to containing hydrophilic groups which facilitate their dispersion in polymeric matrices [57,70–75].

2.1.1.2. Silica-based Filler Reinforced Nanocomposite Materials

Among the spherical particles fumed silica are well-known fillers, and they are used to control the rheological properties of the matrix and increase the toughness, thermal property, and wear resistance of the polymers [76]. According to their high mechanical properties and significantly small size, silica has been used in many studies as a reinforcement [77].

Halloysite nanotubes (HNTs), which are first described by Berthier (1826), are clay minerals, and they resemble the structure of MWCNT. The structure of the HNTs is formed of a 1:1 aluminosilicate layer rolled into a tubular structure and shown in Figure 2.7. They have remarkable advantages such as; (1) re-dispersible in aqueous, (2) non-toxic and durable in high strength shearing, and (3) cheaper than nano-sized carbonaceous fillers [78–80]. As carbonaceous nano-sized fillers HNTs have also some challenges like; (1) they tend to agglomeration into clusters, and (2) due to having low polar functional groups on the surface of the HNTs, weak interfacial interaction occurs between the particle and matrix materials. These issues should be overcome to increase the mechanical properties of epoxy with the incorporation of HNTs [78].

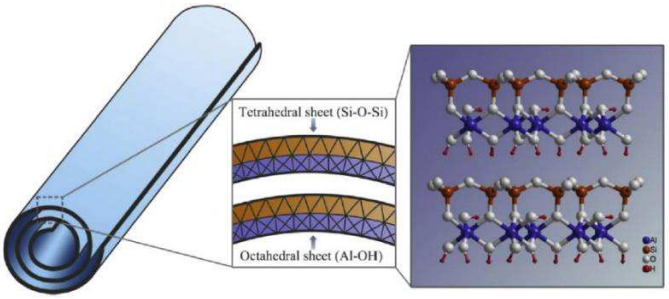

Figure 2.7 Schematic structure of HNTs from single tubular appearance to crystalline structure (Source: Zeng et al., 2014)

2.1.2. Cylindrical Composite Material

The industry would rather the low-cost process and light-weight products. Composite materials provide the desired light-weight. Especially, FW composite materials, which are generally cylindrical with different cross-sectional shapes, are traditionally used in high-pressure areas, chemical storage, space, nuclear, defense sectors, gas and/or oil tanks, and transfers [81]. These applications demand a high stiffness and strength due to high-pressure exposure and these demands are generally met by composite materials. The failure of composite materials does not fail as metals do. Cylindrical composites have many advantages like less lifetime, weight (with nearly the same thickness), and cost. Aramid fiber reinforced cylindrical composites are generally used for rocket motors. Glass and carbon fiber reinforced cylindrical composites are also the other types of composites that have been widely used in long-term pressure vessel applications [82]. GF-based CFRPCs have been widely used for pressure vessel applications according to their high strength, stiffness, and good fatigue resistance.

2.1.2.1. Manufacturing of CFRPCs

There are numerous methods to manufacture the FRPCs according to the matrix types; thermoplastic or thermoset. The production methods for thermoset matrix

(polyester, vinyl ester, and epoxy) based FRPCs are given in Figure 2.8 according to the fiber type.

Among the production methods, the filament winding method is a widely used method for manufacturing high strength continuous fiber-reinforced thermoset composites like uni-and multi-directional lamina, pipes, tanks, etc.

Among the fabrication methods of composite production with a continuous fiber, filament winding ensures the final product with;

- An excellent weight-to-strength ratio,
- A good resin distribution,
- A high fiber content, which provides high strength, and
- A desired fiber orientation/winding angle.

However, it has disadvantages like other production techniques;

- Limited production shapes, and
- Expensive mandrel [83].

While the filament winding process is a cost-effective method, it is a complex and incomprehensible process. Besides, it has manufacturing problems (delamination, layer waviness, local fiber buckling, cracks, voids, etc.) that influence the mechanical properties of the resultant product. The quality of resultant composites is influenced by [84];

- Fiber tension and bundles during the manufacturing process,
- Wettability of the fibers by the predetermined resin at optimum viscosity.

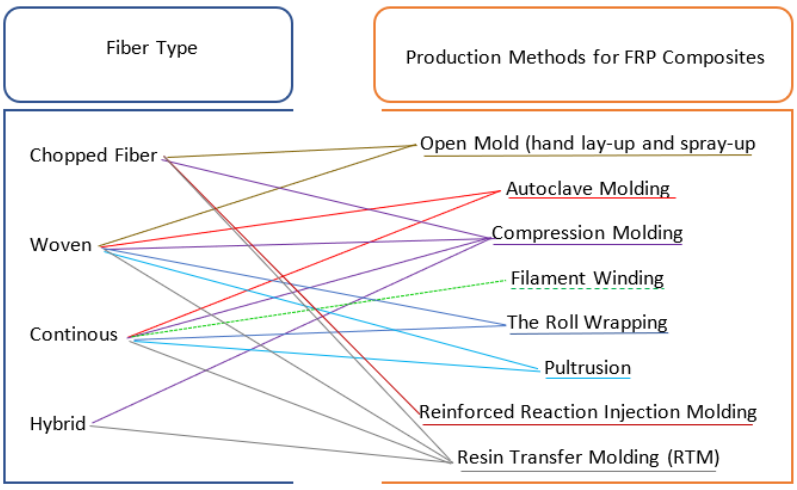

Figure 2.8 Classification of production methods for FRPCs according to the fiber type

2.1.2.2. Definition of the Filament Winding Technique

Filament winding is an automated fabrication method used in the production of cylindrical structures by winding the predetermined resin impregnated continuous fiber onto a mandrel. The filament winding process provides great convenience to manufacturing complex geometries due to having three or more axis of motion. The filament winding method is widely used in the production of different shapes and volumes such as; rocket motor, pressure vessels, power transmission shafts, piping and tubing systems, some non-axisymmetric components, etc. The schematic illustration of the filament winding process is briefly shown in Figure 2.9 (a). During the filament winding processes continuous fiber is firstly impregnated in a resin bath and then wound under tension around a mandrel/liner with a defined geometric pattern controlled by a software system [82,85]. Impregnation of resin can be carried out by the most three methods; roller, cascade, and dip impregnation. Roller impregnation is preferred because winding can be performed with minimum fiber damage and a minimum amount of excess resin (Figure 2.9 (b)). Before the fiber is impregnated within the resin, the fiber is fed to the resin bath by a comb device. Tension devices (spools) are also used to directly control the fiber alignment, resin pick-up, and the fiber tension that affect the properties of the composite. Resin impregnated fiber is eliminated from the excess resin by a wiping device placed right after the resin bath. As the last step of the winding process, continuous fibers are accurately positioned on the mandrel by the pay-out eye (Figure 2.9 (c)). Part geometry, winding angle, winding speed, and several layers have been controlled by software to command winding machine [86]. After the end of the winding process, the FW product is cured at the desired temperatures in an oven. The mandrel used during the winding process may or may not be an integral part of the assembling composites. The FW composite part can be removed from the mandrel after the curing process [87,88].

The filament winding process provides fiber orientations for three basic winding patterns, which are helical, hoop, and polar, and shown in Figure 2.10. While the winding angle is 90^0 for hoop winding, for the helical winding it is usually higher than 45^0. Polar winding is applicable for manufacturing the pressure vessels, in which fiber is wound on the mandrel from polar to polar tangentially [90].

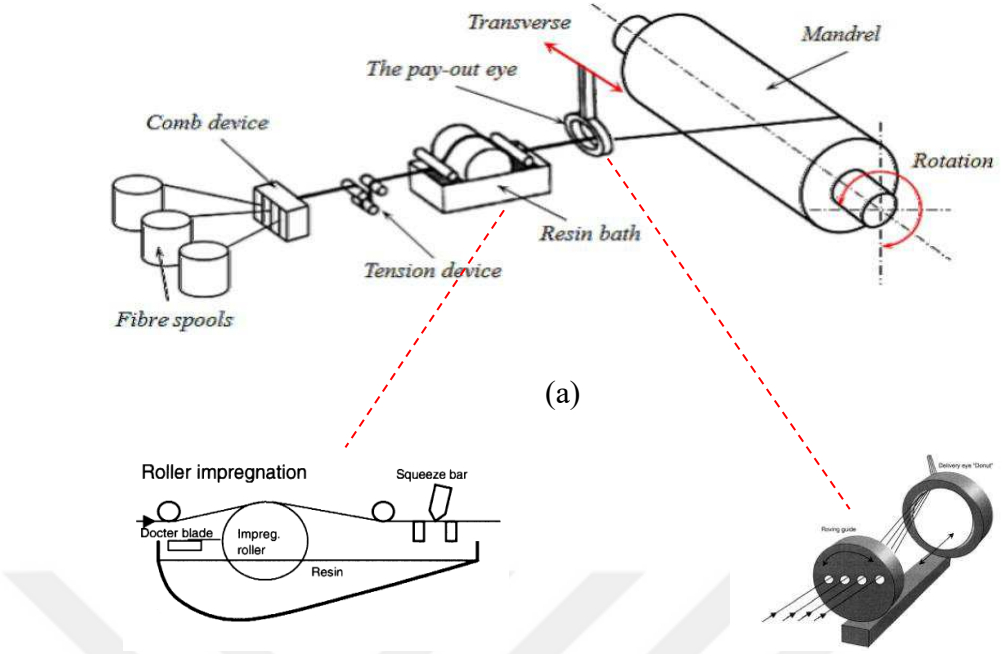

Figure 2.9 Schematic illustration of (a) The filament winding process (Source: Quanjin et al., 2017)[89], (b) Roller impregnation method, and (c) Pay-out eye (Source: Kelly et al., 2000)

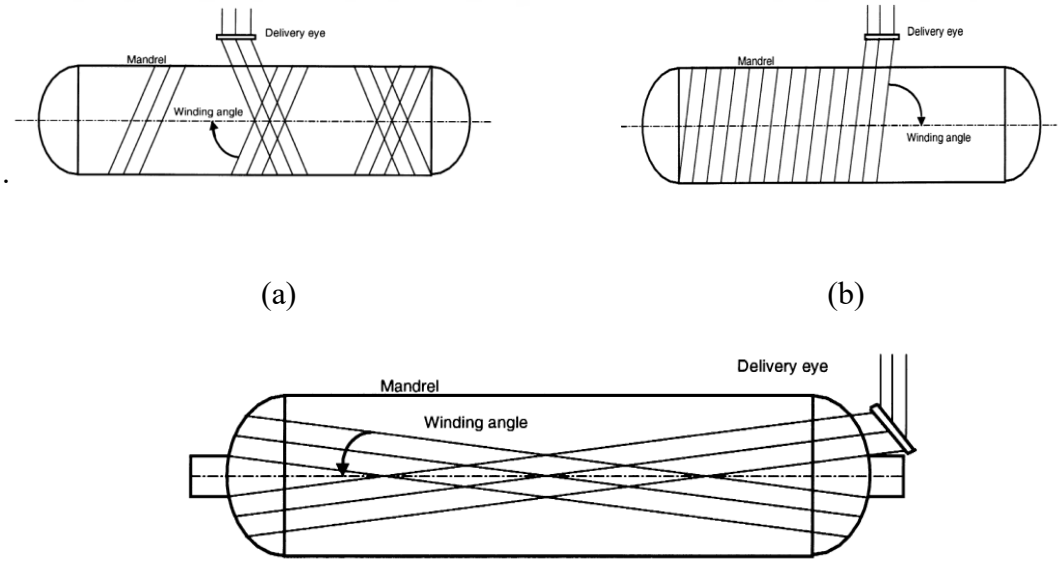

Figure 2.10 Schematic illustration of the filament winding process rotating mandrel in three different patterns; (a) Helical, (b) Hoop, and (c) Polar (Source: Kelly et al., 2000)

Because pressure vessel requires a closed-end structure, a mandrel is used to reduce the openings on the structure ends. Thus, composite pressure vessels are usually produced by the winding of the fiber directly on a mandrel (a thin metallic (Type III) or thermoplastic liner (Type IV)). FW composite pressure vessels are being used for storing either gas or liquids in both aerospace and commercial applications [85]. According to the applications of the composite pressure vessels, they can be exposed to impact loads. FRPCs are not durable to the transverse impact loading and under load pressure vessels can be exposed to fiber fracture, delamination, shear failure, and matrix crack [91]. Damage in FW tanks starts firstly at epoxy and follows by the formation of leakage path, delamination, and finally fiber breakage [12,92]. In decades inorganic fillers are often used to increase the stiffness of the polymer matrix materials. Nevertheless, the usage of high concentrations of commercial fillers is not appropriate for the process of the filament winding, due to the increment of the viscosity to the high levels [93]. Thereby, impregnation of nano-sized fillers at low concentrations can enhance the interlaminar shear strength, interlaminar fracture toughness, and load transferability of FW fiber-reinforced storage vessels by the pull-out, rupture, and crack bridging mechanisms [31,51].

2.2. Mechanical Properties of NCs and Multi-functional FRPCs

The mechanical performance of the NCs and multi-functional FRPCs highly depend on the production process, and interfacial interaction between the materials (fiber, matrix, and nano-sized filler). Especially for the utilization of a nano-sized filler reinforced matrix for the production of FRPCs, dispersion quality of the filler within the matrix is an important matter. The performance of the final composite is affected by the dispersion process and time, nano-sized filler type, the ratio of nano-sized filler to the matrix, etc. [94]. The physical methods and interfacial modifications with a chemical router are important steps for enhancing the homogeneous dispersion of nano-sized fillers within the resin [29,94].

Based on the literature review, the mechanical properties of nano-sized filler reinforced epoxy NCs are summarized in Appendix A. Herein the mechanical properties of NCs were classified according to the production process, matrix type, and nano-size

filler type. As summarized in Appendix A, the tensile strength, flexural strength, and fracture toughness of epoxy can be improved with the incorporation of nano-sized fillers within epoxy.

2.2.1. Interface and Nano-sized Filler Type Approach

The high surface area increases the interacting surface between the filler and the matrix while causing the fillers to agglomerate among themselves. As mentioned earlier, spherical shaped fillers have a lower surface area. For example, CB has a low surface area when compared to GNPs and CNTs. However, according to the literature these properties can be range according to their type. A study that compares the effect of incorporation of GNPs (~8 layers of graphene) and CB within the epoxy matrix to the mechanical properties of epoxy showed that; while the tensile strength decreased with the incorporation of GNPs, it improved with the incorporation of CB. Also, the ductility behavior is enhanced with the incorporation of CB within the epoxy. The fact is that the surface area is greater for used CB (1250 m^2/g) than used GNPs (350 m^2/g) because a high surface area provides more contact area with the matrix [95]. Also, particle size, concentration, and interface with the polymer highly affect the mechanical properties of polymers. Carbas et al. demonstrated that tensile properties did not significantly improve with the incorporation of smaller size CB. However, CB with larger size enhanced the mechanical properties of epoxy at low content of particle, due to the large interface interaction between filler and matrix [96]. Chatterjee et al. studied the size and synergetic effects of nano-sized fillers in the mechanical properties of epoxy. They used two different nano-sized fillers; GNPs with 5µm and 25µm in flake size and MWCNT. According to the results, GNPs in larger flake sizes showed a better mechanical performance when incorporated within the epoxy. Also, a combination of MWCNT with GNPs improved the fracture toughness according to the high aspect ratio of CNTs and the large surface area of GNPs [97].

Nano-sized stiff fillers (nano-silica, halloysite, CNTs, CB, GNPs, etc.) improve the performance of polymers based on the high aspect ratio, alignment, load transfer, and stress transfer [34,98]. These performances can be enhanced by a homogeneous dispersion

of nano-sized fillers within the matrix. The dispersion quality of the nano-sized fillers depends on a decrease interaction between the fillers and increase interaction between filler and matrix by a chemical router. Many studies in the literature have been focused on the functionalization of GNPs and CNTs according to manufactured NCs applications [37,56,105,61,94,99–104].

Surface modified graphene sheets -especially, GO and its derivatives- are widely studied in literature to improve the performance of epoxy-based matrices [56,99–101,106,107]. Qiu et al. concluded during the crack propagation GO incorporated epoxy NCs showed a larger amount of plastic deformation than graphene incorporated epoxy. So, the fracture toughness was improved by retarding the crack propagations by GO [99].

Interfacial modifications of CNT can be achieved with a chemical router. The chemical router improves the bonding and adhesion by a covalent and non-covalent functionalization, which are illustrated for CNT in Figure 2.11. The covalent functionalization of CNTs is the covalent bonding of functional groups (usually carboxylic or hydroxyl groups) on to the CNT walls [54,108]. However, covalent functionalization damages CNTs, which leads to a reduction in the mechanical properties of CNTs [54,109]. Non-covalent functionalization, which consists of surfactant assembling on the CNT walls, does not deteriorate the sp^2 bonding of CNTs and blocks the re-agglomeration of the CNTs within the matrix. Three different surfactants as cationic, anionic, and non-ionic surfactants, are used for the non-covalent functionalization [104,110–113]. Geng et al. while silane and non-ionic surfactant treated MWCNT incorporation showed larger improvement on flexural properties of epoxy than pristine MWCNT, pristine and non-ionic surfactant treated MWCNT incorporation increased the impact fracture toughness of epoxy by almost the same rate [112]. Gallego et al. compared the functionalization of the MWCNT effect on the tensile strength of nanocomposites. According to the acid treatment of MWCNT, the wettability and interfacial adhesion between oxidized MWCNT (o-MWCNT) and epoxy were improved with the presence of functional groups. A good adhesion provided a better performance of o-MWCNT/epoxy than MWCNT/epoxy [102].

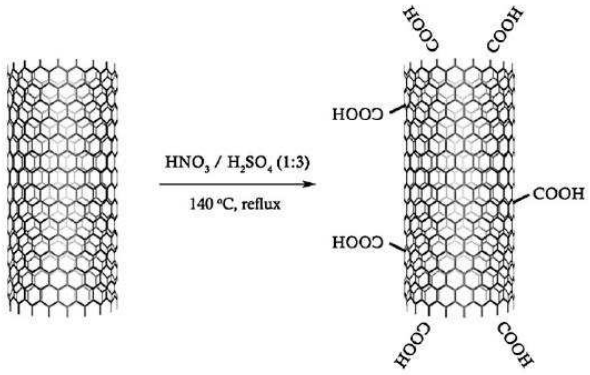

(a)

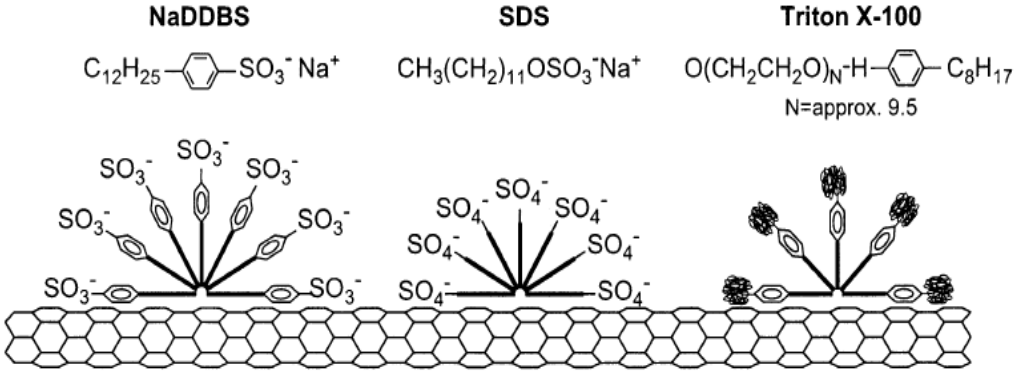

(b)

Figure 2.11 (a) Covalent (Source: Ribeiro et al., 2017) and (b) Non-covalent functionalization (Source: Islam et al., 2003) of CNT

For the size and modification effects of nano-sized filler impact on the mechanical properties, Chandrasekaran et al. examined the fracture toughness of the epoxy with the addition of three different types of carbonaceous fillers; GNPs, TRGO, and MWCNT. The effect of TRGO on fracture toughness is greater, while the effect of MWCNT was lower at the same concentrations. This is due to the good dispersion of layers depending on having functional groups on the graphene [34].

For achieving a better dispersion of clay-based nano-sized fillers-HNT-into the epoxy resin by providing extra sites for interactions with epoxy, surface modification of HNTs has been carried out in lots of studies. To eliminate the aggregation of HNTs in epoxy resins, chemical treatment of HNTs has been utilized. A comparison study of Sun et al. showed that the silane-modified HNTs exhibited improved dispersion within the

epoxy and improved interfacial interaction with the epoxy matrix when compared with pristine HNTs. Thus, tensile strength and toughness of epoxy were improved with the incorporation of treated HNTs [114]. Phenylphosphonic acid (PPA) and potassium acetate (PA) are widely used agents that could reduce the cluster size of HNT with the help of ball mill homogenization. Tang et al. presented the effects of the processing methods on the fracture toughness of PPA-treated HNT/epoxy composites. The processing methods used for manufacturing are mechanical mixing and ball milling homogenization. According to the results, the ball milling homogenization method significantly ensures uniform dispersion of the halloysite contents of 10 wt.%. Consequently, the fracture toughness of epoxy was improved with the addition of halloysite [115]. Zeng et al. studied the improvement of the dispersibility of HNTs within the epoxy resin. HNTs were treated with a low concentration of sodium hydroxide (NaOH) to form hydroxyl groups on the surface of the HNTs. The higher level of dispersion of HNTs in epoxy led to considerable enhancement in both stiffness and toughness for the resultant NCs [78]. Deng et al. showed that, while treatment of HNTs did not affect the intercalating halloysite layers, PA treatment reduced the size of the clusters of particles. Also, silane and cetyl trimethyl ammonium chloride (CTAC) treatment caused agglomeration of HNT [116].

In rundown interface is an important issue for the nano-sized filler incorporated polymeric composites. Since the interface of filler and polymer in the composite systems has a significant effect on morphological features, chemical compositions, and mechanical and physical properties of the resultant composite structure, studies of nano-sized filler incorporated polymeric composites have been widely conducted in many decades. Besides, mechanical properties related to the interface of FRPCs were widely studied in previous studies in the literature. FRPCs with strong fiber/matrix interface has high stiffness and strength, but also low toughness. In recent studies, the production of multi-scale reinforced composites draws attention. Generally, multi-scale reinforced composites consist of three different phases, which are, (1) matrix (polymer), (2) micro-sized reinforcement (glass fiber, carbon fiber, basalt fiber, etc.), and (3) nano-sized reinforcement (CNT, graphene, nano-silica, etc.) [117]. Since among the nano-sized filler, CNT and GNPs have a larger interfacial area per particle than classical mineral fillers, usage of CNTs and GNPs for the production of multi-scale reinforced composites draws the most attention in the literature [118]. For the production of multi-scale reinforced composites, nano-enabling approaches can be carried by (1) bulk resin, (2) fiber/matrix interphase, and (3) interlaminar modification. These multi-scale reinforced composites

are also called “novel hybrid” or “hierarchical” composite systems [32]. The hierarchical structures are already found in nature, for example; plant cell walls, animal shells, and skeletons [119]. Configuration of micro-and nano-sized fillers for the formation of the hierarchical composites is the most technological promise combining top-down and bottom-up processing. However, there are challenges to designing, processing, and characterization [120].

FRPCs already have high mechanical properties such as high stiffness and strength, the incorporation of nano-sized fillers within the matrix or at the interface of FRPC is not expected to improve these properties. However, since mechanical properties like shear strength and fracture toughness are matrix- and interface-dominated properties, integration of nano-sized fillers for the production of the FRPCs has a direct effect on these properties. The role of the matrix in the composites is to hold the system together and govern the out-of-plane properties of composites. The major role of nanotechnology is improving the out-of-plane properties of FRPCs [117]. Due to fracture toughness is very important for many FRPC applications (e.g., aerospace and oil/gas industries), it is essential to improve the fracture toughness, which is dominated by the matrix. Additionally, when the polymer segments are attractive to the particle surface, the density of the polymer segments that close to the fibers is much higher which leads to a storage change in chain dynamics. Although considerable efforts have been made to understand the interface between the micro-scale fiber and polymer, more studies should be carried out to fill the gap in understanding interfaces in nano-scale fillers [120].

Among the aforementioned multi-scale reinforced composites production methods, bulk resin modification enhanced homogeneous dispersion of nano-sized fillers within the polymeric matrix via mechanical stirrer, calendaring, ultrasonication, etc. As previously explained, appropriate dispersion methods should be used to hinder the agglomeration and destruction of CNTs. In addition to the increase in the stiffness and the toughness of the polymers with the nano-sized filler incorporation, the usage of the nano-sized filler reinforced polymeric matrix in the production of FRPCs is also likely to provide lateral support to the load-bearing fibers. Another main concept also is the viscosity of the CNT reinforced matrix, such that it increases dramatically with increasing CNT concentration. Highly viscous matrix suspension causes difficulties in the production of FRPCs, as well as increases the agglomeration of CNTs, which results in infiltration during production. To eliminate the filtration problem the filament winding is an alternative for FRPC production [119].

The FW fiber-reinforced storage vessels and pressure pipes for high pressure are expected to have high stiffness and strength. The properties of the FW composite structures are affected by (1) the fiber properties, (2) winding angles, and (3) wall thickness. Also, the axial and hoop stiffness affect the properties of the FW CFRPCs, which is directly affected by the matrix modulus. Indeed, when a load is applied to the composite, it is transferred from the matrix to the fibers through the interface between the fiber and matrix. Thus, interfacial strength between the fiber and matrix highly affects the toughness and the strength of FRP composites [121]. In decades inorganic fillers are often used to increase the stiffness of the polymer matrix materials by absorption of some deformation energy. Thereby, impregnation of nano-sized fillers enhances interlaminar shear strength, fracture toughness, and load transferability of FW fiber-reinforced storage vessels by the pull-out, rupture, and crack bridging mechanisms [31,51].

2.2.2. Dispersion of Nano-sized Fillers Approach

There are several physical methods for enhancing the distribution of micro-and nano-sized fillers within the thermoset resin. The most popular ones are;

- Solution mixing,
- Mechanical stirrer,
- Ultra-sonication,
- Calendaring (3-roll-mill), and
- Ball milling processes[30].

According to the Van der Waals forces, nano-sized fillers tend to agglomerate. Agglomeration of the fillers can act as a stress concentration, which reduces the tensile strength of the NCs. Thus, a homogeneous dispersion of nano-sized fillers within the epoxy resin is a critical issue to ensure the load transfer from the matrix to the nano-sized filler.

Solution mixing is a widely used dispersion method to disperse CNTs, GNPs within the resin in the presence of an organic solution for study on the mechanical properties of nanocomposites [122–125]. Another widely used method is the *ultra-sonication* method, which generates ultrasound energy with an ultrasonic probe [30]. However, to

avoid serious damage, ultrasonication should be implemented appropriately. Lu et al. defined the significant damages that may occur during a high-energy ultrasound applied to the CNTs. They observed bending and buckling in CNTs after sonication according to TEM images (Figure 2.12). Since the duration of sonication is a critical concern for damaging the CNT structure, serious damage and even breakages in the structure may occur at high sonication time. This results in a reduction in the mechanical properties of CNTs. Likewise, a high energy level of the ultrasound can cause more serious damages to the other carbonaceous nano-sized particles even more than CNTs. In the ultrasonication process, due to the production of local energy ultrasounds can cause damage and rupture on the structure of nano-sized particles when dispersion is accomplished within a high viscous resin -such as epoxy [126,127]. So, nano-sized particles are usually mixed in a solution-based mixture first by ultrasound. Even if CNTs are separated in a low viscous liquid like acetone at low frequencies, after mixing the suspension with epoxy and removing the acetone with heat, agglomerates will remain (Figure 2.13) [31]. Besides, not removing the solvent completely from the mixture after the sonication process will affect the curing degree of the epoxy, which results in a decrease in the mechanical properties of NCs [128].

Rafiee et al. used the sonication method to disperse GNPs within the epoxy and the results showed that graphene platelets improved tensile strength, Young's modulus, and fracture toughness better than CNTs [129]. According to the study of Gkikas et al., the amplitude and duration of the sonication process highly affected the fracture toughness but not the storage modulus of MWCNT reinforced epoxy NCs [130].

Mechanical stirring is the other widely used method for the dispersion of nano-sized particles in a liquid system. In the mechanical stirrer process, shear forces are applied by the rotation of the propeller. The parameters like the shape, size, and speed of the propeller and temperature affect the quality of nano-sized filler dispersion within the viscous resin [30,31,94]. Sandler et al. reached a good dispersion after the intensive stirring of MWCNTs in epoxy resin [131].

The *calendaring method* is another common technique for dispersing the micro-scale particles as well as nano-scale particles in different viscous matrices without causing damage and rupture to nano-sized particles when compared to the sonication and high

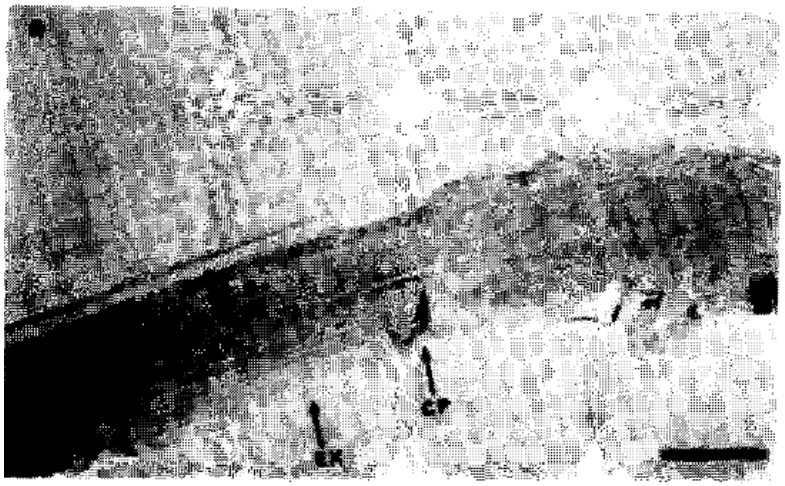

Figure 2.12 TEM images of bending and buckling in CNT after sonication process (Source: Lu et al.,1996)

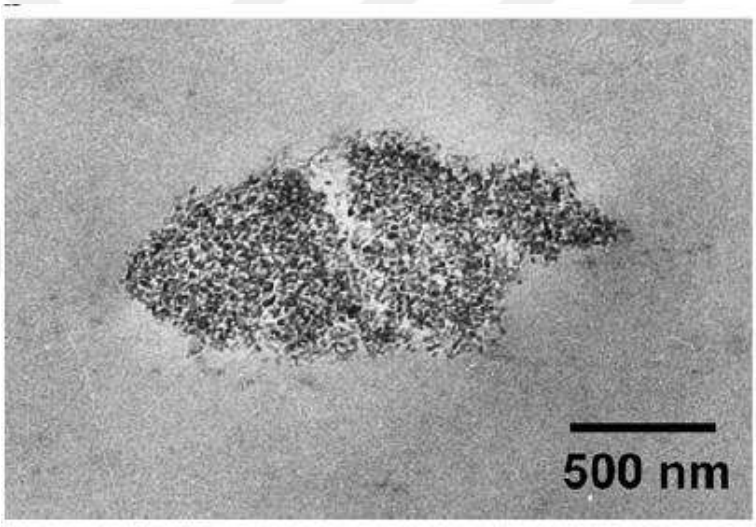

Figure 2.13 TEM images of CNT/epoxy nanocomposites produced by the ultra-sonication process (Source: Fiedler et al., 2016)

shear mixing methods [31,33,97,132,133]. During calendaring, high shear stress is applied to disentangle CNT bundles and allow a homogeneous dispersion. However, Fu et al. observed a length reduction of CNTs after calendar processing. This can be explained due to the minimum gap between the rollers (<5μm), which is almost equal to the length of the CNTs [134]. Residence time, the number of times the mixture is feed, the gaps between the rolls, and the force between the rolls of the calendar affect the mixing quality. Jiménez-Suárez et al. investigated two different calendaring methods, which are the sequential batch and time-controlled methods. In the sequential method, the bundles of

the nano-scale reinforcements were disaggregated according to a progressive decrease in gap size. However, a time-controlled method is more difficult because of longer processing times. Slight differences were observed between two different manufactured nanocomposites [135]. Thostenson et al. applied the calendaring method for two different gaps (5 and 10 μm), and according to the SEM images, a large number of CNTs were dispersed in the continuous matrix at 5μm gap [136].

Ball milling is a grinding method that generates high pressure. Because it reduces the size of the particles, it can damage the structure of the nano-sized fillers [30]. According to Tan et al., while the flexural modulus was significantly improved, the flexural strength was slightly improved with the incorporation of RGO. Also, the ball milling technique highly affected the flexural strength of the nanocomposites compared to the ultra-sonication technique, while the flexural modulus is not affected by the dispersion method [61].

2.2.3. Interlaminar Failure Approach

While laminated FRPCs have high strength in the in-plane direction, the strength is low throughout the thickness. This flaw leads to damage and interlaminar failure as a result of a high impact. This damage may create a catastrophic failure to the composite. To prevent this catastrophic result, improving the delamination resistance of the FRPCs is substantial. There are several studies in the literature to improve the delamination resistance of laminated structures by techniques aiming to increase the strength throughout the thickness. These techniques are;

- Three-dimensional (3D) weaving [137],
- Z-pinning [138],
- Braiding, knitting and stitching [139],
- Fiber hybridization [140],
- Interleaving film, fibers, or particles between the composite [141–144], and
- Toughening the matrix material with micro/nano-sized fillers (alumina, silica, carbon black, graphene, carbon nanotubes) [145–147].

Since to aware of the interlaminar failure of the produced multi-functional composites, researchers have used many test methods to determine the effectiveness of these techniques. The widely used test methods are;

- The double cantilever beam (DCB) test to utilize the Mode I fracture toughness,
- The end-notched flexure (ENF) test to investigate the Mode II fracture toughness and,
- The short beam shear (SBS) test to determine interlaminar shear strength (ILSS) [148].

SBS test specimen exposes to the interlaminar shear stress and shear stress, then fails in transverse shear. However, all-composite specimens do not fail in transverse shear. Besides, DCB characterizes the resistance to delamination. Delamination occurs near the stress risers, such as micro-cracks, holes, etc. [149]. During the delamination, the loading pattern starts as tension and gradually becomes shear. Catastrophic results may occur without the mechanism to prevent delamination. So, delamination will be more damaging to the laminates than for transverse shear.

Nano-sized filler addition to the FRPCs motivates to reduce the limitations correlated with the matrix dominated properties. Nano-sized fillers, such as CNT, ensure an improvement of delamination resistance without compromising the in-plane properties of FRPCs, besides they enhance the multi-functionality [119,150,151]. These newly developed composites should resist the initiation of cracks and their propagation under external load for preventing catastrophic failure. In this context, the most important issue of laminated composite materials during damage is delamination. The objective is here to manufacture FRPC with nano-sized filler incorporated polymeric matrix to enhance the damage resistance and tolerance of the FRPCs.

2.2.3.1. Interlaminar Shear Strength

While in-plane properties of FRPCs are not directly affected by the incorporation of nano-sized filler within the polymer, out-of-plane properties are highly affected by nano-sized filler incorporation. ILSS is a matrix dominated property, and the interlaminar

shear properties of FRP is important for many applications, due to be a limiting characteristic design feature. In the past decades, the ILSS property of conventional fiber-reinforced composites (basalt, glass, and carbon fiber) was improved by 7-50% with the incorporation of CNTs within the polymer matrix [51,76,159,160,146,152–158] (See Appendix B for the literature review of ILSS of multi-scale FRPCs).

Matrix modification with nano-sized fillers is an effective way to improve the interlaminar shear properties of FRPCs. While in the study of Qiu et al., GF-based FRPCs manufactured with 1 wt.% o-MWCNT reinforced epoxy by vacuum-assisted resin transfer molding (VARTM) exhibited a 7.9% improvement in ILSS, Fan et al. obtained a higher improvement on ILSS of GF/epoxy composites that manufactured with injection and followed by double vacuum-assisted resin transfer molding (IDVARTM) and 2 wt.% o-MWCNT incorporation [153,155]. Amino functionalized CNTs at 0.3 wt.% incorporations enhanced further ILSS improvement regardless of the production method of FRPCs [51,76,154,156]. Besides the usage of bulk resin modification methods, the usage of fiber coated with the nano-solvent suspension to manufacture multi-scale FRPCs is also improved the ILSS [161,162]. Furthermore, besides CNTs, the other nano-sized fillers like graphene, silica, alumina, etc., and in their other forms have been widely used to improve the ILSS of the multi-scale FRPCs, but the improvement has mostly not as much as the CNT contribution [35,146,163–169].

Furthermore, curved composite structures can be exposed to external forces, especially due to their usage areas. Since the damage in FW CFRPCs starts firstly at epoxy, the measurement of the interlaminar shear force is a very important parameter for CFRPC. In a study, ILSS of FW Naval Ordinance Laboratory-ring (NOL-ring) improved 28% with 6 wt.% MWCNT-NH_2 incorporations [159]. In another study, a synergetic effect of core-shell rubber and a rigid nano-sized SiO_2 incorporation on the mechanical properties of FW CF/epoxy NOL-ring was studied. In addition to other mechanical properties, ILSS was also improved [168].

2.2.3.2. Delamination Fracture Toughness

Definition of Delamination:

The separation of two adjacent layers from the layered composites is called "delamination" or "fracture toughness". It is the most common fracture mode in laminated composite structures and is defined as the "Achilles heel" of composite materials [170]. As delamination has an important role in determining the durability and damage tolerance, it is an essential issue to address for laminated composites. Delamination can occur by mismatch material usage, the shear stress between the layers and material, and/or initial geometrical imperfections (broken fibers, void containing, structural imperfections, delamination regions, cracks in matrix material, foreign material inclusion, etc.) [171,172]. Since delamination damage mode decreases the stiffness and strength of the composite materials, with the enlargement of the delamination, failure is completed.

Delamination modes and mechanisms:

Interlaminar fracture toughness is a failure mode for laminated composite structures and characterized in terms of the critical strain energy release rate, G_c. This failure occurs according to the high out-of-plane loads (fibers cannot resist this loading) and therefore, the production of multi-scale composites has been attracted a lot of attention [32,169]. The delamination of FRPCs can occur when the composite subjected to three different modes;

- Peel mode (Mode I (G_{Ic}))-tensile load,
- Shear mode (Mode II (G_{IIc}))-shear load, and
- Tearing mode (Mode III (G_{IIIc}))-combined load [173].

All delamination modes were illustrated in Figure 2.14. As illustrated in Figure 2.15 (a), the delamination of FRPCs starts with the delamination initiation, followed by crack jump and then steady-state growth. Figure 2.15 (b) shows the morphology of the fracture surfaces during crack growth. Delamination initiation between resin interlayer is seen as a honey-comb shape on the fractured surface. Crack jumps from interlayer to between interlayer and lamina layer, then steady-state growth takes place, and finally, here fibers can be seen on the fracture surface [174].

Among the delamination modes, Mode I interlaminar fracture toughness has attracted a lot of attention among the researchers, due to the low delamination initiation energy during the shear mode. While delamination occurs between the laminates, fibers tend to bridge between two separated sub-laminates behind the crack tip. This tendency

is called “the fiber-bridging” effect, which increases the critical strain energy release rate with delamination extension. This increases the fracture toughness, which is characterized by the resistance curves (R-curves). R-curves consists of three main stages;

- Initiation toughness (G_{ini}),
- Steady-state toughness (G_{ss}), and
- Steady-state fiber-bridging length (L_{FB}).

R-curves do not depend on the material properties, but it highly depends on the specimen size and geometry (initial crack length, width, thickness, and curvature) [175]. While the curvature of the composite does not affect the initiation toughness, it affects the steady-state toughness and fiber-bridging length [176].

Fracture toughness depends on several parameters such as;

- Fiber sizing/coating and adhesion between the fiber and matrix [177,178],
- Specimen geometry [179],
- The inserted film features [180],
- Fiber volume fraction [181],
- Stacking sequence [182],
- Loading rate [183],
- Crack length [184,185],
- Environmental conditions [186], etc.

To increase the fracture toughness, the fiber-bridging mechanism should be improved behind the pre-crack. This can be achieved by producing multi-scale composites with the aforementioned techniques to enhances the performance of the laminated composite structures through the thickness. However, most of these techniques, such as 3D weaving, Z-pinning, braiding, stitching can lead to a reduction in-plane mechanical properties [142,187]. Interlaminar fracture toughness can be improved with the micro-and nano-sized filler toughened matrix technique. As summarized in Appendix B, comprehensive studies of multi-functional FRPCs have been conducted to achieving superior properties without sacrificing in-plane properties with the incorporation of nano-sized fillers such as CNTs [146,152,188–195], graphene [146], nano-silica [167,168], halloysite [35], alumina [165,169], etc. within the matrix.

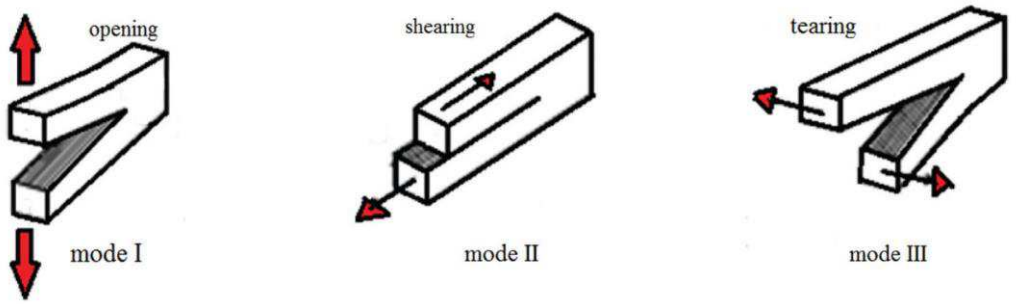

Figure 2.14 Modes of delamination (Source: Manjunatha et al., 2015)

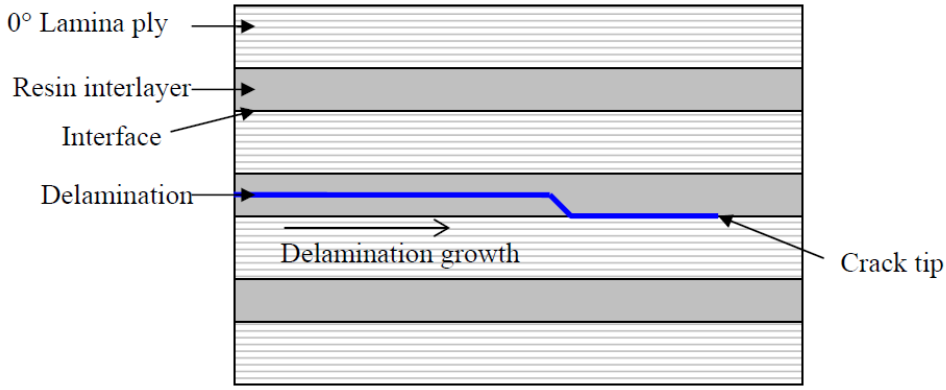

(a)

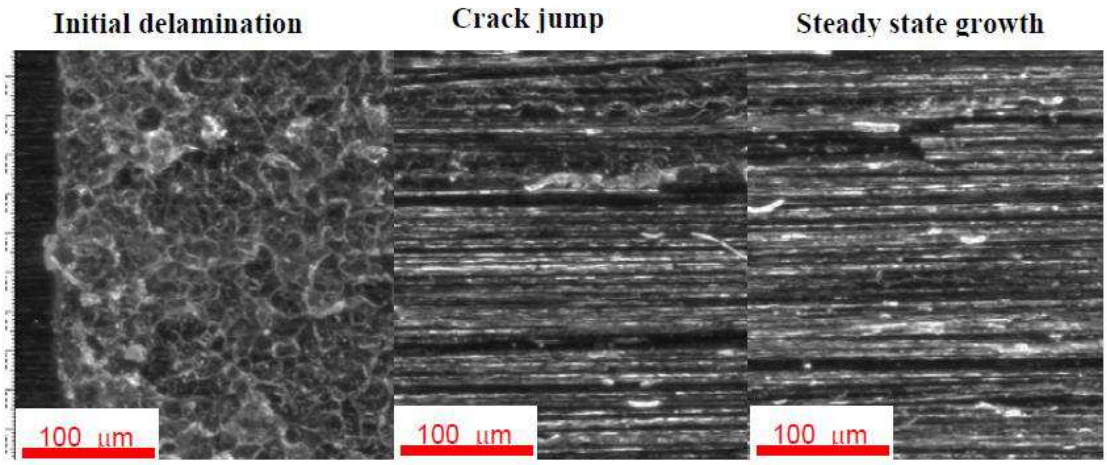

(b)

Figure 2.15 (a) Crack growth during delamination and (b) Fracture surface morphology of Unidirectional Torayca T800H/3900-2 graphite/epoxy (Source: Zhao, 2011)

2.2.3.3. Delamination Fracture Toughness of CFRPCs

Delamination is a damage type that occurs throughout the circumferential directions in CFRPCs. When the force is applied to the CFRPC structures, curved regions of CFRPCs are exposed to bending moment, which results in delamination in the curved regions. Therefore, the determination of interlaminar fracture toughness of curved composites is of great importance for their performance. There are several numerical and experimental studies in the literature for determining the delamination propagation of CFRPCs [176,184,185,196–199]. In both experimental and numerical studies of Ghadirdokht, FW flat and curved laminated composites were tested under Mode I load. While the curvature does not affect the initiation toughness, curvature increases steady-state toughness but decreases fiber-bridging length (Figure 2.16). Based on the numerical studies, they showed that delamination modeling in curved samples can be assumed to be the same as flat samples [176]. In another study by Liu et al., curved carbon fiber reinforced polymeric composites showed significantly higher Mode-I fracture toughness values than the strait one [197].

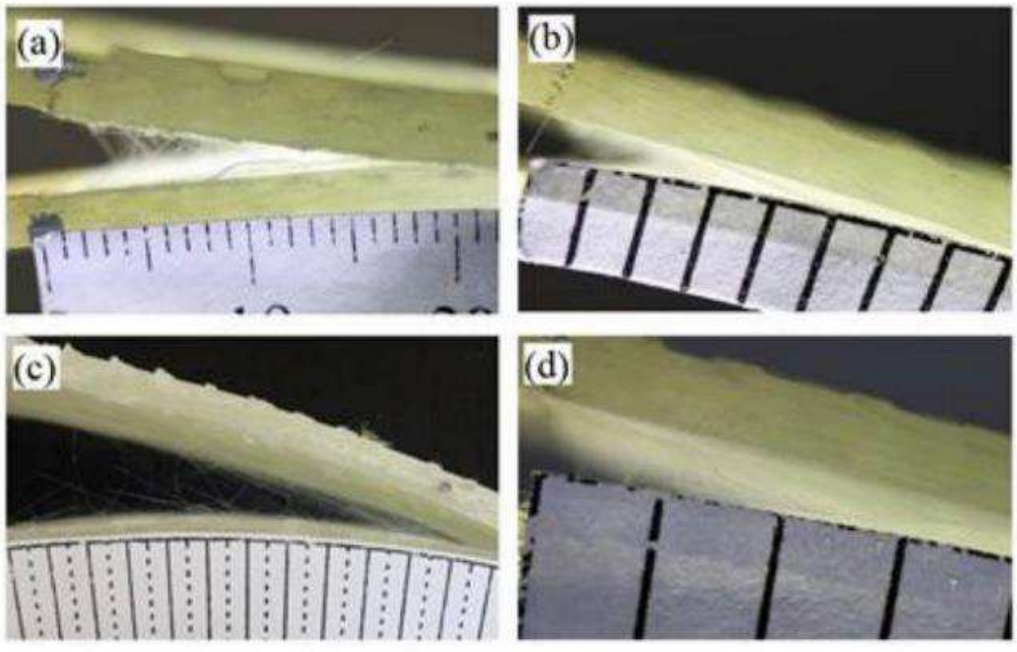

Figure 2.16 Fiber-bridging phenomenon of (a) Flat DCB specimen and (b), (c), and (d) Curved specimen with increasing curvature (Source: Ghadirdokht, 2019)

It was stated in the previous subtitle that fracture toughness depends on many parameters. Some of these parameters for curved samples were reviewed by researchers. Especially for the FW CFRPCs, the angle of the fiber and number of the layers influence the delamination fracture toughness. A study by Ozdil et al. showed that initiation fracture toughness was increased with increasing fiber angle for both thin and thick beam cut from the FW CFRPCs longitudinally. The experimental results were coherent with analytical results [198]. In addition to the angle of the fiber and thickness of the specimen, the pre-crack length of CFRPCs extremely affects the interlaminar fracture toughness by fiber-bridging length, as shown in Figure 2.17 [185]. Also, some researchers showed that compliance (C) is not influenced by the curvature at the composite sample and pre-crack length, significantly [176,198]. As Figure 2.17 illustrates that, while calculated compliance values with the progress of the delamination for different pre-crack lengths are overlapped [196], compliance graphics for samples with different curvatures nearly overlapped [185].

Guedes et al. used the modified compliance calibration (MCC) and compliance-based beam method (CBBM) for the calculation of the Mode I fracture toughness. According to the numerical and experimental results, both methods are accurate to each other [199].

Toughening of the polymeric matrix with nano-sized fillers will enhance the matrix thickness in the space between commercial fibers. In this context, the interaction between commercial fiber and epoxy will increase, and the delamination resistance will also increase. Consequently, the resistance of FRPCs to blast loading or hard object impact loading will increase.

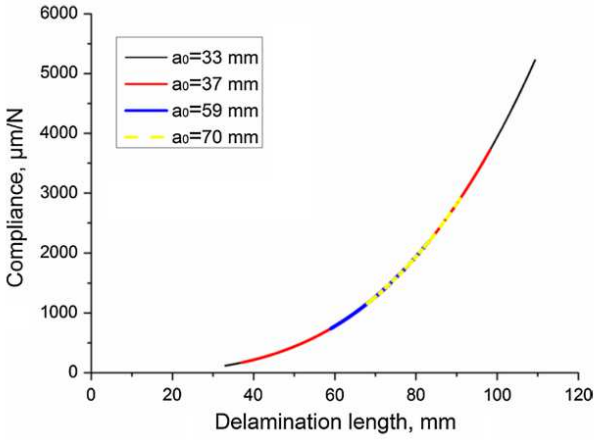

(a)

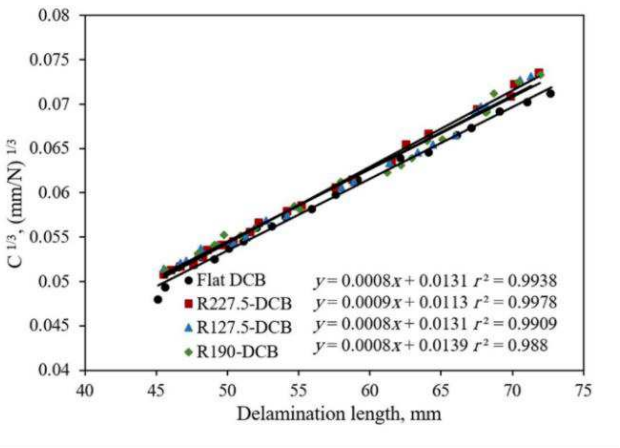

(b)

Figure 2.17 Compliance curves for (a) Different pre-crack length (Source: Mohammed et al., 2018), and (b) Flat and curved samples in increasing curvature (Source: Laid et al., 2018) of CFRPCs

2.2.4. Toughening the Matrix Material Technique with CNT

According to the high aspect ratio of CNTs, the reinforcement of the FRPCs with CNTs leads to entanglement between CNTs and fibers that result in an extra energy requirement to pull-out the CNTs from the host matrix. Consequently, CNT toughens the matrix and hinder the propagation of cracks by enhancing the load transfer, and that results in a delamination resistance in the FRPCs. However, there are some limitations to the usage of CNT reinforced thermoset polymeric matrix for the production of multi-functional FRPCs; (1) agglomeration of CNT within the epoxy resin, (2) increasing viscosity, (3) filtration of CNTs during production, etc. While the necessary steps to solve the agglomeration problem have been considered in the previous titles, the viscosity will be mentioned in the following titles. When filtration is considered, CNT bundles by preform mesh during FRPC fabrication are another problem, an increase in concentration can induce the filtration of agglomerated nano-sized filler especially during RTM processes [200].

For taking the advantage of the mechanical properties of CNT, to enhance the performance of the composites, it is essential to obtain a homogeneous dispersion in the

composite. Particularly, the dispersion of CNTs within the thermoset polymeric matrix is challenging due to the Van der Walls attraction between particles. However, there are previously mentioned techniques to overcome this challenge. These techniques are (1) physical methods and (2) interfacial modifications with a chemical router (covalent and non-covalent functionalization). The most used physical methods are shear mixing, calendaring, extrusion, ultrasonication, ball milling, and the combinations of these techniques [30]. In the literature, widely used physical methods are high shear mixing, ultrasonication, or their combinations for producing multi-functional FRPCs [35,154,156,157,160,193,201]. The calendaring method is also used, due to breaking CNT bundles with a small gap between the mills by high shear [76,152,158]. The aforementioned functionalization techniques of CNTs highly affects the mechanical properties of multi-scale FRPCs. Functionalized CNT improve the strengthening mechanism of FRPCs, due to enhancing the stress transfer. Covalent functionalization of CNT especially for SWCNT can lead to a reduction in the performance of CNTs by damaging the CNT walls. There are several studies about the incorporation of covalently functionalized CNTs to multi-functional FRPCs [152,188,192,193]. Non-covalent functionalization of CNT ensures the dispersibility of CNT within the polymeric matrix without damaging CNT walls [109]. However, there are few studies about non-covalently functionalized CNT incorporation for the production of multi-functional FRPCs [160,189]. Therefore, in this thesis, the focus will be on the interlaminar fracture toughness behavior of composite laminates using non-covalently functionalized CNT reinforced matrices.

A study by Sánchez et al. emphasizes the significance of functionalized CNT utilization on the performance of multi-scale FRPCs. Amino functionalized CNT, which prevents the formation of micro-agglomerates, was dispersed within the epoxy matrix by the calendaring method. The results demonstrated that the performance of the multi-scale composites was increased with the incorporation of functionalized CNTs [158]. In another study by Rahman et. al, the physical properties of GF-based FRPCs were described with enhancing the crosslink density by an effective and low contribution of nano-sized filler addition, which is amino-functionalized MWCNT. The dispersion of CNT is carried out by a combination of ultrasonication, calendaring method, and shear mixing [156]. In another study using amino-functionalized CNT; CNTs were dispersed within the polyester resin via a 3-roll milling technique, and for preventing the agglomerations of CNTs on the fibers VARTM technique is used. However, while some physical properties of multi-functional FRPCs are enhanced, some of them decreased slightly [152].

2.2.5. Toughening Mechanisms

Several toughening mechanisms define the fracture toughness properties of micro-particle (spherical or fibrous) reinforced brittle thermosets. These mechanisms depend on the particle size and morphology, interfacial bonding between particle and matrix, volume/weight fraction of the particles in the matrix, mechanical properties of both filler and matrix, phase transformation, etc. [31]. The toughening mechanisms are generally categorized according to the effect of rigid particles on the brittle thermoset polymers; on-/round-plane (crack pinning and crack deflection, in which crack front encounter with particles) and off-/away-plane (debonding and plastic void growth, in which the damage is occurred in away from the crack tip) [77,202]. The rigid micro-sized fillers incorporation toughen the epoxy through the crack pinning, crack deflection, micro-cracking and plastic void growth, particle/fiber debonding, particle/fiber deformation, or breaking at the crack tip [31,34,203–205]. However, understanding the toughening mechanisms of nano-sized filler incorporated epoxy composites is important because plastic zone size is small for the epoxy resin. The size and geometry of the fillers affect the distribution of the filler within the matrix. A smaller sized filler ensures a further amount of particles that contribute to the plastic zone deformation process during crack propagation than a larger sized filler [31]. However, the toughness effect of nano-sized fillers on the epoxy composites are not completely definite yet. According to Fiedler et al., toughness mechanisms for micro-sized rigid filler reinforced epoxy composites can offer basic assumptions for explaining the toughness effect of nano-sized filler within the epoxy [31]. Still, wide studies are needed to understand the toughening mechanisms of nano-sized fillers [34].

Crack pinning (crack bowing) mechanism can be defined for micro-and nano-sized particles. This mechanism is parallel to the precipitation hardening, which has an interaction between the particles and dislocations within the matrix. Crack is entrapped and blocked by the crack pinning mechanism due to the blunting of the crack tip with localized plastic deformation. This mechanism firstly defined by Lange [206] as inhomogeneous dispersion of a second phase within the matrix causes obstacles and delays the crack propagation by the crack pinning mechanism. This delay depends on the particle size and spacing between the particles. As shown in Figure 2.18, during the crack

propagation, bowing lines are presented between the second phase dispersion, which is shown by an arc of a circle with a 2R diameter. When the crack meets the obstacles, crack propagation pins and encounters, and finally bow out with forming a non-linear crack propagation. Because bowing needs more energy, the crack resistance is enhanced with the increase of the crack length by the formation of a non-linear crack (secondary cracks, which provides energy dissipation during crack propagation) that assumed as a "line energy". Secondary cracks are formed as a result of the branching of the initial crack, which improves the fracture toughness of the matrix. Crack pinning toughening is increased with a high content of filler, a high aspect ratio of filler, average distance among the fillers, and high mechanical properties of the filler [207–209].

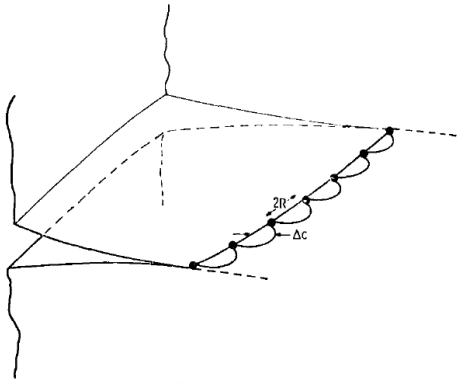

Figure 2.18 The model of crack pinning mechanism (Source: Lange, 1970)

Crack deflection is a toughening effect that occurs when the crack front tilts and twists due to the interaction between the reinforcement and the crack front. Faber and Evans [210] used the fracture mechanics approach to the analysis of the crack deflection process. When the crack first meets and intercepts by a micro-sized filler, it will tilt at an angle that depends on the orientation and position of the initial crack (Figure 2.19 (a)). Then, it may be followed by twisting and tilting of the crack as the deflected crack intercepts by further particles (Figure 2.19 (b)). Three different crack models can occur; (1) flat crack in Mode I (opening), (2) tilt crack in Mode I and Mode II (sliding), and (3) twist crack in Mode I and Mode III (tearing). Fracture under Mode II and Mode III load need more energy than Mode I. As the deflected crack experiences mixed-mode loading, fracture energy increases. Hence, it results in great energy absorption as a result of local stress intensities at the crack fonts [211,212]. Crack deflection toughening increases when

twisting is more dominant than the tilt of the crack. Also, the high content of filler and high aspect ratio of filler increases the crack deflection toughness. While the aspect ratio of the rod has little effect on the tilting of the crack, the aspect ratio has a great effect on twisting (Figure 2.20) [210].

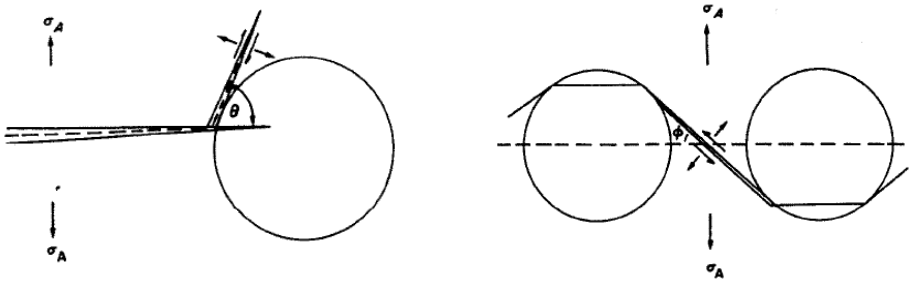

(a) (b)

Figure 2.19 Schematic illustrations of (a) Tilt crack front, and (b) Twist crack front (Source: Faber and Evans, 1983)

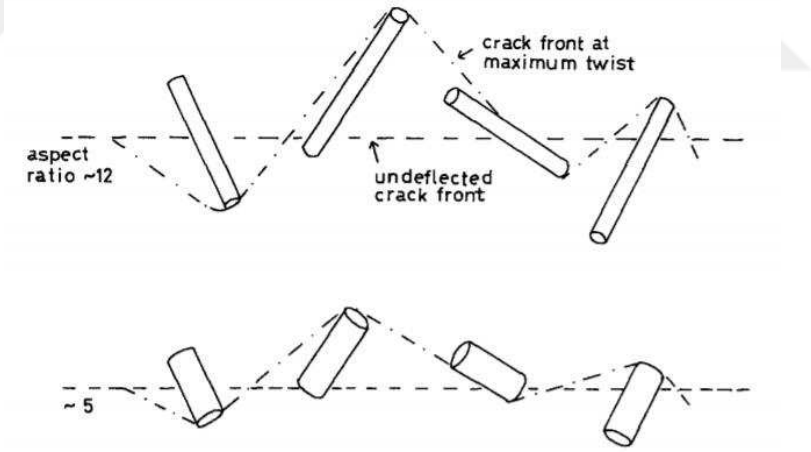

Figure 2.20 Schematic illustrations of twist of a crack front with different aspect ratios of rods (Source: Faber and Evans, 1983)

The interface or immobilized layer of polymer around the particle formation is another mechanism [77]. In this mechanism surrounding polymer (interface) is immobilized by the particles. Immobilized is affected by the interfacial bonding, which depends on the "effective volume fraction" [213]. For an effective volume fraction model, an effective

particle volume fraction, and a constant effective interface thickness are needed. When the particle radius increases, interface volume and effective volume ratio decrease which lowers the elastic properties of the composite [214]. This local fluctuation at the matrix created by the particles may influence the fracture mechanisms like the pinning mechanism [209].

The separation of the filler from the matrix called "*debonding*", which reduces the stress at the crack tip. Debonding and the subsequent plastic deformation via a void growth play an important role in the toughening mechanism of filler reinforced epoxy composites [77,203]. Localized plastic deformation produces a network at the front of the crack tip, which strongly depends on the interfacial adhesion between filler and matrix [215]. Among the plastics, thermosets have resistance to plastic deformation due to their cross-linked network structure. Plastic shear yielding plays an important role in the toughening mechanisms of the thermoset-based composites due to leading crack initiation. Plastic shear yielding can be induced by the presence of rigid fillers. When the adhesion between the rigid filler and the matrix is weak, and the filler size is relatively large, interfacial debonding may occur and follow by plastic deformation, due to the poor adhesion between the filler and the matrix acts as stress concentrations or micro-cracks at the crack tip after debonding [212,216]. Localized plastic shear yielding exists at the crack tip surroundings and results in cavitation in the matrix. In the circumstances, small-sized fillers have a better toughening effect than larger ones. But it should be noted that debonding can be also occurred by the presence of flaws, air bubbles, or molecular inhomogeneities that act as stress concentrations.

Fiber pull-out occurs behind the crack tip separation of the fibers from the matrix while energy is observed due to the shear stress at the fiber and the matrix interface [217]. Kelly studied the effect of the aspect ratio on the toughened of the FRPCs [218]. When the fiber length was below the critical fiber length, pull-out was observed. However, when the length exceeded the critical fiber length, fiber failure occurred. Fiber pull-out relates to the interfacial friction between fiber and a broken matrix [219]. So, it is clear that the aspect ratio is a crucial issue for determining the fracture toughness mechanisms. For particles with larger aspect ratios than for rods like short GFs are much more coherent with fiber pull-out than crack deflection [219]. The size and geometry of the filler highly affect the growth of the process zone in front of the crack tip. The higher aspect ratio (length/diameter ratio) and higher specific surface area (SSA) both together provide a desirable interface for a better stress transfer. CNTs have larger SSA than conventional

fibers. Thus, contribution to the plastic zone deformation is going to be larger when CNTs are used as a reinforcement for epoxy-based NCs [31,51]. Homogeneous dispersion of CNTs is crucial for estimating the pull-out mechanism especially for nano-sized incorporated epoxy because CNTs tend to agglomerate [31].

For the fiber-reinforced polymers, the contribution of the fibers to the process zone in front of the crack tip and a strong interface adhesion enables crack bridging [103,220]. During the crack propagation, the crack jumps from one fiber-matrix interface to another without damaging the fibers [196]. So, because fibers carry out the stress under the load, fiber-bridging improves the fracture toughness of epoxy via reducing the stress at the crack tip and hinder the crack propagation. For the bridging effect of CNTs, it shows the extensibility behavior of CNT. That leads a partial debonding and bridging mechanisms, which is shown in Figure 2.21 (a). Also, a weak interfacial bonding between CNT and matrix, pull-out takes place shown in Figure 2.21 (b). When the pull-out occurs in the composites, there is a large process-zone development, which leads to an enormous matrix deformation [37,220].

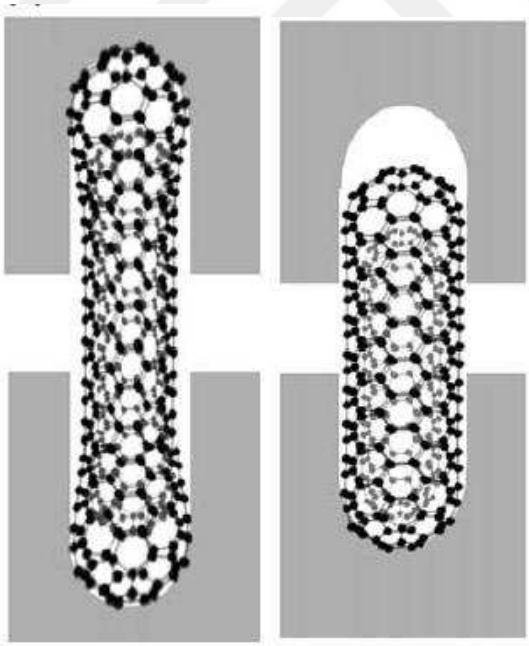

(a) (b)

Figure 2.21 (a) Partial debonding and bridging, and (b) Pull-out due to debonding of CNT reinforced epoxy NCs (Source: Gojny et al., 2005)

2.3. Rheological Properties of Nano-sized Incorporated Polymeric Matrices

The rheological property of epoxy is highly affected by the incorporation of nano-sized fillers. Rheological property plays an important role in the quality of the production and mechanical features of produced NCs and multi-functional FRPCs. Thus, understanding the rheological behavior of epoxy resins with the incorporation of nano-sized filler is crucial for developing the production process and mechanical properties of composites [80]. Incorporation of rigid nano-sized fillers within the epoxy matrix generally results in (1) viscosity build-up, and (2) a shear-thinning (viscosity reduction) according to the aspect ratio and dispersion level of the fillers. Figure 2.22 (a) and (b) illustrates the viscosity behavior depending on the exfoliation level of ZrP nanoplatelets within the epoxy, and the different aspect ratios but the same amount of ZrP nanoplatelets at room temperature, respectively. For the well-dispersed system viscosity build-up and shear-thinning exhibit higher than for poor dispersed system. Also, a high aspect ratio of the nanoplatelet addition within the epoxy exhibits a great increase in viscosity and high shear-thinning behavior [221].

The rheological property of the resins varies with the dispersion level of the filler as well as the interfacial interaction between the filler and the resin. Due to the surface modification, the dispersion level of the fillers improved and exhibit a higher shear-thinning behavior [222–224]. Kim et al. studied the effect of pure, acid oxidized, amine-functionalized, and plasma oxidized MWCNTs on the rheological behavior of epoxy. According to the results, surface treated MWCNT showed stronger shear-thinning behavior and higher shear viscosity than those for pure MWCNT [222]. Abdalla et al. also demonstrated that the fluorinated MWCNT incorporated epoxy exhibit higher viscosity and a more noticeable shear-thinning behavior than neat epoxy and unmodified MWCNT incorporated epoxy [224].

Rigid fillers generally increase the viscosity of the resin, which affects the manufacturing quality for the production of FRPCs [77,225,226]. Especially for the filament winding process, a low viscous resin is required for obtaining a complete wet of the fibers and removing the air bubbles from the resin easily. Appropriate working viscosity is in the range of from 350-1500 cP at room temperature. Extremely viscous resins cause

uneven fiber wetting and winding, excessive stress in the fiber, fiber spray in a resin bath, etc., which will affect the properties of resultant material [226].

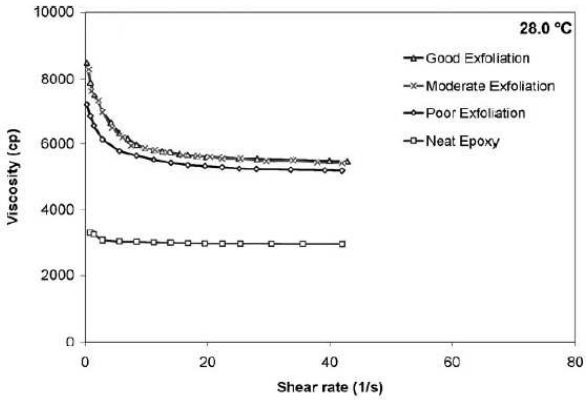

(a)

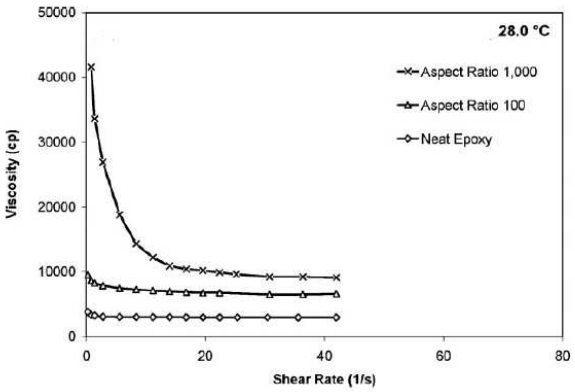

(b)

Figure 2.22 Viscosity behavior with increasing shear rate due to (a) The exfoliation, and (b) Aspect ratio of ZrP nanoplatelets at room temperature (Source: Sun et al., 2009)

2.4. Literature Review on FW CFRPCs

CFRPC pipes and vessels are designed to resist either internal pressures sourced from the fluid transport and storage or external pressures caused by underwater or underground and transportation applications. The main concern is to improve the

performance of CFRPC in case of the internal and external pressure caused by their applications and failure mechanisms depending on their service life. Common failure mechanisms of CFRPCs are; (1) functional failure (leakage, etc.), and (2) structural failure (burst failure, etc.). These failures can be occurred separately or concomitantly depending on the loading type. The critical properties of the CFRPC are burst pressure, and buckling due to the bending, durability, and corrosion [227–229].

Since designing the CFRPC numerical simulation and optimization is essential especially for pressure vessels, several numerical studies are available in the literature. Finite element analysis is commonly used to overcome numerical problems in the design of cylindrical pressure vessels with a complex structure. Thereby, cylindrical composite optimization deals with the improvement of weight, strength, reliability, and life by designing the fiber winding angle, and composite geometry and thickness. An optimum winding angle is defined by expected loading cases, such as; purely uniaxial loading (±75˚), and combined internal pressure and axial loading (±55˚) [230]. For the prediction of the real-time performance burst analysis of CFRPC is a critical issue. For the burst analysis, CFRPC is subjected to varied pressures caused by different liquids such as water, gas, chemicals, etc. Furthermore, there are many studies that CFRPC has been exposed to impact loading for determining the material and structural responses by the delamination and fiber fracture mechanisms.

Onder et. al studied the burst pressure of FW composite pressure vessels with varying fiber orientations under internal pressure and hygrothermal force. The optimum winding angle is obtained as 55^0 for the composite vessels under internal pressure. However, hygrothermal loading did not affect the burst pressure of vessels. Also, results obtained analytical methods were compatible with the experimental results [231]. In another study, Erkal et al. investigated the optimal angle-ply orientation of symmetric cylindrical composites under fatigue loading. The FW cylindrical composites were fabricated from e-glass and epoxy in $[\pm75°]_2$, $[\pm60°]_2$, $[\pm55°]_2$, and $[\pm45°]_2$ orientations. Burst pressures measured experimentally under alternating pure internal pressure and the failure mechanisms were investigated for the cylindrical composites. The optimum winding angle was obtained as $[\pm45^0]_2$ under internal fatigue pressure for cylindrical composites [232].

Demir et. al studied the performance of FW GF/epoxy vessels fabricated from fibers oriented $[+55/-55-/+55/-55]_{2s}$ on burst pressure under varying impact energy levels; 10, 15, 20, 25, and 30 J for empty vessels and 10, 15, 20, and 25 J for water-filled vessels

at 25^0C and 70^0C. As a result of repeated transverse impact load, the burst pressure decreased with increasing impact load and temperature [12].

As mentioned before, in FRPCs, it has been become prominent to increase the toughness of the matrix material due to delaying the progression of the matrix crack and increasing the performance of composites. The most important problem is leakage, which results from the permeation of the fluids (gas or liquid) from the vessel or pipe to the outside by the matrix cracking. For the internal pressure development of FW CFRPCs, split-disk tests are generally performed experimentally [233]. As matrix cracking is a major problem for the pressure vessel and pipe applications and it plays an important role to determine the fracture toughness, Demirci et al. studied the fracture toughness improvement of FW basal fiber-based pipes with the incorporation of nano-sized silica. They studied the hoop tensile stress, strain for notched and un-notched ring specimens, and performed split-disk tests. They came up with an idea and calculate the fracture toughness (Mode I) of 4 wt.% SiO_2 filled and unfilled $\pm[55]_6$ FW basalt fiber composites for the single-edge notched ring specimens. The mechanical properties of the FW composites were enhanced with the incorporation of SiO_2. Ranges of 27.7-30.3% increment monitored for the hoop tensile stress with the incorporation of SiO_2. Mode I fracture toughness was also increased 43-50% for SiO_2 filled basalt fiber-based filament wound composites [215].

Until about 10 years ago, as the primary load was carried by fiber in composite pressure vessels, the burst strength is dominated by fibers, and the matrix resin is neglected. However, because the use of fiber in pressure vessel production is higher than the matrix resin, the cost and the density increase. Therefore, the reduction of process time and the cost can be reduced by reducing the amount of used fiber for the composite pressure vessel production. Accordingly, the optimum design should be used to overcome the required strength of the vessels with a minimum amount of fiber [229]. In some studies, nano-sized fillers were used for the production of composite pressure vessels. Among these studies, the more common one is to use the nano-sized fillers incorporated matrix resin for the production of vessels [227,229], but nano-sized fillers incorporated liners were also used [234].

Thunhorst et al. studied the nano-silica concentration effect on the performance of both the epoxy matrix and their usage of FW CF reinforced composites. The target of the study is to specify the appropriate nano-silica doped resin ranging from 0-33 wt.% for the FW process (first in the hoop direction, then in the helical direction, till liner

overwrapped by fibers). Epoxy resin properties showed an improvement with increasing nano-silica concentration. Further, the burst pressure, the total fiber delivered strength and the fatigue life of the FW type III vessels were also enhanced by the contribution of nano-silica with a balanced weight and cost [229]. Bashar et al. investigated the effect of nano-sized organic and inorganic fillers (silicate clay and tri-block-copolymer) incorporation to the epoxy for the matrix cracking of the FW basalt fiber reinforced pipes with ±60 winding angle. According to the result, moderate improvements were obtained in the leakage failure strain of the composites [201].

CHAPTER 3

THEORETICAL FRAMEWORK

As a result of the extensive literature review, the theoretical framework was created for the thesis study. Based on the aim of this thesis, firstly improvement of the matrix material (Bisphenol-A epoxy) performance was studied experimentally, and then performance-enhanced epoxy was adapted for the production of FW CFRPCs. In light of this, a flowchart was constituted, and shown in Figure 3.1.

The use of functionalized fillers is important as adhesion between the filler and the matrix highly affects the performance of the final composite. In many studies in the literature, the performance of composites has been improved by using covalent functionalized CNT. However, many researchers approved that, the CNT structure is damaged by the covalent functionalization. Therefore, it is aimed to increase the performance of the epoxy matrix and FRPCs without compromising the properties of the CNT by using the non-covalent functionalized CNT that does not damage the CNT structure.

The other substantial issue is the dispersion of the CNT within the epoxy matrix. According to the result of the literature review, the calendaring method, which applies a high shear, is appropriate because it disentangles the CNT bundles with a small distance between the rolls.

For this thesis to achieve its essential purpose, a toughened matrix was used for the production of CFRPCs. Since the filament winding ensures to manufacture of type III composite vessel for hydrogen gas storage, CFRPCs were manufactured by the filament winding process with literature approved winding angle. The effect of the usage of toughened epoxy for the production of CFRPCs on the performance of the materials used for the production of pressure vessel applications was experimentally studied.

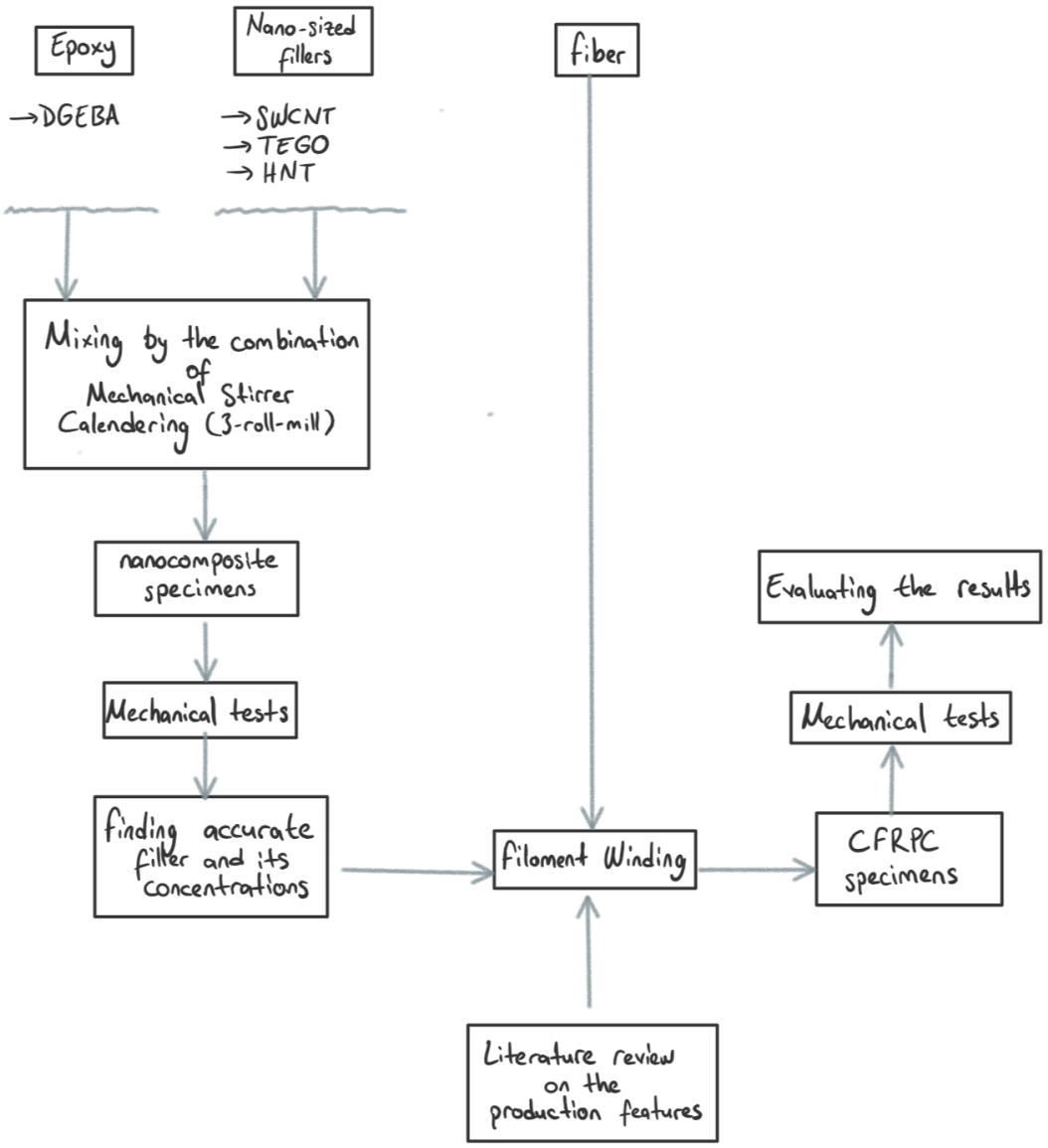

Figure 3.1 Schematic illustration of the thesis flowchart

CHAPTER 4

EXPERIMENTAL METHOD AND INSTRUMENTATION

4.1. Material Preparation

4.1.1. Materials

In this thesis, micro-and nano-sized fillers were utilized to manufacture nano-sized (SWCNT, TEGO, and HNT) incorporated epoxy NCs and FW CFRPCs with SWCNT incorporated epoxy.

For the fabrication of cylindrical composite structures, a continuous fiber was used as an essential reinforcement suitable for the filament winding process. Continuous E-glass fiber (FWR06 1200 tex) with a density of 2.56 g/cm^3 and a 17 μm diameter were supplied from Sisecam Elyaf Sanayii Inc., Turkey. The thermoset epoxy resin Araldite® MY740, and its curing agent Aradur® HY918, and accelerator DY062 were used as a matrix material with the weight ratio of 100:85:1.3, respectively.

Three different nano-sized fillers were used as reinforcements in this study; (1) Chemical Vapor Deposition (CVD) grown SWCNTs, which were non-covalently functionalized with ethoxylated alcohol (TUBALL™ Matrix 301), (2) TEGO and, (3) Silane-treated halloysite.

As-received pure and non-covalently functionalized SWCNT with 2 nm outer mean diameter and >5 μm length was supplied from Pinhas Inc. of Turkey and examined under SEM (Figure 4.1). As-received TEGO, which was obtained through two processes; (1) graphene oxidation and (2) thermal expansion of GO in high quality and at low cost, was received from Nanografen™ Inc, Turkey. Silane-treated halloysite with under 45μm in grain size was obtained from Esan Eczacıbaşı Industrial Raw Materials Co. SEM images of layered as-received TEGO and silane-treated halloysite are shown in Figure

4.2. Technical properties of the fillers obtained from datasheets were summarized in Table 4.1.

(a)

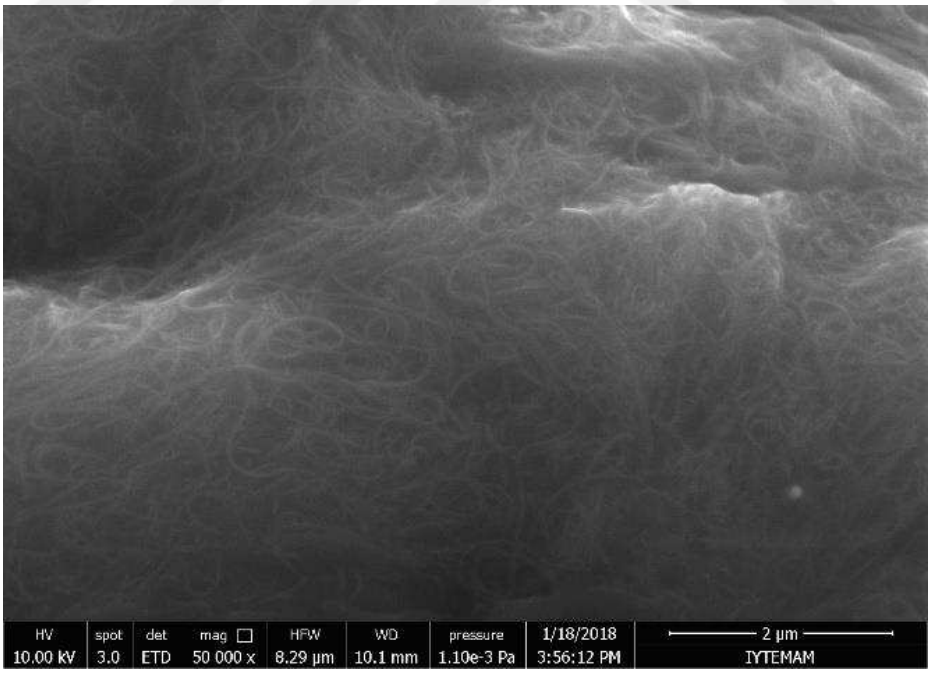

(b)

Figure 4.1 SEM images of as-received (a) Pure SWCNT, and (b) Functionalized SWCNT

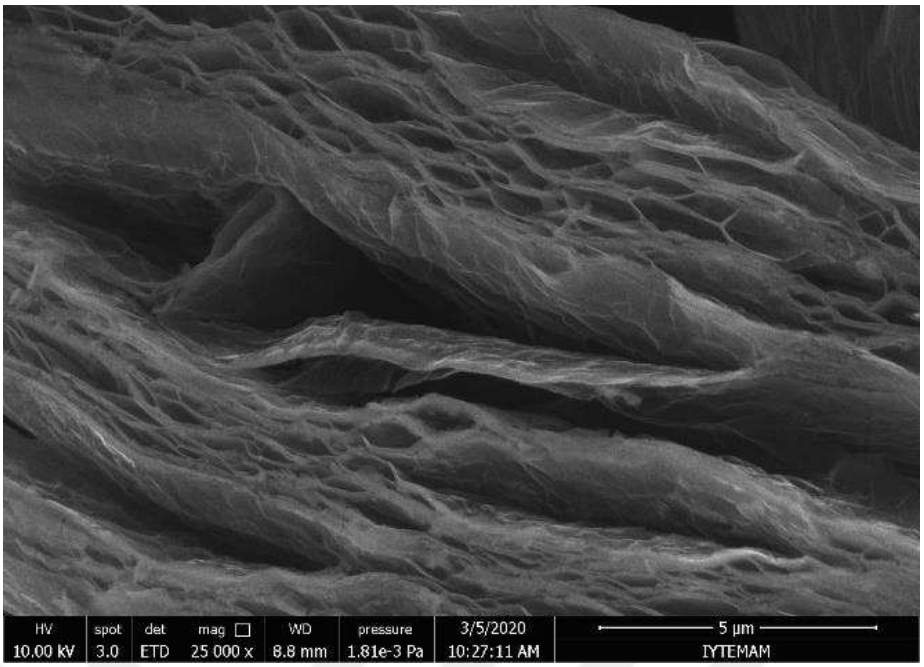

(a)

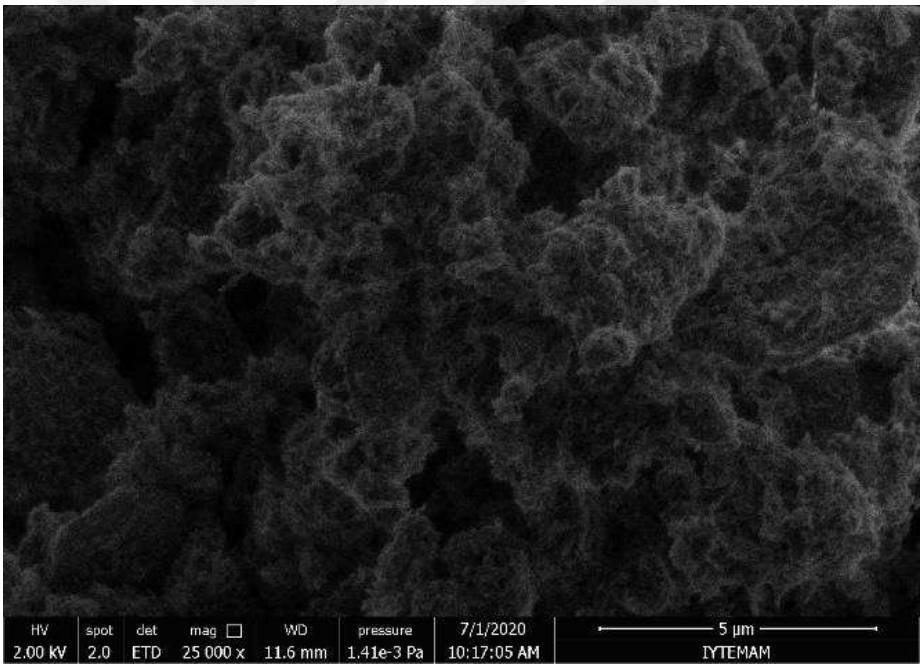

(b)

Figure 4.2 SEM images of as-received (a) TEGO, and (b) Silane-treated halloysite

Table 4.1 Technical properties of used micro-and nano-sized fillers

Filler	Length (μm)	Diameter (nm)	Density (g/ml)
HNT	1.2	d_{outer} = 40 d_{inner} = 20	2.1-2.6
TEGO			1.188
SWCNT	>5	d_{outer} = 2	0.97
GF		$17x10^3$ (filament diameter)	2.56

4.1.2. Synthesis of NCs

Nano-sized filler incorporated epoxy was prepared by the calendaring method at different nano-sized fillers with various concentrations to be used to produce the NCs and GF-based CFRPCs.

For the production of NCs, nano-sized filler types, and their concentrations in percentage by weight were listed in Table 4.2. Abbreviations of the NCs were constituted as followed by the contents of nano-sized fillers (x), nano-sized filler type, and matrix, respectively.

Table 4.2 Abbreviations of NCs according to the types of nano-sized fillers and their concentrations

Abbreviations of NCs	**Nano-sized fillers**	**(x) Contents of Fillers (wt.%)**
xSWCNT/epoxy	SWCNT(Matrix301)	0.0125, 0.025, 0.05, 0.1, 0.3, 0.5
xTEGO/epoxy	TEGO	0.025, 0.05, 0.1
xHNT/epoxy	HNT (Z-6040 silane)	0.5

As it can be seen in Figure 4.3, nano-sized filler reinforced epoxy NCs were fabricated in five main steps;

- 1st step; neat and nano-sized fillers incorporated epoxy was mixed by a mechanical stirrer at 1000 rpm,

- 2nd step; the mixtures were exposed to the high shear with a three-roll-mill (Exakt™ 80 E calendar equipment) with the 5µm gap size and different milling speeds for six stages, and the mixtures were collected immediately after every mixing stage (see in Table 4.3).
- 3rd step; neat and nano-sized filler incorporated epoxy blends were blended with the hardener (HY918) and accelerator (DY062).
- 4th step; the final suspensions were degassed in a vacuum oven at 80 mbar for half an hour to remove the air bubbles from the mixture.
- 5th step; the prepared mixtures were cast in silicone molds, and neat epoxy and NCs were cured at 80^{0}C for 2 hours and followed with a post-curing at 120^{0}C for 2 hours within a controlled oven.

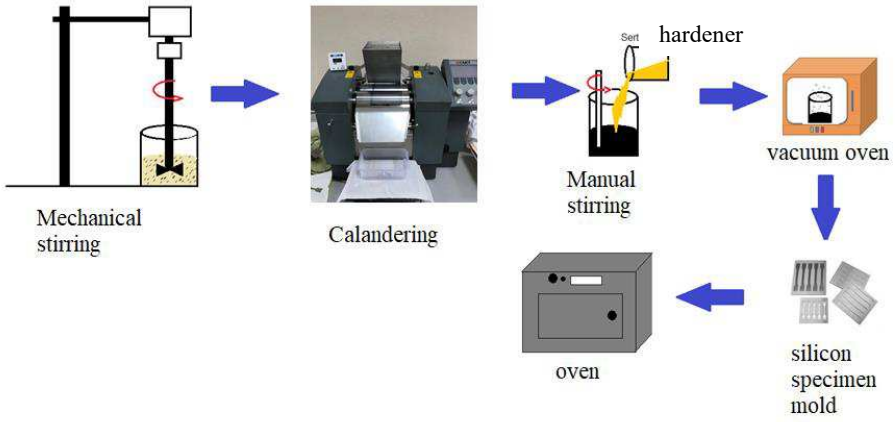

Figure 4.3 The schematization of NC preparation

Table 4.3 Mixing stages for the preparation of epoxy mixtures at 5 µm gap sized and variable mill speeds

Mixing stage	Gap size (µm)	Mill speed (rpm)
1st	5	180
2nd	5	200
3rd	5	220
4th	5	240
5th	5	260
6th	5	280

4.1.3. Fabrication of CFRPCs

Neat and SWCNT (0.05 and 0.1 wt.%) incorporated epoxy blends from the 3rd step of the production process of NCs were used for manufacturing the reference and SWCNT incorporated GF-based CFRPCs by filament winding method, which is conducted with CADWIND CAM[99] software. Two different CFRPCs with an inner diameter of 60 and 275mm were prepared with $[\pm 55^0]_n$ fiber direction. The layer number of composites was n=4 and n=2 for cylindrical composites with an inner diameter of 60 and 275 mm, respectively. While the filament winding process for CFRPCs with an inner diameter of 60 and 275mm as illustrated in Figure 4.4, Figure 4.5 shows the fiber direction during the filament winding. CFRPCs with an inner diameter of 60 and 275mm were manufactured for the reason of performing the split-disk tests, and double cantilever beam test (DCB), respectively. A non-adhesive release layer with a thickness of 19 µm was inserted between the 1st and 2nd laminates during the filament winding process to create an initiated crack along the interlaminar region of the DCB test specimens in the longitudinal and transverse directions.

With the purpose of the trial, only the outer layer/s of CFRPCs wound with SWCNT reinforced epoxy. Specimen abbreviations were constituted as followed by GF, SWCNT incorporation with percent content by weight in the matrix, and matrix material, respectively. The cured reinforced resin was burn-off to weigh both resin and fiber following ASTM D2584-94 standard [235]. A burn-off test was carried out for at least 3 specimens for each composite. Weight percentages were calculated according to the equation (4.1). The calculated fiber weight and abbreviation of FW GF-based specimens according to their inner diameter and SWCNT content are given in Table 4.4.

$$W_f = \frac{M_f}{M_c} \times 100 \tag{4.1}$$

Where; W_f fiber weight percentage, M_c and M_f mass of the composite and the fiber, respectively.

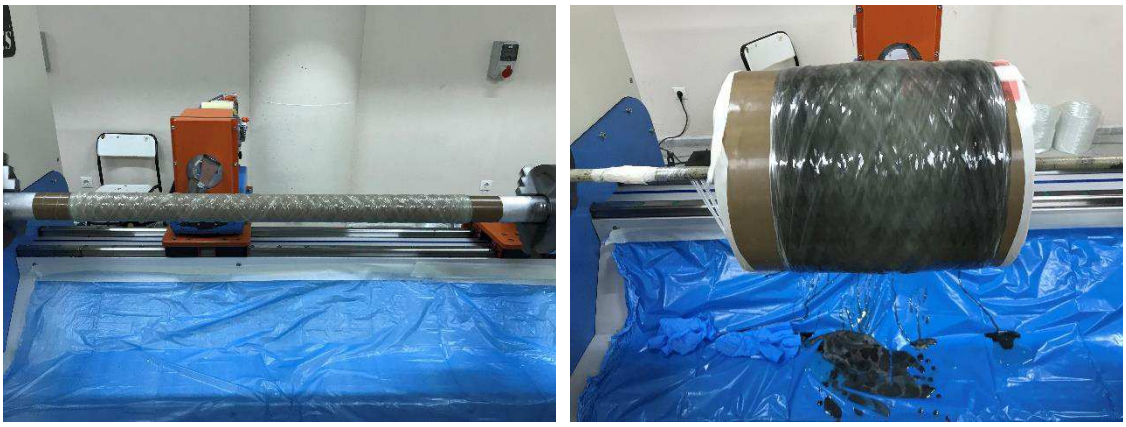

(a) (b)

Figure 4.4 Filament winding process of GF-based CFRPCs with an inner diameter of (a) 60 mm and (b) 275 mm

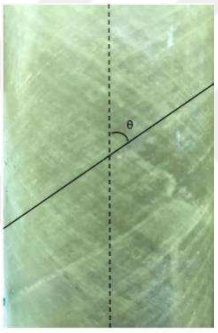

$\Theta=\pm55^0$

Figure 4.5 The fiber angle of FW GF-based CFRPCs

Table 4.4 Abbreviation of the specimens, SWCNT contents, and W_f of the cylindrical composites according to their inner diameter.

Specimen abbreviation	**SWCNT content (wt.%)**	**Fiber weight percentage (W_f)**	
		d_{inner}=60mm	d_{inner}=275mm
GF/epoxy	0	0.38	0.53
GF/005SWCNT/epoxy	0.05	0.47	0.54
GF /01SWCNT/epoxy	0.1	0.37	0.55

4.2. Instrumentation and Testing

4.2.1. Mechanical Characterisation of Composites

To determine the impact of nano-sized fillers on the mechanical and thermomechanical properties of epoxy and GF-based CFRPCs, a series of mechanical tests, such as tensile, single-edge notch bending (SENB) and three-point bending tests for NCs, and split-disk, double cantilever beam (DCB) and three-point bending tests for CFRPCs were performed. All tests were performed for at least five specimens per each batch following the relevant ASTM standards at room temperature and ambient conditions.

4.2.1.1 Tensile and Spilt-Disk Testsing

The tensile tests were carried out for test specimens at a constant crosshead speed of 2.0 mm/min up to failure by 100kN Shimadzu AG-IC tester, which is shown in Figure 4.6 (a). The axial strain and tensile modulus values of the specimens were measured by a video extensometer during the tensile test. The dog-bone shaped test specimens were prepared following ASTM-D638 standard [236]. According to the tensile test results tensile strength and modulus of the reference and nano-sized filler incorporated epoxy NCs were calculated.

The split-disk test method was performed for test specimens at ambient conditions by using a universal tensile testing machine (100kN Shimadzu AG-IC tester). The split-disk test for GF/epoxy, GF/005SWCNT/epoxy, and GF/01SWCNT/epoxy rings with an inner diameter of 60 mm is shown in Figure 4.6 (b). Each test specimen was loaded with a constant crosshead speed of 5 mm/min. Notched and unnotched $[\pm 55^0]_4$ composite ring specimens were tested under the split-disk test method. Apparent hoop tensile strength for unnotched ring specimens and fracture toughness (Mode-I) for notched ring specimens were calculated according to ASTM D2290-0ϵ1 and ASTM E399, respectively

[237,238]. Pipes were drilled in a group with a 4 axis CNC machine, then ring specimens were cut from the group with a diamond saw. The dimensions of the cut ring test samples are shown in Figure 4.7 (a). To generate notched ring specimens, the notches were opened with a rotating diamond saw from the drilled side of the ring specimens, and the notched length is shown in Figure 4.7 (b).

(a) (b)

Figure 4.6 Images of (a) The tensile and (b) Split-disk tests

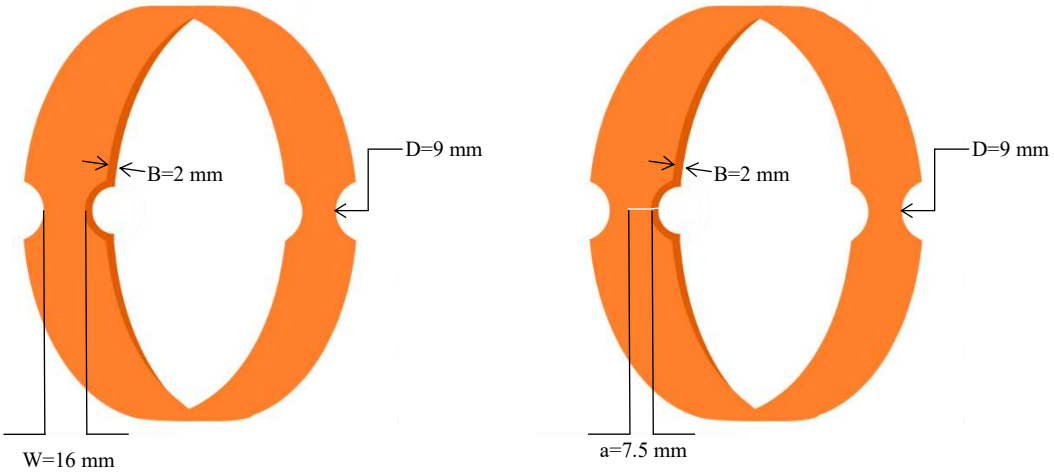

(a) (b)

Figure 4.7 Schematic illustration of the ring specimens for (a) Unnotched and (b) Notched split-disk tests

Apparent Hoop tensile strength was calculated for each batch of at least five specimens from the formula given below;

$$\sigma_a = {}^{P_b}/_{2(BW)} \tag{4.2}$$

Where; σ_a is the ultimate tensile strength in MPa, P_b is the maximum load in N, W is the width in mm, and B is the thickness in mm.

4.2.1.2 SENB Test

For measuring the Mode I fracture toughness of NCs, the SENB test was carried out for each specimen by a 5kN Shimadzu AGS-X tester. The test specimens were produced according to ASTM-D 5045 standard [239]. A 3 mm notch was opened via a rotating diamond saw and then a 1.5 mm pre-crack was generated with a razor blade to generate a very sharp pre-crack and prevent residual stress around the crack tip. The equations shown below were used for calculating the toughness parameters.

$$K_Q = \left(\frac{P_Q}{BW^{\frac{1}{2}}}\right) f({}^{a}/_{W}) \tag{4.3}$$

$$f(a \Big/ W) = \frac{2+{}^{a}/_{W}}{\left(1-{}^{a}/_{W}\right)^{1.5}} \begin{bmatrix} 0.886 + 4.64\left(\frac{a}{W}\right) - \\ 13.32\left(\frac{a}{W}\right)^2 + 14.72\left(\frac{a}{W}\right)^3 - \\ 56\left(\frac{a}{W}\right)^4 \end{bmatrix} \tag{4.4}$$

In Equations 4.3 and 4.4; K_Q is the fracture toughness in MPa.m$^{1/2}$, P_Q is the load in kN, B is the thickness of the specimen in mm, w is the width of the specimen in mm, and a is the crack length in mm.

4.2.1.3 Three-point Bending Tests

Three-point bending tests were performed for the calculation of the flexural properties and interlaminar shear strength (ILSS) of the composites. The flexural

properties of the neat epoxy and xTEGO/epoxy nanocomposites, and reference GF/epoxy, GF/005SWCNT/epoxy, and GF/01SWCNT/epoxy composites cut from the pipe with an inner diameter of 60 and 275 mm were studied. Figure 4.8 illustrates the flexural test of xTEGO/epoxy and GF/xSWCNT/epoxy composites, and the short beam shear (SBS) test of GF/xSWCNT/epoxy composites. A support span-to-depth ratio for all composites were 32:1. The rate of crosshead motion was calculated according to ASTM D 790-03 [240]. The SBS test was performed for ILSS behavior of GF/epoxy, GF/005SWCNT/epoxy, and GF/01SWCNT/epoxy composites cut from the pipe with an inner diameter of 60 and 275 mm. SBS test specimens were prepared in an accordance with ASTM D 2344 [241]. Three-point bending tests were accomplished by a 5kN Shimadzu AGS-X tester for each specimen. Flexural strength (σ_f) and modulus ($\in_f$) were calculated with the equations (4.5) and (4.6) given below;

$$\sigma_f = {}^{3PL}/_{2bd^2} \tag{4.5}$$

$$\in_f = {}^{6Dd}/_{L^2} \tag{4.6}$$

Where; P is the applied load (N), L is the support span length (mm), b is the width (mm), d is the thickness (mm), and D is the deflection (mm).

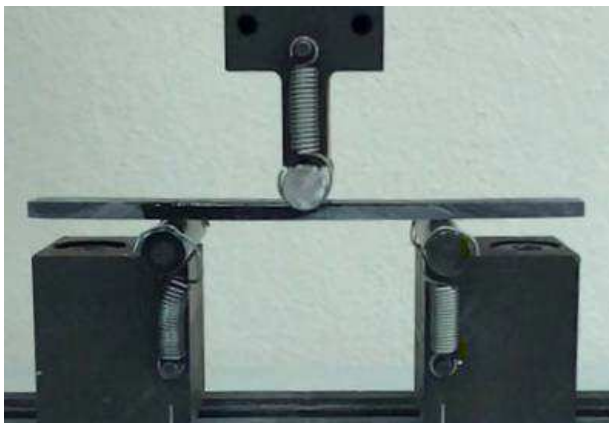

(a)

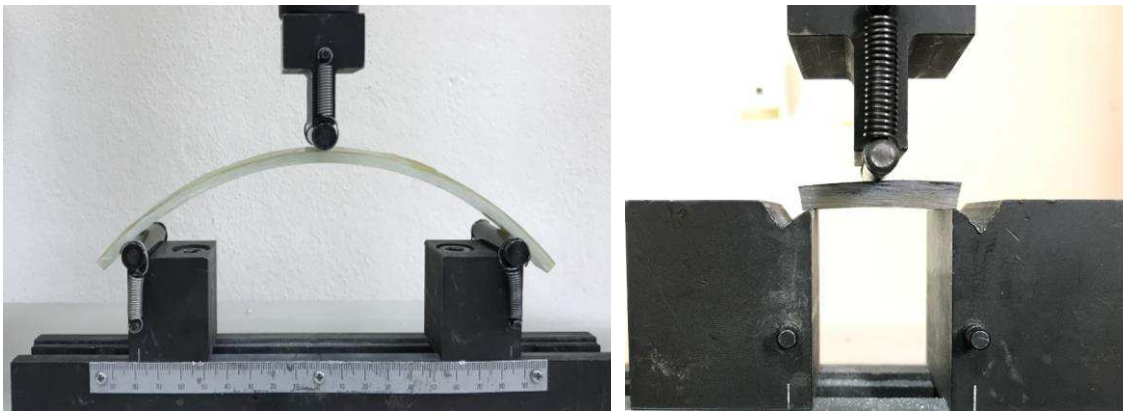

(b) (c)

Figure 4.8 Images of the flexural test of (a) xTEGO/epoxy and (b) GF/xSWCNT/epoxy composites, and (c) the SBS test of GF/xSWCNT/epoxy composites

The short beam strength (F^{sbs}) for reference GF/epoxy and GF/xSWCNT/epoxy pipes with an inner diameter of 60 and 275mm was calculated according to the equation below;

$$F^{sbs} = 0.75 \times \frac{P_m}{b \times h} \tag{4.7}$$

Where P_m is the maximum load (N), b is the width (mm), and h is the thickness (mm).

4.2.1.4 Mode-I Interlaminar Fracture Toughness Test

The Mode I interlaminar fracture toughness (G_{Ic}) of the GF-based CFRPCs with an inner diameter of 275 mm was carried out by a double cantilever beam (DCB) test. Test specimens were cut from the pipe with an inner diameter of 275 mm via a diamond saw from both transverse and longitudinal directions, which are shown in Figure 4.9 (a). The dimensions of the longitudinal and transverse DCB specimens are shown in Figure 4.9 (b) and (c), respectively. All specimens were $L = 150$ mm in length, $b = 30$ mm in

width, and $h = 5$ mm in thickness. Also, the crack length of the specimens was $a_0 = 60$ mm. The aluminum loading blocks were bonded to sanded outer surfaces of the specimens -where the initial crack starts- with a polyurethane-based adhesive (Denlaks Pu 99). Curing of the epoxy-based adhesive was accomplished for 24 hours at room temperature and followed with a post-curing at 60^0C in an oven for 2 hours. Before testing, the edges of the samples were painted with a white dye after the initial crack and marked with 1 mm intervals to record the progress of the crack. DCB tests were performed by 5kN Shimadzu AGS-X tester for at least 5 specimens for each batch, according to ASTM D5528-01 standard [242]. The crosshead speed was 2 mm/min. After allowing 5 mm crack formation, specimens were unloaded. Then, the specimens were loaded until the crack propagation was completed. The Mode-I critical energy release rate (G_I) can be determined experimentally by (1) modified beam theory (MBT), (2) compliance calibration (CC), and (3) modified compliance calibration (MCC). Among these three reduction methods to calculate interlaminar fracture toughness, MBT is recommended due to its conservative values. Consequently, for this study the energy release rate (G_I) of DCB test specimens was calculated from the MBT data reduction method given as follows;

$$G_I = \frac{F}{N}\frac{3P\delta}{2b(a+|\Delta|)} \tag{4.8}$$

Where P is the applied load, δ is the load point displacement, b is the specimen width, a is the delamination length, and Δ is a value that can be determined experimentally by generating a least-squares plot of the cube root of the compliance ($C^{1/3}$) as a function of delamination length. Compliance (C) is a ratio of the load point displacement to the applied load (δ/P). F and N are the correction parameters according to the large displacement and end block corrections. These correction parameters were calculated with the equations (4.9) and (4.10) as follows;

$$F = 1 - \left(\frac{3}{10}\right)\left(\frac{\delta}{a}\right)^2 - \left(\frac{3}{2}\right)\left(\frac{\delta t}{a^2}\right) \tag{4.9}$$

$$N = 1 - \left(\frac{L'}{a}\right)^3 - \left(\frac{9}{8}\right)\left[1 - \left(\frac{L'}{a}\right)^2\right]\left(\frac{\delta t}{a^2}\right) - \frac{9}{35}\left(\frac{\delta}{a}\right)^2 \tag{4.10}$$

Where t, L', and $h/4$ were shown in Figure 4.10. Mode I interlaminar fracture toughness (G_{Ic}) was calculated and the R-curve was drowned as a function to characterize the initiation and prorogation of delamination. At the first stage of the DCB loading, samples were loaded till 5mm delamination length was read on the samples and the G_{Ic} initiation ($G_{Ic,ini}$) was calculated for the first created crack. After that, the sample is unloaded, and it followed by DCB loading again. The G_{Ic} propagation ($G_{Ic,prop}$) was calculated for the first created crack at this stage. Also, the maximum G_{Ic} ($G_{Ic,max}$) value was taken as the maximum G_{Ic} value of the samples.

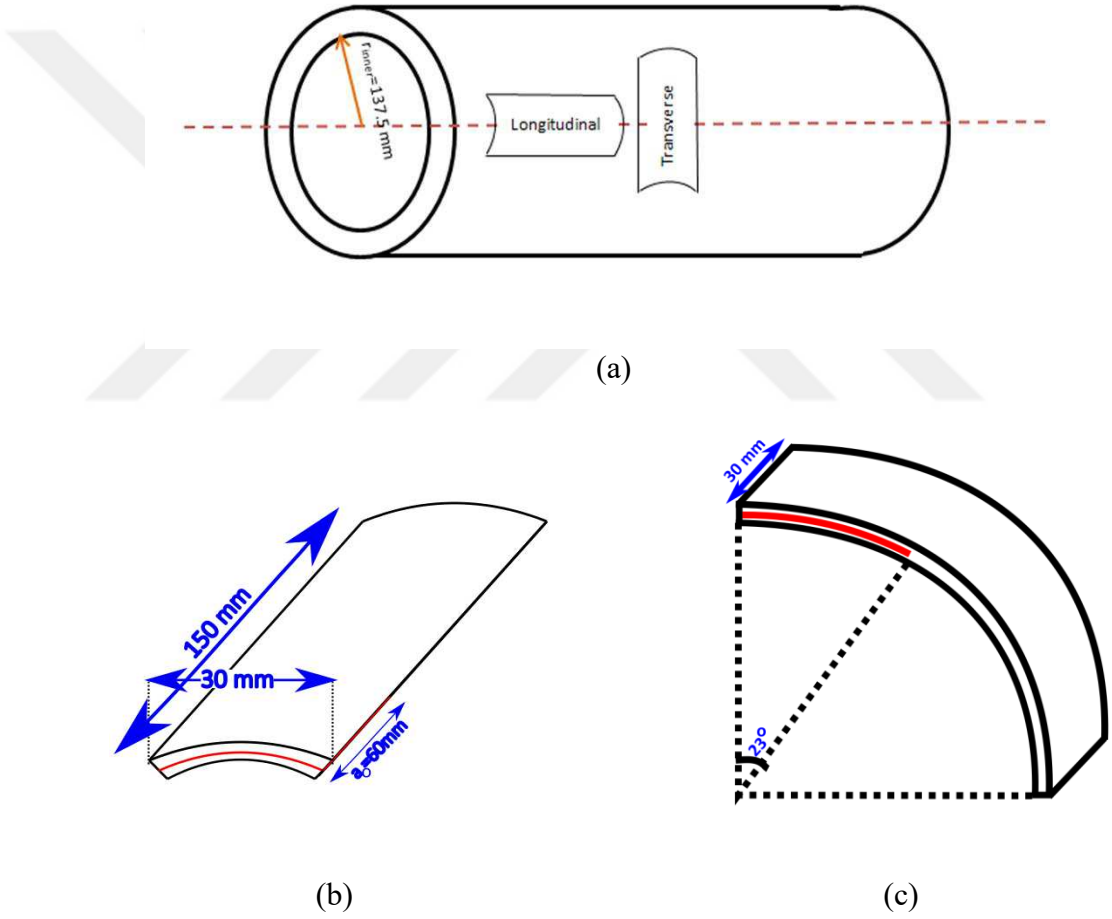

(a)

(b) (c)

Figure 4.9 Schematically illustrations of (a) Cylindrical composite with an inner diameter of 275 mm, (b) Longitudinal DCB test specimen with a fiber direction of $[\pm 55^0]_2$ and (c) Transverse DCB test specimen with a fiber direction of $[35^0]_2$

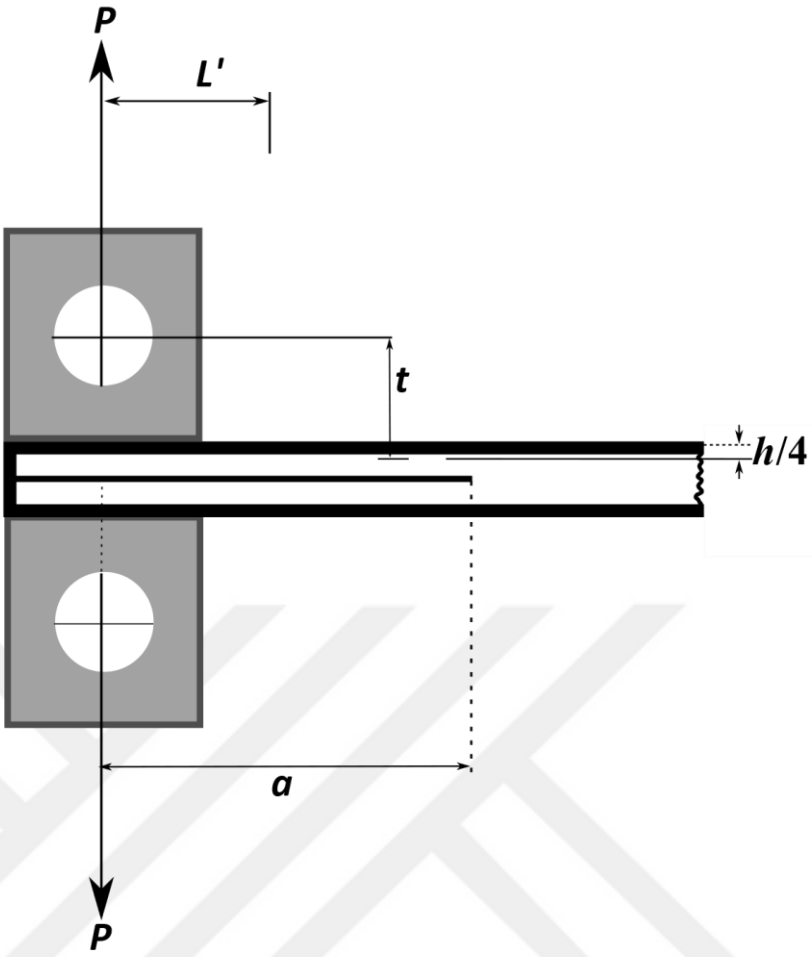

Figure 4.10 Schematic representation of DCB test specimen

4.2.2. Scanning Electron Microscopy (SEM) Analysis and Thermomechanical Tests

Scanning electron microscopy (SEM) images were taken for fractured surfaces of the composites to determine the failure modes and evaluate the delamination and toughening mechanisms. The specimens were coated with a thin gold layer using a sputter-coating for 90 seconds and examined under a Quanta 250FEG SEM at various magnifications.

The dynamic mechanical analysis (DMA) of the composites was carried out for composites using TA™ Q800 equipment in dual cantilever mode. At least three test specimens were produced and tested according to the ASTM D4065-01 standard [243].

During the DMA test, a dynamic force was applied to the specimens at a frequency of 1 Hz in a three-point bending mode. The temperature range was 20^0C to 250^0C, with a ramp of 3^0C/min. The accurate glass transition temperature (T_g) of composites was taken as the temperature at the maximum peak of the tanδ vs temperature curve. DMA specimens for GF-based composites were cut from pipes with an inner diameter of 275 mm. Test specimens were cut with a diamond saw from both transverse and longitudinal directions (Figure 4.11).

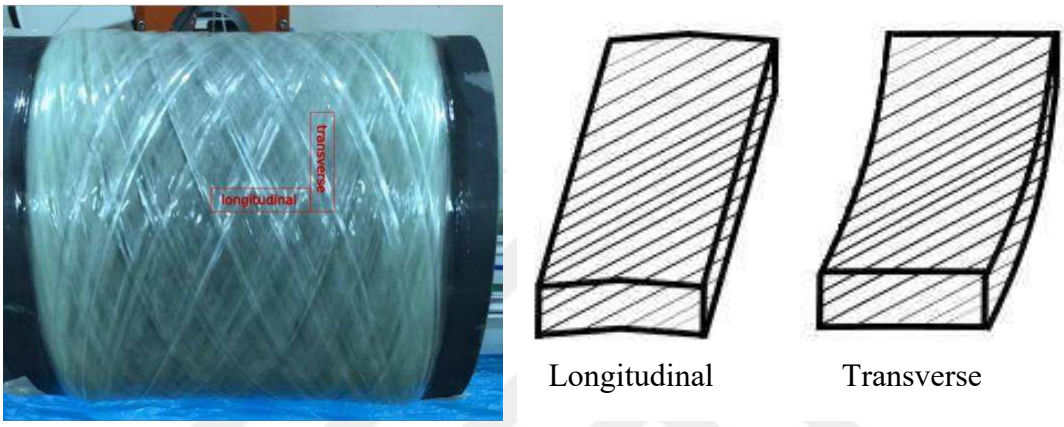

Figure 4.11 The transverse and longitudinal specimens (a) illustrated on the cylindrical composite and (b) curvature illustrations of the samples for DMA samples.

4.2.3. Rheological Characterizations and Contact Angle Measurements

The rheological behaviors of reference and SWCNT incorporated epoxy suspensions prepared as described in the title of 4.1.2 were measured by an oscillatory rheometer (TA Instruments^{TM}) with a 25 mm parallel plate geometry and 0.5 mm sample gap. The oscillating experiments were performed at 25^0C for reference and SWCNT (0.0125, 0.025, 0.05, 0.1, 0.3 and 0.5 wt.%) incorporated suspensions. Pre-shear was implemented at 1 s^{-1} for 30 seconds. Three repeats were carried out for each sample of measurements at varying shear rates, which are between 0.005 and 1000 s^{-1}. Also, the rheological properties of reference and SWCNT (0.05 and 0.1 wt.%) incorporated

suspensions at temperatures between 25-120^{0}C were measured while a constant shear rate (100 s^{-1}) was applied for at least three repeats of all suspensions.

An optic tensiometer (Biolin Scientific Attension Theta) was used to measure the contact angle values according to the pendant drop method. The wettability behavior of fiber depending on SWCNT incorporation within the epoxy was determined. Reference and SWCNT (0.1 wt.%) incorporated suspensions prepared as described in the title of 4.1.2 were dropped on GF by a micropipette with a 5 μm in volume, and the volumetric change in the drop was monitored for 200 seconds. The measurements were carried out at least three times for all suspensions.

CHAPTER 5

RESULTS AND DISCUSSION

5.1. Effects of Nano-Sized Fillers on the Tensile Properties of Epoxy

Tensile properties of dog-bone test specimens subjected to unidirectional force were examined with the load-displacement curves obtained from the computer, which were converted to the stress-strain curves. Corresponding with the stress-strain curves and fracture behavior of the NCs the certain material properties and morphology of the samples were determined and discussed.

Figure 5.1, Figure 5.4, and Figure 5.7 show the stress-strain curves of SWCNT, TEGO, and HNT incorporated epoxy NCs, respectively. With an overview of the stress-strain curves, while neat epoxy showed brittleness, the incorporation of stiff nanofillers (SWCNT and HNT) improved the strength of the epoxy. However, since TEGO incorporated epoxy nanocomposites failed before the neat epoxy composites, the incorporation of TEGO decreased the strength of the epoxy. The morphological structure of the NCs after the tensile test was examined with the SEM, and shown in Figure 5.2, Figure 5.3, Figure 5.5, Figure 5.6, and Figure 5.8. Based on the tensile test results, toughness (area under the stress-strain curve), elastic modulus, ultimate tensile strength (UTS), and strain at failure values were also calculated from the results obtained from the stress-strain curves and these results were given in Table 5.1 with the abbreviations of NCs.

Figure 5.1 shows the stress-strain curves of neat and SWCNT incorporated epoxy NCs. The tensile test results revealed that epoxy-based NCs exhibit higher strain at failure, strength, and toughness values due to the incorporation of SWCNT at low concentrations (0.0125, 0.025, and 0.05 wt.%). 0.0125, 0.025, and 0.05 wt.% SWCNT incorporated epoxy NCs have large deformation before failure when compared to the neat epoxy, which showed a brittle fracture behavior. Young's modulus was effectively enhanced with the incorporation of SWCNT. On the other hand, the strength was

increased from 76.14±2.55 MPa to a maximum value of 87.39±5.34 MPa with the incorporation of 0.025 wt.% SWCNT, which corresponds to a 15% increase. The incorporation of the stiff nano-sized filler at high concentrations reduced the strain at failure because the epoxy became more rigid. However, strain at failure increased from 0.029±0.002 mm/mm to 0.063±0.006 mm/mm, and 0.047±0.014 mm/mm with the incorporation of SWCNT at 0.0125, and 0.025 wt.%, respectively. It was also observed that the calculated toughness values from the area under the stress-strain curves increased maximum by about 211% for 00125SWCNT/epoxy and decreased for NCs with high concentrations of SWCNT (above 0.05 wt.%). NCs containing SWCNT at low concentrations (0.0125, 0.025, and 0.05 wt.%) absorb great energy before the failure. This relates to how tough the NC is.

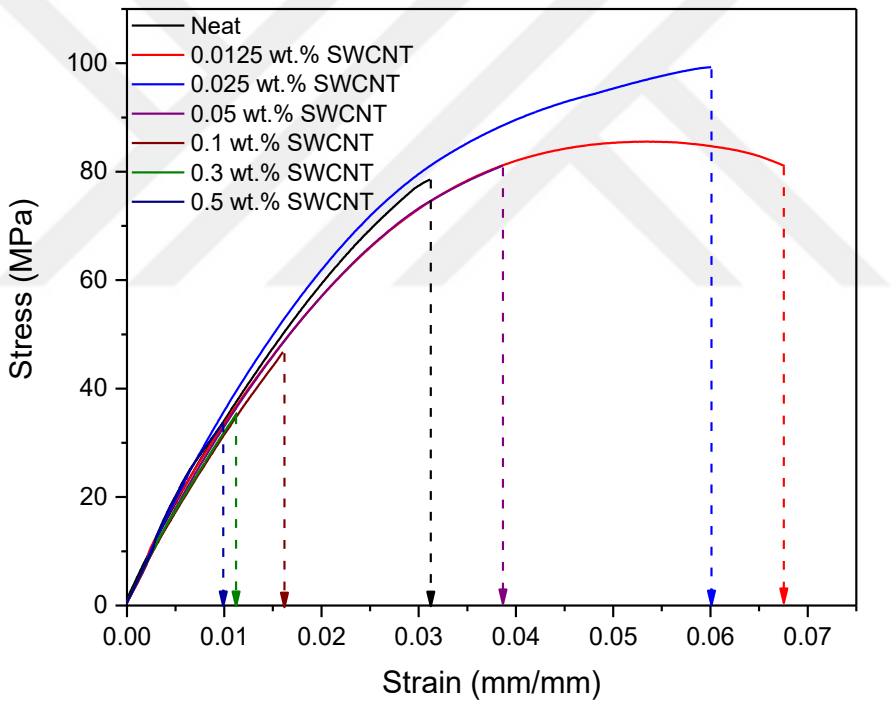

Figure 5.1 The stress-strain curve of neat and SWCNT incorporated epoxy nanocomposites

The improvement of the tensile test properties obtained through this study is more significant compared to those reported in the literature [31,52,68,136]. In summary, while the incorporation of SWCNT at low concentrations increased the ductility of the epoxy, it also significantly improved the tensile properties. This translates to the better dispersion enhanced by the incorporation of SWCNT at low concentrations within the epoxy resin

together with better interfacial interaction between the matrix and SWCNT and consequently resulted in a good load transfer from the matrix to the nano-sized filler. But tensile properties decreased at high concentrations of SWCNT (above 0.05 wt.%), due to the agglomeration tendency of CNTs. The CNT clusters also can cause microscopic defects (voids, microcracks, etc.) and promote the formation of micro-cracks during tensile loading.

SEM images of the fractured surfaces of the neat epoxy and SWCNT incorporated epoxy NCs after the tensile test are shown in Figure 5.2. The neat epoxy showed a relatively smooth fracture surface, which indicated a typical brittle fracture behavior with no clear plastic deformation (Figure 5.2 (a)). The roughness of fractured surfaces was increased with the incorporation of stiff SWCNT, especially for NCs containing SWCNT at low content (0.0125 and 0.025 wt.% SWCNT) (Figure 5.2 (b) and (c)). The roughness resulted in a delay of the crack propagation encountering the SWNCTs, which enhance the toughness of the epoxy by debonding mechanisms. However, surface roughness decreased for 01SWCNT/epoxy, 0.3 SWCNT/epoxy, and 0.5 SWCNT/epoxy NCs and the content of micro-voids (about 0.5 μm in size) also increased at the same time (Figure 5.2 (e), (f) and (g)). This is due to the difficulty in getting rid of the bubbles during degassing depending on the high viscosity of the suspension.

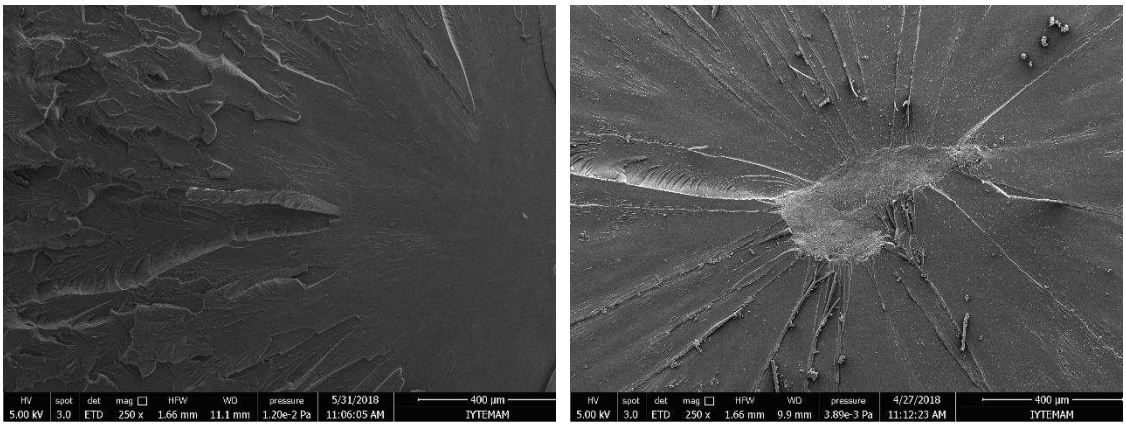

(a) (b)

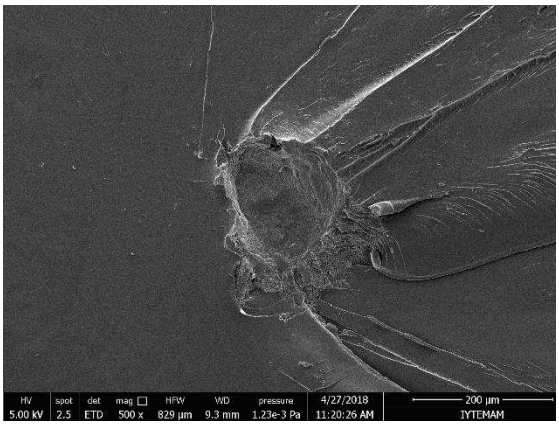

(c)

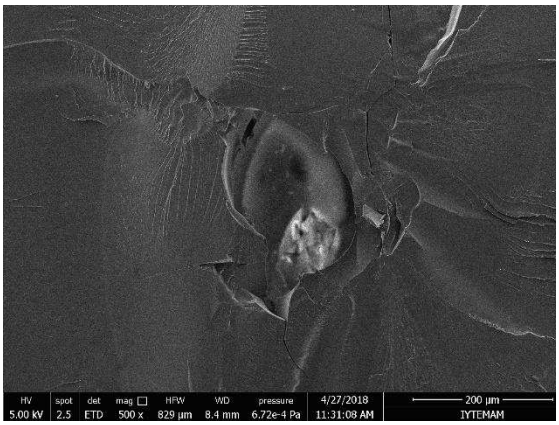

(d)

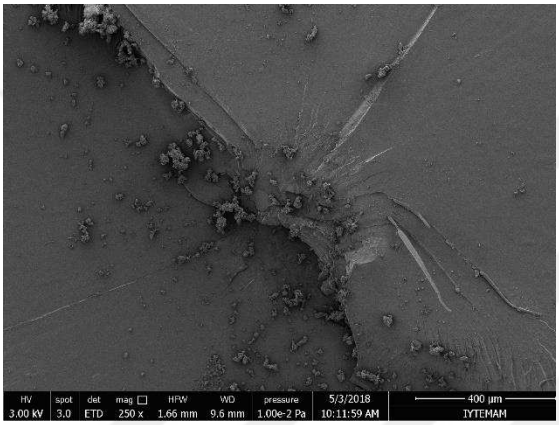

(e)

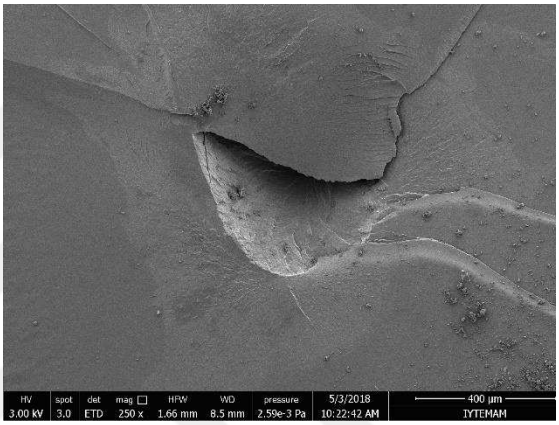

(f)

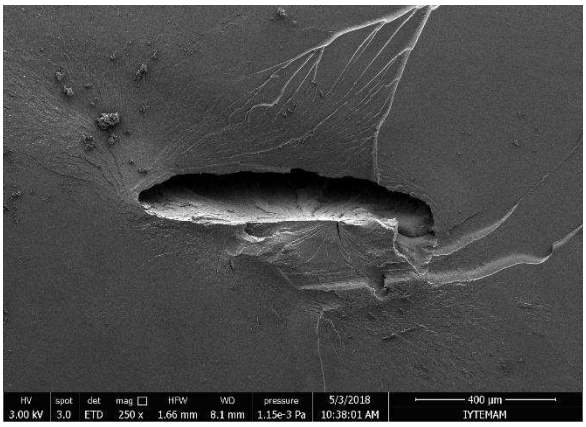

(g)

Figure 5.2 SEM images of the fractured surface of (a) Neat epoxy, (b) 00125SWCNT/epoxy, (c) 0025SWCNT/epoxy, (d) 005SWCNT/epoxy, (e) 01SWCNT/epoxy, (f) 03SWCNT/epoxy, and (g) 05SWCNT/epoxy NCs after the tensile test

SWCNT-rich regions on the fractured surfaced were examined under SEM at higher magnifications. Figure 5.3 shows the SEM images of the fractured surface of 0025SWCNT/epoxy nanocomposite, which showed a higher tensile property among the other SWCNT reinforced epoxy NCs at 25000x and 100000x magnifications after the tensile test. The distribution of SWCNT within the epoxy seems quite homogeneous in Figure 5.3 (a). Figure 5.3 (b) and (c) focused on the fiber-bridging mechanism, which delays the crack propagation during the tensile test. The roughness of the fractured surfaces observed in the SEM images resulted in a delay of the crack propagation encountering with SWCNTs. Improvement of the roughness and plastic deformation of NC can be defined by the "fiber-bridging" mechanism is seen that reveals a strong

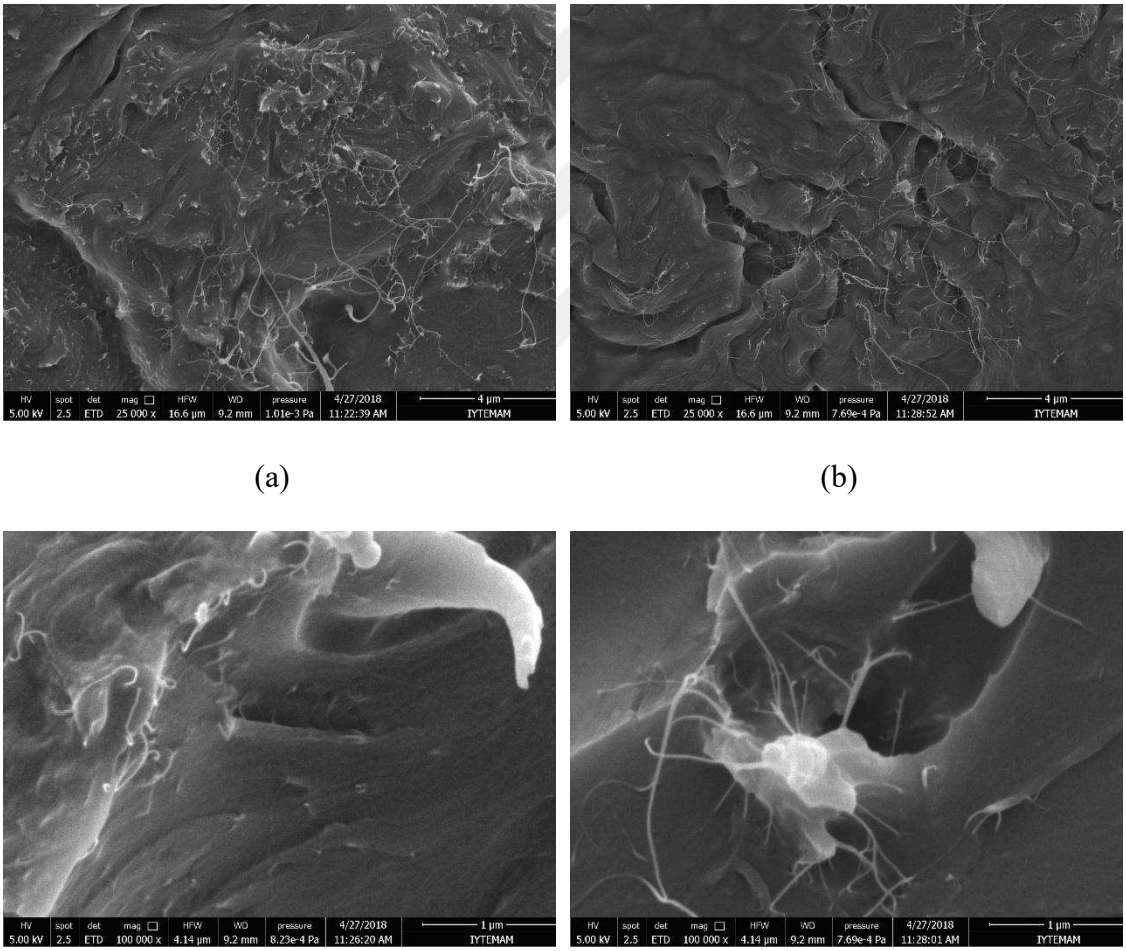

(a) (b)

(c) (d)

Figure 5.3 SEM images of the fractured surface of 0025SWCNT/epoxy NC at (a), and (b) 25000x and (c), and (d) 100000x magnifications after the tensile test

interfacial interaction between SWCNT and epoxy [108]. Also, Figure 5.3 (d) shows the small agglomerates and SWCNT pulled-out from the epoxy during the crack propagation. However, the agglomerates are below the micrometers in the size.

Based on the tensile test of results shown in Figure 5.4, the tensile strength, and strain at failure values were decreased; however, the modulus of elasticity values was slightly increased due to the incorporation of TEGO. The improvement of the modulus is shown as the slope of the stress-strain curve in the upper left corner of Figure 5.4. The Young's modulus of NCs at low contents of TEGO (0.05 and 0.1 wt.%) was not significantly changed when compared to the neat epoxy system (Table 5.1). However, while Young's modulus showed a prominent increase for 015TEGO/epoxy NCs, the improvement was diminished for 03TEGO/epoxy nanocomposites. For 015TEGO/epoxy NCs, the average elastic modulus improved by about 15 %. According to the SEM images of as-received TEGO, TEGO has a wrinkled structure, which induces the extension and rotation of the graphene sheets along the applied tensile direction. As a result of this, graphene limited the tensile modulus improvement [61]. Tensile strength showed a decline with the incorporation of TEGO within the epoxy, which is typical behavior for graphene

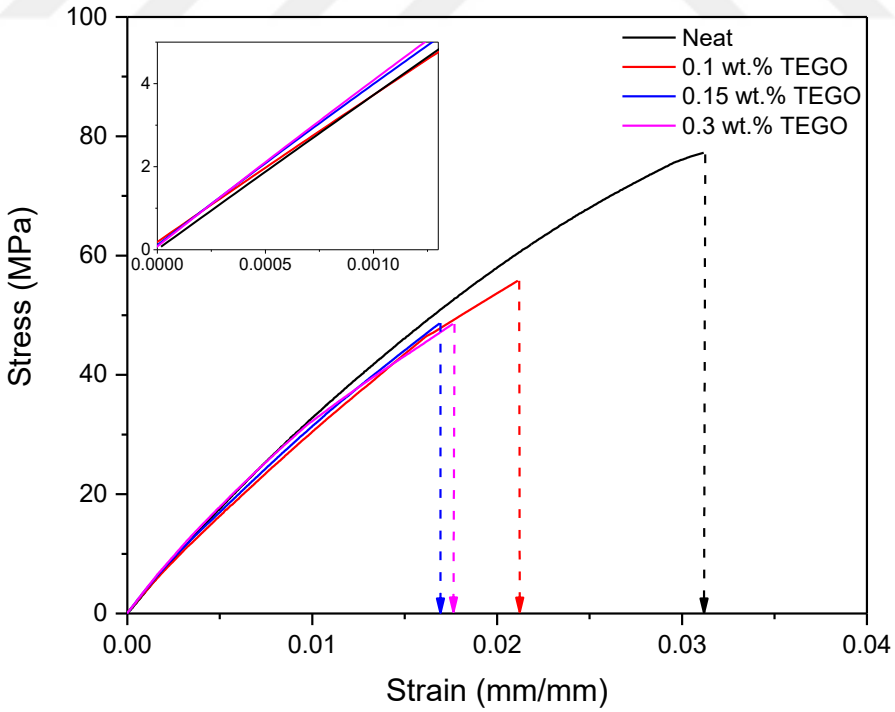

Figure 5.4 The stress-strain curves of neat and TEGO incorporated epoxy NCs

reinforced rigid matrix in the literature [244]. Matrix stiffness is important for the addition of layered additives. GNP generally improves the tensile strength of the ductile matrix, but once they are incorporated within a rigid matrix (e.g. epoxy), it usually decreases the tensile strength [245] as in this study. The drop in the strength of the NCs may be related to the weak load transfer from the epoxy to GNPs as a result of the weak interfacial interaction between the filler and matrix. The other reason can be because of the agglomeration formation according to Van der Waals forces. Agglomerates act as a stress concentrator and induce slipping between the sheets during tensile loading [61].

SEM images of the fractured tensile surfaces of the neat epoxy and TEGO incorporated epoxy NCs at 250x magnification is presented in Figure 5.5. As shown in Figure 5.5 (b), (c), (d), and (e), the roughness of the fractured surface was increased with increasing contents of TEGO, especially for 015TEGO/epoxy, and 03TEGO/epoxy NCs. Figure 5.6 presents the fractured surface of 01TEGO/epoxy NC, where the break occurred, at higher magnifications. Since the graphene layers seem parallel to the fractured surfaces, slipping between the clustered graphene layers with weak bonds between them may have occurred during the tensile loading (Figure 5.6 (a)). Peeled-off thick graphene layers can be seen in Figure 5.6 (b). This is proof of the crack that underwent tilt and twisting when it encountered the stiff graphene layers. So, during the crack propagation, GNP pulled off from the epoxy. On the other hand, thick graphene layers are shown in Figure 5.6 (b) completely wetted by the epoxy.

Figure 5.7 demonstrates the stress-strain curve of the neat epoxy and 05HNT/epoxy NC. According to the tensile test results, the strength, strain at failure, and toughness of epoxy NCs were improved with the incorporation of HNT. Enhancement of the tensile properties refers to their effectiveness according to their large aspect ratio [116]. However, while tensile strength was slightly improved by about %4, Young's modulus was slightly decreased with the incorporation of HNT within the epoxy. This can be the result of the potential presence of HNT aggregates within the epoxy. Calculated area-under stress-strain curves for toughness properties of neat epoxy and 05HNT/epoxy NC were increased by 35% with the incorporation of 0.5 wt.% HNT within the epoxy. The improvement in the toughness relates to the content of silane groups in the halloysite, which ensures a good interaction with the matrix.

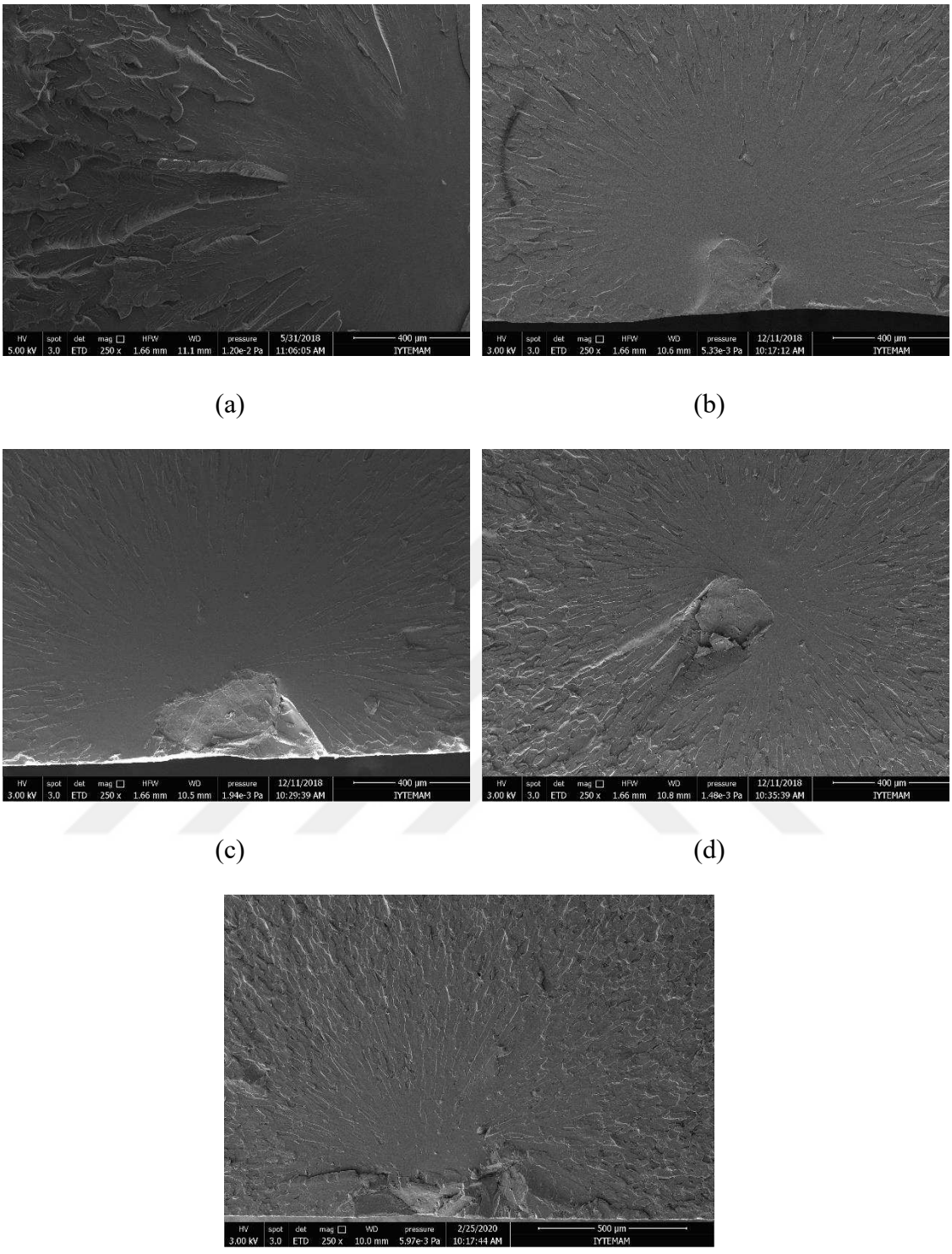

Figure 5.5 SEM images of the fractured surface of (a) Neat epoxy, (b) 005TEGO/epoxy, (c) 01TEGO/epoxy, (d), 015TEGO/epoxy and, (e) 03TEG0/epoxy NCs at 250 magnification after the tensile test

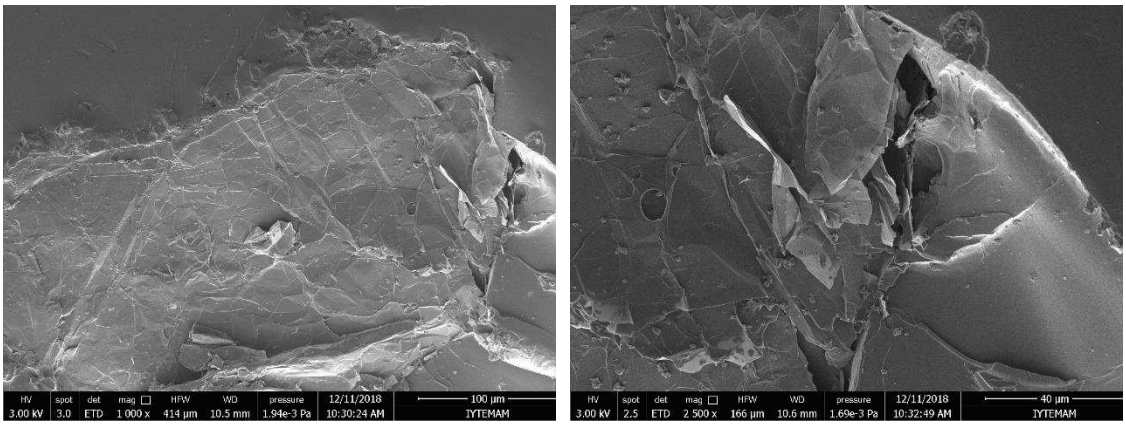

(a) (b)

Figure 5.6 SEM images of the fractured surface of 01TEGO/epoxy at (a) 1000x, and (b) 2500x magnifications

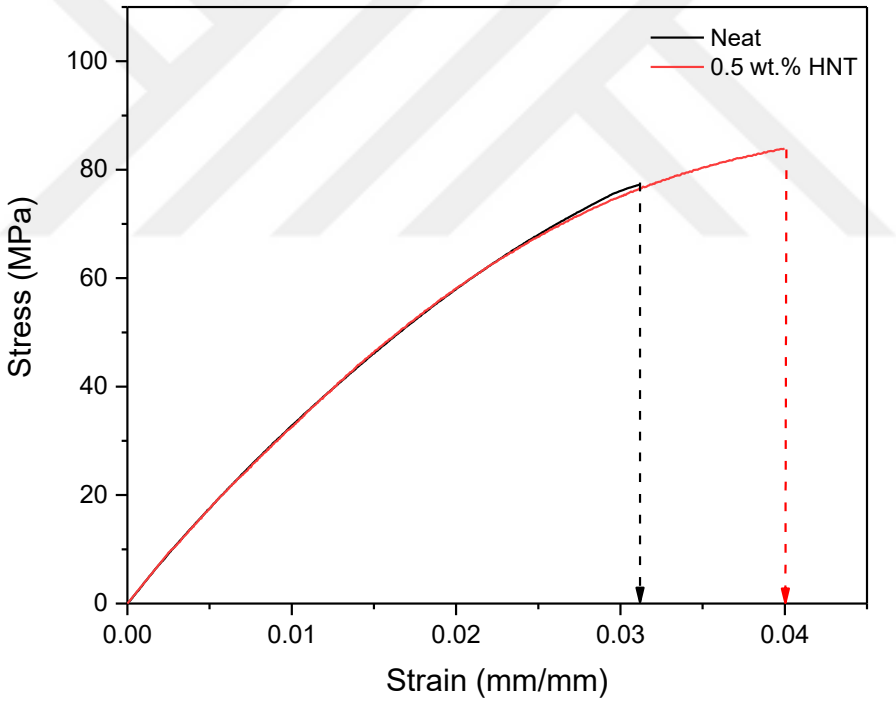

Figure 5.7 The stress-strain curve of neat and HNT incorporated epoxy NC

The fractured surface of 05HNT/epoxy NC after the tensile test was shown in Figure 5.8 with a typical rough surface when compared to the neat epoxy system. The reason for this is the strengthening effect of HNT on the epoxy that is provided to a delayed failure. The fracture lines on the fractured surface of 05HNT/epoxy NC created a rough fracture surface, which relates to a large surface area, and thereby much higher

energy was consumed when compared with neat epoxy [78]. Indeed, the area under the stress-strain curve showed an enhancement with the incorporation of HNT. Eventually, the increment of the resistance to the crack propagation improved the tensile properties of 05HNT/epoxy NCs.

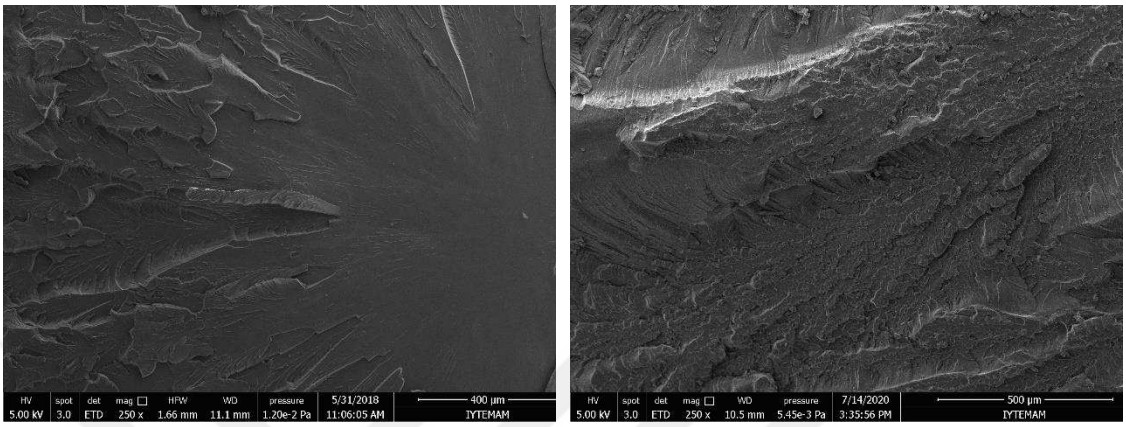

(a) (b)

Figure 5.8 SEM images of the fractured surface of (a) Neat epoxy, and (b) 05HNT/epoxy NC at 250 magnification after the tensile test

5.2. Effects of Nano-Sized Fillers on the Fracture Toughness Properties of Epoxy

The plane-strain fracture toughness (K_{Ic}) gives the resistance of a material to fracture in the presence of a sharp crack. For plastic materials, K_{Ic} is determined with the SENB test. Figure 5.9 illustrates a comparison between the Mode I fracture toughness values calculated from the SENB test results of SWCNT, TEGO, and HNT incorporated epoxy NCs and neat epoxy. The average fracture toughness value was measured as 1.04±0.09 MPa.m$^{1/2}$ for the neat epoxy. Maximum improvement on fracture toughness of epoxy was obtained for NCs reinforced with SWCNT and HNT as +182% and +208%, respectively. However, TEGO incorporation has less effect on fracture toughness of epoxy (about +60%).

Table 5.1 Tensile properties, calculated toughness, and abbreviations of nanocomposites

Filler type	Filler content (wt.%)	Ultimate Tensile Strength (MPa)	Strain at Failure (mm/mm)	Area Under Stress-Strain curve (J/m)	Young's Modulus (MPa)	Abbreviation of NCs
Neat	-	76.14±2.55	0.029±0.002	1.30±0.15	3.54±0.12	Neat epoxy
SWCNT	0.0125	82.82±2.45	0.063±0.006	4.04±0.59	3.53±0.16	00125SWCNT/epoxy
	0.025	87.39±5.34	0.047±0.014	2.85±1.18	3.93±0.37	0025SWCNT/epoxy
	0.05	77.89±4.97	0.035±0.004	1.68±0.38	3.60±0.42	005SWCNT/epoxy
	0.1	50.04±9.12	0.025±0.015	0.50±0.12	3.56±0.16	01SWCNT/epoxy
	0.3	30.16±4.78	0.012±0.003	0.24±0.13	3.64±0.42	03WCNT/epoxy
	0.5	28.51±5.12	0.008±0.002	0.14±0.77	3.69±0.66	05SWCNT/epoxy
TEGO	0.05	53.85±6.42	0.016±0.003	0.52±0.16	3.40±0.24	005TEGO/epoxy
	0.1	47.26±7.18	0.014±0.003	0.40±0.11	3.47±0.03	01TEGO/epoxy
	0.15	51.99±1.14	0.015±0.003	0.51±0.44	3.89±0.35	015TEGO/epoxy
	0.3	52.87±3.71	0.016±0.001	0.52±0.83	3.37±0.37	03TEGO/epoxy
HNT	0.5	79.38±7.71	0.034±0.007	1.75±0.58	3.20±0.10	05HNT/epoxy

The Mode I plane strain fracture toughness was improved from 1.04±0.09 MPa.m$^{1/2}$ to 2.93±0.58 MPa.m$^{1/2}$, 2.92±0.27 MPa.m$^{1/2}$, and 3.20 ±0.31 MPa.m$^{1/2}$ for 0025SWCNT/epoxy, 005SWCNT/epoxy, and 05HNT/epoxy NCs, respectively. This increment of the fracture toughness is based on the bridging and crack front pinning mechanisms. Since, CNTs and HNTs are fiber-like structures, the effect of these fillers on the fracture mechanism of the epoxy NCs can be understood by the classical models (a micro-mechanical mechanism) [31,103,246]. If there is a strong interfacial interaction between the epoxy matrix and CNT or HNT, the crack prorogation can be delayed by the fibers. During the fracture of fibrous reinforced epoxy composites; crack pinning, crack deflection, crack bridging, fiber debonding, and fiber pull-out are responsible for the fracture mechanism. At high concentrations of SWCNT, toughness was reduced by the ineffective fabrications of NCs (because of the possible agglomeration of SWCNTs, and the inability to remove the voids due to high viscosity). But NCs at high SWCNT content have never reached the lowest fracture toughness levels of the neat epoxy. It means that agglomeration of SWCNT resembled micro-sized rigid particles which can cause crack deflection and twist during the crack propagation. However, these micro-sized SWCNT agglomerates have a more limited effect on cracking and fracture energy. Also, according to the calculated area under stress-strain results for 0.0125 wt.% SWCNT incorporated epoxy NC, the energy absorbed to fracture increased up to 213%. That is to say, the calculated fracture toughness results verified with the calculated toughness values from the stress-strain curve. Also, it is important to point out that the enhancement of the toughness values of SWCNT reinforced epoxy NCs is greater than those values reported in the literature [31,52,68,103,136,247,248].

The incorporation of TEGO within the epoxy results in a significant improvement in the fracture toughness of NCs. The maximum improvement of the fracture toughness reached 1.66±0.31 MPa.m$^{1/2}$ for 015TEGO/epoxy NC. The obtained value is the greatest among the results of studies reported in the literature (see Appendix A). TEGO particles resembled micro-sized rigid particles, which may cause branching and crack deflection during the crack propagation. On the other hand, the fracture toughness value slightly decreased at higher contents of TEGO (0.3 wt.%). This trend has been reported in the literature and explained that the nano-sized filler content above a certain weight ratio leads to a decrease in fracture toughness. This could be due to the ineffective dispersion and agglomeration tendency in consequence of Van der Waals forces between graphene

sheets of TEGO at high concentrations. However, the decrease in the fracture toughness was not reached to the neat epoxy due to the hydroxyl group on the graphene sheets induced a covalent bonding between the filler and epoxy [249].

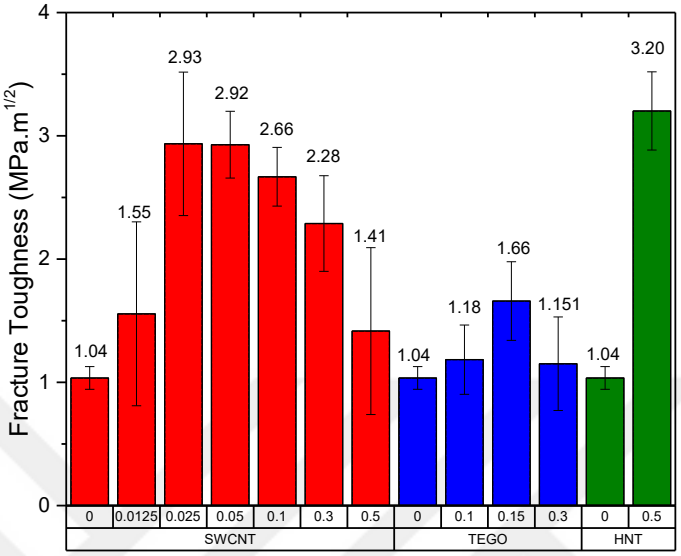

Figure 5.9 Effect of the nano-sized filler content on the fracture toughness of the epoxy

SEM images of the fractured surfaces of the neat epoxy and NCs reinforced with various content of SWCNT, TEGO, and HNT after the SENB test are shown in Figure 5.10. The part that looks sandy in the SEM images is the notch opened for the SENB test. Thus, the crack propagation direction is from bottom to top for SWCNT, and TEGO incorporated NCs, left to right for HNT incorporated NCs in SEM images. Neat epoxy showed a typical brittle fracture according to their weakness against the crack initiation and propagation (Figure 5.10 (a)) [203]. As shown in Figure 5. 10 (b), (c), and (d), the contribution of rigid filler increased the roughness of the fractured surface. During the SENB test, the crack firstly starts to propagate behind the pre-crack, then encounters the rigid fillers, and finally crack propagation is delayed. Besides, the formation of rough surfaces according to the crack propagation inhibition of NCs during the SENB test. Additionally, during the crack propagation energy dissipation also occurs, which leads to the fracture mechanism. A river-like structure on the rough fracture surfaces of NCs, which are correlated with the formation of the “crack tip blunting”, was formed.

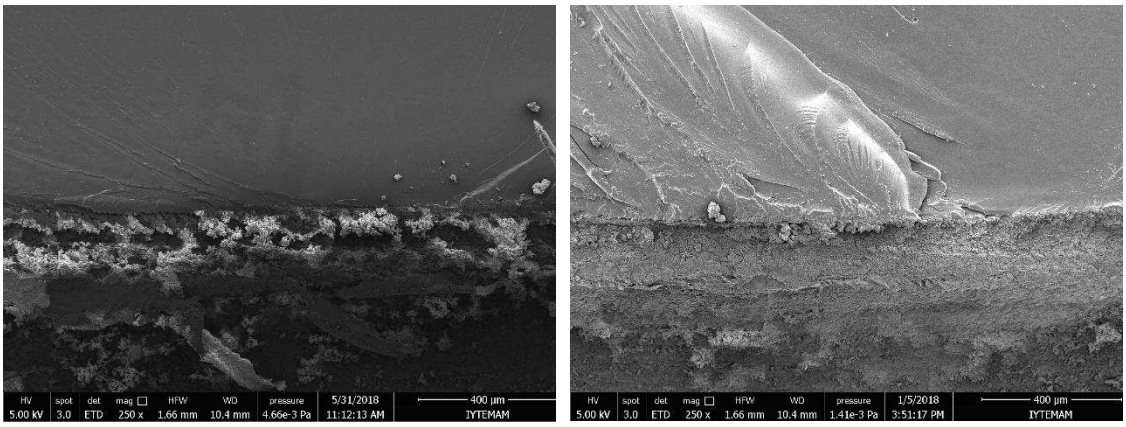

(a) (b)

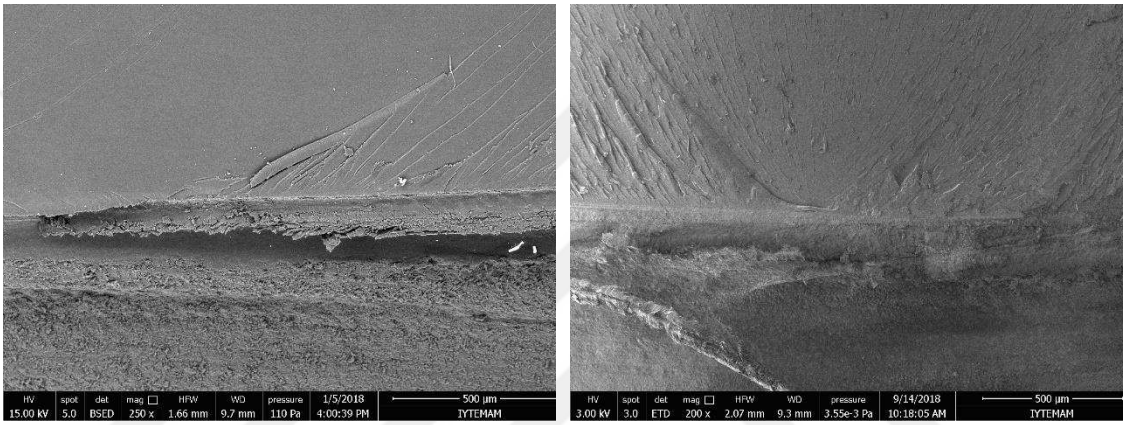

(c) (d)

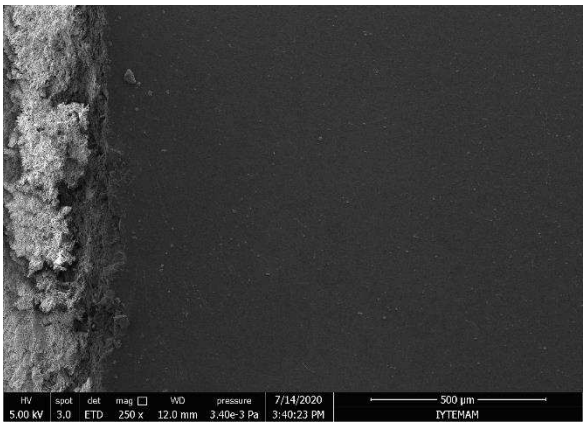

(e)

Figure 5.10 SEM images of the fractured surface of (a) Neat epoxy, (b) 01SWCNT/epoxy NC, and (c) 03SWCNT/epoxy NC at 250x magnification, (d) 015TEGO/epoxy NC at 200x magnification and (e) 05HNT/epoxy NC at 250x magnification after SENB test

On account of a further investigation of the toughness properties of composites, the fractured surfaces of composites were also investigated at higher magnification as shown in Figure 5.11. While there was a relatively uniform distribution of SWCNT on the surface at lower SWCNT content, which was the one that exhibited the highest fracture toughness values (Figure 5.11 (a)), an agglomeration of SWCNT occurred at higher SWCNT content (Figure 5.11 (b)). However, because Gojny et al. suggested that small clusters of nanotubes are favorable [103], it can be said that these clusters of SWCNTs also participated in the fracture toughening mechanisms as micro-sized additives. Since there was a strong interfacial adhesion between the filler and matrix, pull-outs were not

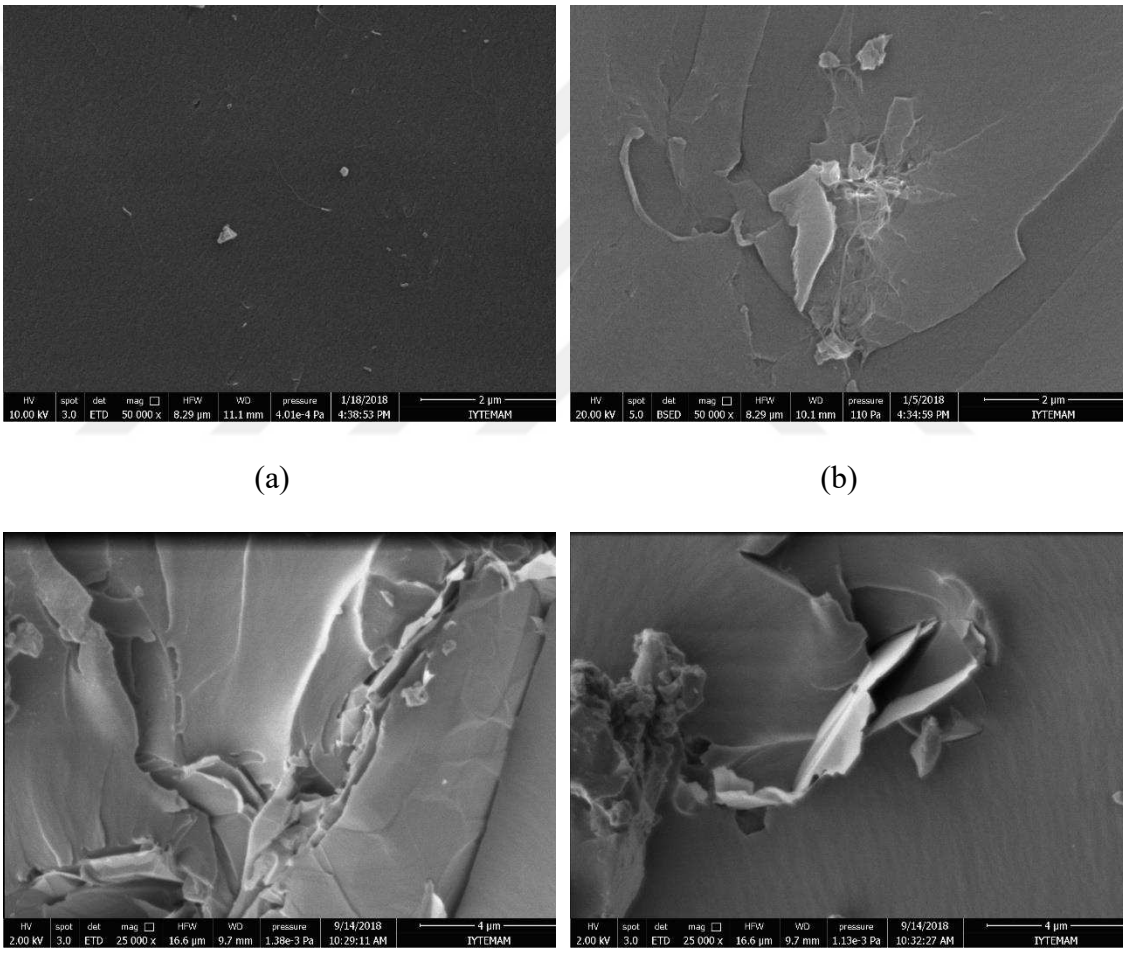

(a) (b)

(c) (d)

Figure 5.11 SEM images of fractured surface of (a) 005SWCNT/epoxy, (b) 03SWCNT/epoxy NCs at 50 000x magnification and (c), and (d) 015TEGO/epoxy NC at 25 000x magnification after SENB test.

observed and SWCNTs were wetted well by the epoxy. The exfoliated layered structures of TEGO can be seen on the right side of Figure 5.11 (c). These parallel positioned GNP layers to the crack propagation participated in the crack deflection mechanism during the crack propagation by inducing the fracture toughness. However, when vertically oriented graphene layers to the crack propagation were examined at higher magnifications, the little gap between the epoxy matrix and graphene sheets was observed, as illustrated in Figure 5.11 (d). This gap could be due to the crack pinning mechanism by vertically oriented graphene layers.

5.3. Effects of Nano-Sized Fillers on the Flexural Properties of Epoxy

The flexural strength and modulus values were determined for the neat epoxy and NCs at various contents of TEGO (0.05, 0.1, and 0.15 wt.%) to observe the effect of the graphene incorporation on the flexural properties of composites. The flexural strength and modulus results are presented in Figure 5.12. According to the results obtained from the flexural test, both flexural strength and modulus values were significantly enhanced at low content of TEGO (maximum enhancement for 0.05 wt.% TEGO/epoxy nanocomposites), but a decline in flexural properties was observed at increasing concentrations of TEGO. The flexural strength and modulus values of neat epoxy were measured as 124 MPa and 2.5 GPa, respectively. The improvement of the flexural strength and modulus values were a maximum of about 26% and 70%, respectively. The improvement in the flexural modulus of NCs with the incorporation of rigid TEGO associates with restricting the mobility of the polymer chain. It is also noted that the decay of the flexural properties due to the high content of TEGO did not go below the flexural properties of neat epoxy. The decline of the flexural properties of the NCs at high content of graphene associates with the agglomeration tendency of the nano-sized particles, which acts as a defect or stress concentration point. These agglomerates resulted in the micro-defects with a relatively lower surface area that interacts with epoxy and accelerated the crack propagation through to forming steric obstacles, which may have led to voids between the filler and matrix [250].

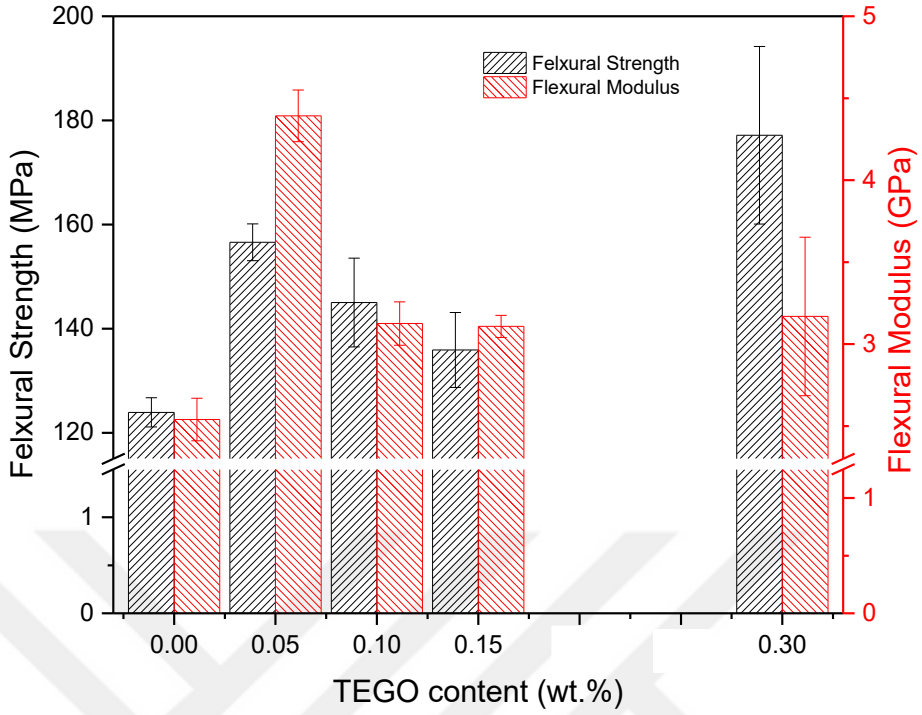

Figure 5.12 Flexural strength and modulus values of the neat epoxy and TEGO/epoxy NCs

5.4. Effects of Nano-Sized Fillers on the Rheological Properties of Epoxy

The viscosity values of the reference and SWCNT blended epoxy suspensions in the presence of hardener and accelerator as a function of shear rate at 25^0C is given in Figure 5.13. The rheological behavior of suspensions at low contents of SWCNT (0.0125 and 0.025 wt.%) was almost the same with the pure epoxy. The viscosity of suspensions highly affected at low and intermediate shear rates with the incorporation of SWCNT, especially at higher contents (0.3 and 0.5 wt.%), but the viscosity of these suspensions was decreased and reached almost the same viscosity value for the reference suspension viscosity at the highest shear rate.

For the reference suspension, there were two distinct regions; the 1st region (at the low shear rate) is the Newtonian region, which is independent of shear rate, and 2nd region is shear thinning, which occurred at an increasing shear rate and resulted in a linear

decline in viscosity [223]. While the Newtonian region was observed for reference suspension, it was disappeared for suspensions with increasing SWCNT concentrations [251]. After the Newtonian region, viscosity linearly decreased with increasing shear rate at the shear thinning region. SWCNT blended suspensions also showed a shear-thinning behavior, according to the viscosity decrease as a function of shear rate- typical behavior for a pseudoplastic fluid. While the orientation of nano-sized fillers was provided by the shear, an increased shear rate could cause breakage of SWCNT bundles [80].

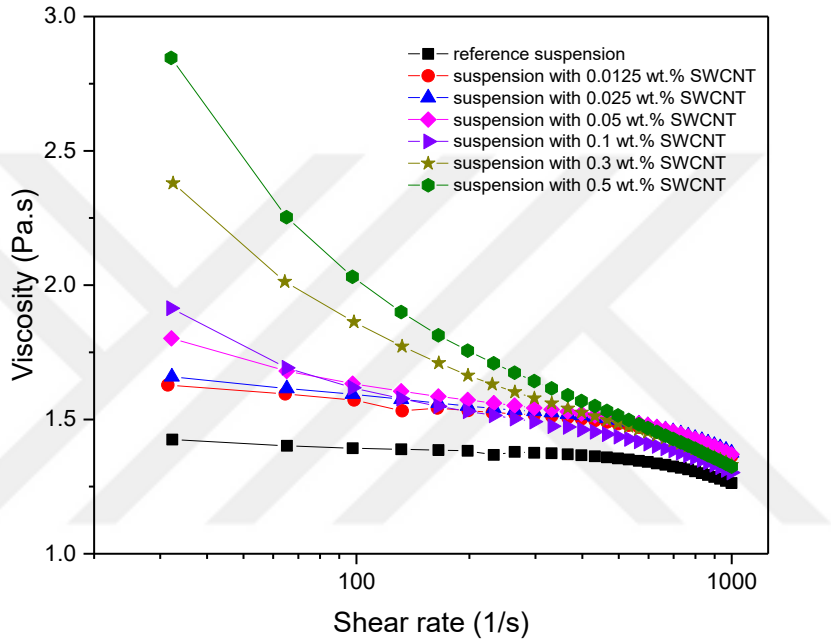

Figure 5.13 The viscosity of the reference and SWCNT blended suspensions at increasing shear rate

Also, at low concentrations of SWCNT (0.0125, 0.025, 0.05, and even 0.1 wt.%), the flow behaviors of suspensions were nearly the same as compared to those for the reference suspension. However, with the incorporation of SWCNT at high concentrations (more than 0.1 wt.%), there was a progressive increase in the low shear rate with an apparent viscosity. This resulted in difficulty for the removal of the air bubbles from the suspension. Consequently, a decrease in the mechanical properties of NCs was taken place, due to the presence of micro-voids.

For the filament winding process, a desirable wet winding of fibers can be provided by epoxy viscosities less than about 5.0 Pa.s (preferred about 2.0 Pa.s) at room temperature (25^0C) [252]. According to the rheological values of reference and 0.0125,

0.025, 0.05, and 0.1 wt.% SWCNT blended suspensions at room temperature (25^0C), and at the low shear rate did not exceed 2.0 Pa.s, which is a suitable viscosity value during filament winding for wetting the continuous filaments.

The viscosity behavior of the reference and SWCNT blended epoxy suspensions, which were used in the production of GF-based CFRPCs, as a function of temperature at 100 1/s shear rate is given in Figure 5.14. The viscosity behavior of the suspensions was not significantly affected by the incorporation of SWCNT at increasing temperature. As expected, viscosity was decreased with increasing temperature. While the curing of composites was completed at 80^0C for 2 hours, post-curing was completed at 120^0C for 2 hours. As seen in the graphic (Figure 5.14), at 80^0C viscosity reached its lowest value.

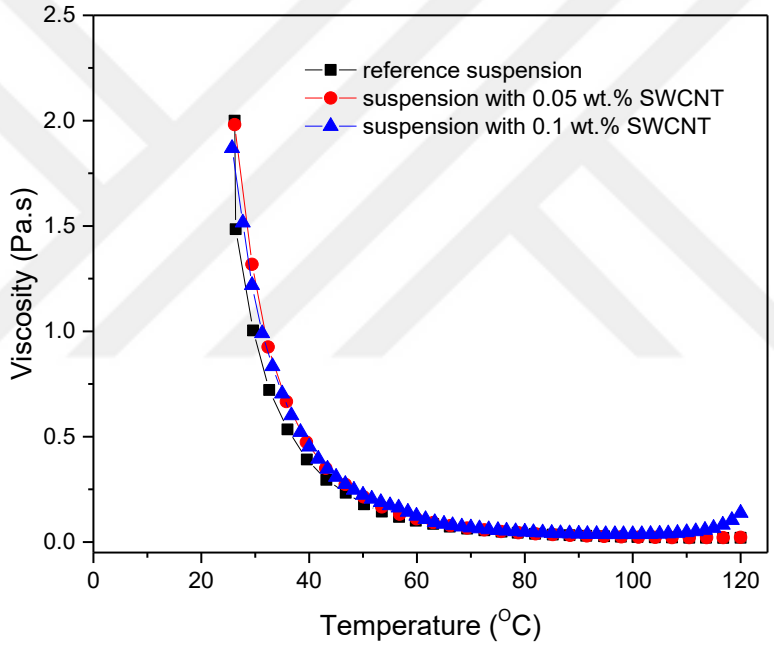

Figure 5.14 Temperature dependency of the viscosity of the reference and SWCNT blended suspensions at 100 1/s shear rate

5.5. Effects of Nano-Sized Fillers on Contact Angle Properties of GF

In the filament winding, the process for complete wetting of the continuous fiber is a critical issue for enhancing the mechanical properties of resultant FW composites. The wettability of the fiber with the epoxy resin can be quantitated with the pendant drop

method, which is an appropriate experimental method for measuring the contact angle of the liquids on the solid surfaces. The wettability is determined by the degree of spread of a liquid on the solid surface and it depends on the interfacial interaction between the liquid and the solid surface. The contact angle between the surface of the wetted solid and a line tangent to the curved surface of the drop at the point of three-phase contact is measured to get information about the interactions between the surfaces [253,254]. Complete wetting of the fibers requires a good adhesion between the ingredients. So, the mechanical properties of the composite material produced by providing a good wettability of GF.

According to the pendant drop method, the spread of the reference, and 0.1 wt.% SWCNT incorporated epoxy suspensions on a single GF surface is shown in Figure 5.15. The absorption of the reference, and 0.1 wt.% SWCNT incorporated epoxy suspensions were approximately the same. So, the wettability of GF is not affected by the presence of SWCNT even at the highest concentration for this study.

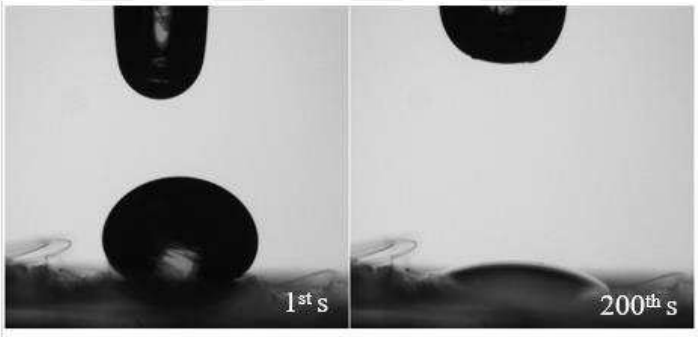

(a)

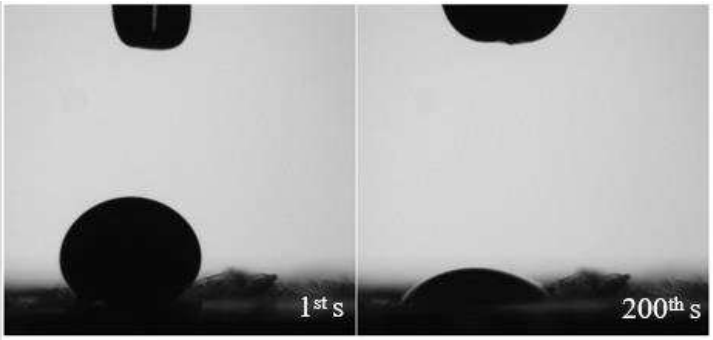

(b)

Figure 5.15 (a) Reference suspension and (b) Suspension with 0.1 wt.% SWCNT drops on a single GF surface in 1st and 200th seconds at room temperature

5.6. Effects of Nano-Sized Fillers on the Apparent Hoop Tensile Strength and Mode I Fracture Toughness Properties of GF-based Composite Rings

Tubular structures are generally used under internal pressure where high hoop stresses are developed. The split-disk test is efficient for determining the performance of these tubular structures [233].

The split-disk tests were performed for the composite rings cut from FW GF/epoxy, GF/005SWCNT/epoxy, and GF/01SWCNT/epoxy with an inner diameter of 60 mm. As illustrated in Figure 5.16, the unnotched and notched composite rings were tested under the tensile force to calculate the hoop tensile strength. While for unnotched composite rings both strength and strain increased with the incorporation of SWCNT, for notched composite rings the strength was improved with the incorporation of SWCNT, but the strain was not affected significantly. According to the strength obtained from the split-disk test, the apparent hoop tensile strength and Mode I fracture toughness with their

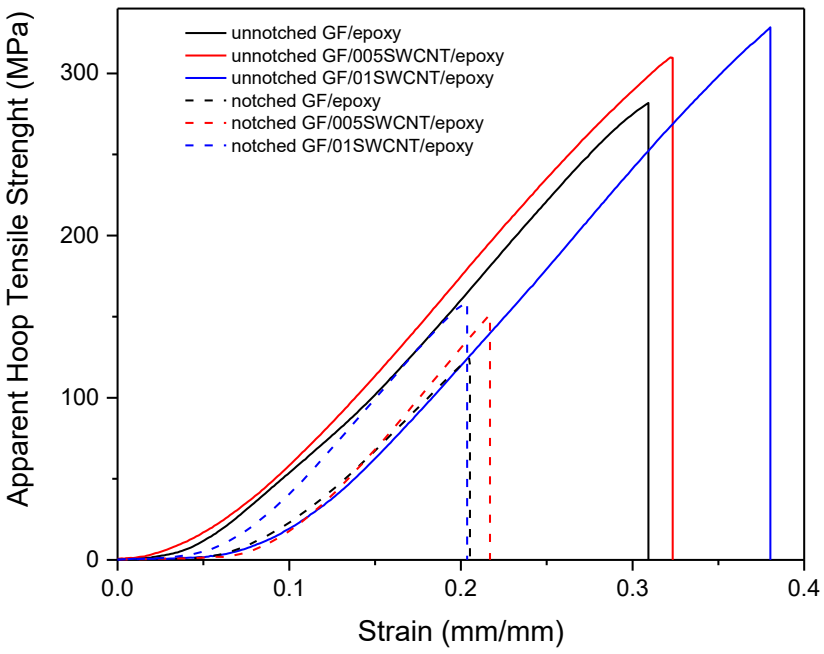

Figure 5.16 The apparent hoop tensile strength of the unnotched and notched FW GF/epoxy, GF/005SWCNT/epoxy, and GF/01SWCNT/epoxy composite rings

standard deviations were calculated and the results are given in Figure 5.17. The apparent hoop tensile strength and Mode I fracture toughness were calculated for GF/epoxy ring as 282.80±29.60 MPa and 273.78±52.83 MPa.m$^{1/2}$, respectively. While the tensile strength was improved by about 16% with the incorporation of 0.1 wt.% SWCNT, the Mode I fracture toughness was increased by about 36% at the same SWCNT concentration.

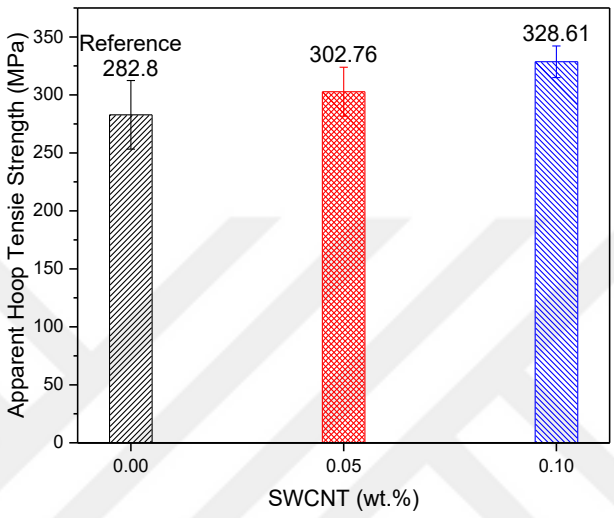

(a)

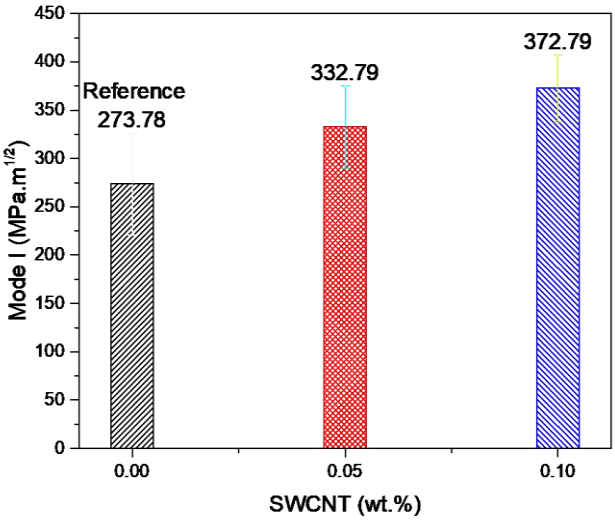

(b)

Figure 5.17 (a) The apparent hoop tensile strength, and (b) Mode I fracture toughness of the composite ring specimens as a function of SWCNT concentration

SWCNT participated more in the fracture mechanism of the epoxy than of GF/epoxy since GF and SWCNT both participate in the fracture mechanism of SWCNT incorporated GF-based epoxy composites. Thus, fracture toughness mechanisms were enhanced by both micro-and nano-sized fillers. As known, the fracture toughness strongly depends on how to crack propagation occurs, and it is defined with mechanisms.

Figure 5.18 shows the fractured surface of GF/epoxy, and GF/01SWCNT/epoxy composite rings after the split-disk test. Since the toughness of the epoxy matrix was enhanced with the incorporation of SWCNT, delamination, which is the matrix failure, was dominant for GF/epoxy composites. Therefore, GF debonding and pull-out failure from the matrix has been seen on the fractured surface of GF/epoxy composites (Figure 5.18 (a)). Furthermore, the propagation of the crack was smoother for GF/epoxy (Figure 5.18 (a)) than for GF/01SWNCT/epoxy composites (Figure 5.18 (b)). This is due to the improvement of the fracture toughness with the incorporation of SWCNT within the epoxy matrix by the fracture toughness mechanisms.

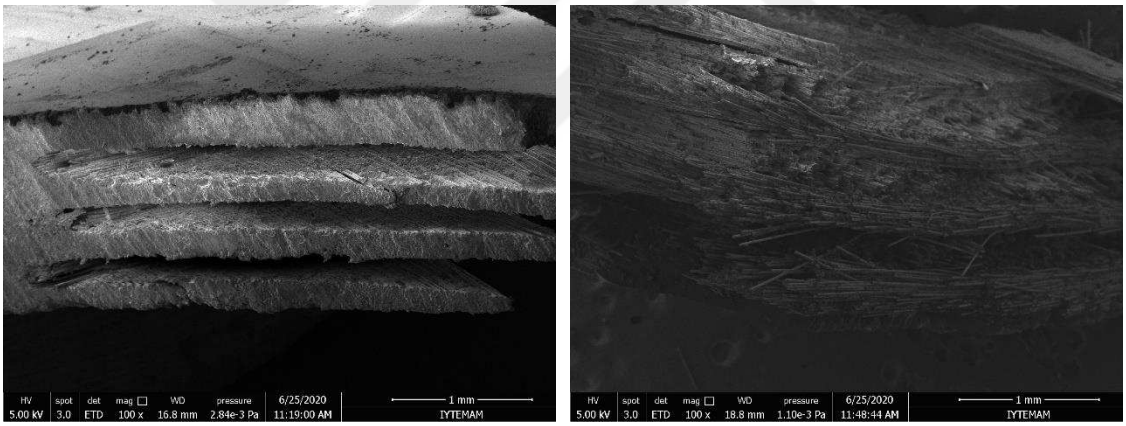

Figure 5.18 SEM images of the fractured surfaces of (a) GF/epoxy, and (b) GF/01SWCNT/epoxy composites after the split-disk test at 100x magnification

Figure 5.19 presents the SEM images of the fractured surfaces of SWCNT reinforced composite rings after the split-disk test at higher magnifications. The micro-sized GF and nano-sized SWCNT embedded in epoxy can be seen in Figure 5.19 (a). The contribution of SWCNT to the fracture toughness by the fiber-bridging mechanisms can be also seen in Figure 5.19 (b). This explains the reason for the less delamination occurred in the GF/01SWCNT/epoxy composites.

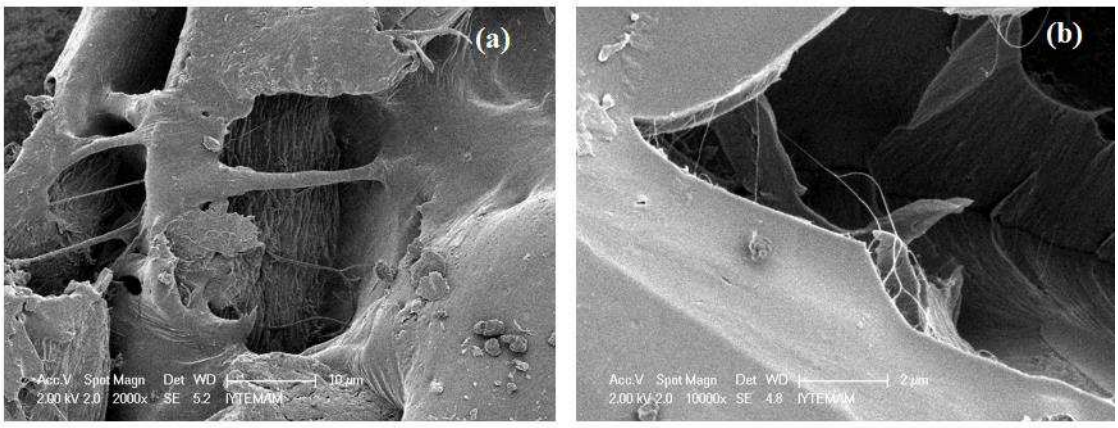

Figure 5.19 SEM images of a fractured surface of GF/01SWCNT/epoxy composites after the split-disk test at (a) 2000x and (b) 10000x magnifications

5.7. Effects of Nano-Sized Fillers on Flexural and ILSS Properties of GF-based CFRPCs

Three-point bending tests were performed to determine the flexural and ILSS properties of cylindrical GF/epoxy, GF/005SWCNT/epoxy, and GF/01SWCNT/epoxy composites with an inner diameter of 60 mm and 275 mm. Figure 5.20 shows the force vs displacement curves of GF/epoxy, GF/005SWCNT/epoxy, and GF/01SWCNT/epoxy composite samples with an inner diameter of 60 and 275mm under three-point bending loading. While the load was improved from 0.395 kN to 0.577 kN with 0.05 wt.% SWCNT incorporation for CFRPCs with 60 mm inner diameter (Figure 5.20 (a)), the load was enhanced from 0.795 kN to 2.209 kN with 0.1 wt% SWCNT incorporation for CFRPCs with 275 mm inner diameter (Figure 5.20 (b)). The slope of the load vs displacement curves for both types of CFRPCs was increased with increasing concentration of SWCNT as a consequence of the resistance to crack propagation enhancement by SWCNT. Besides, Figure 5.21 shows SWCNT improved the calculated flexural strength of CFRPCs with 60 and 275mm inner diameter. While the maximum improvements were obtained as 16% and 37% for 0.1 wt.% SWCNT incorporated CFRPCs with an inner diameter of 60 and 275mm, respectively.

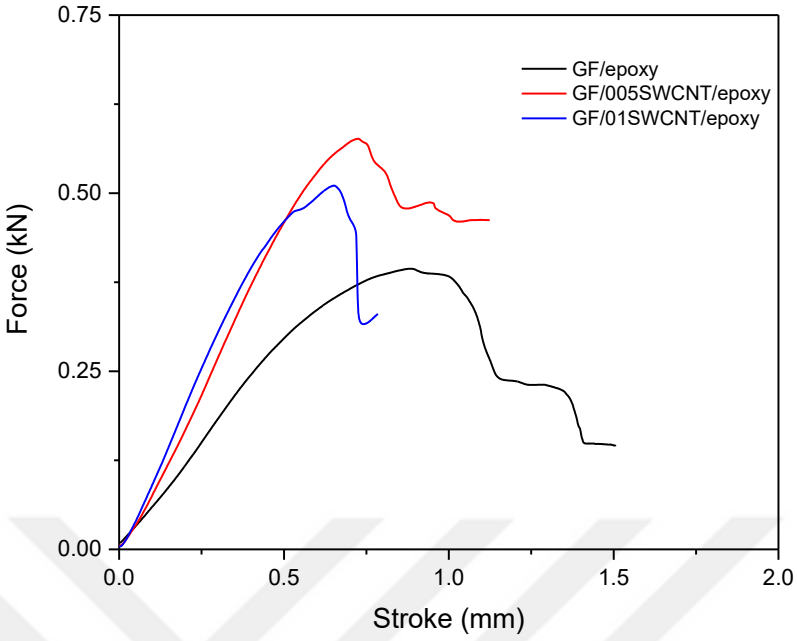

(a)

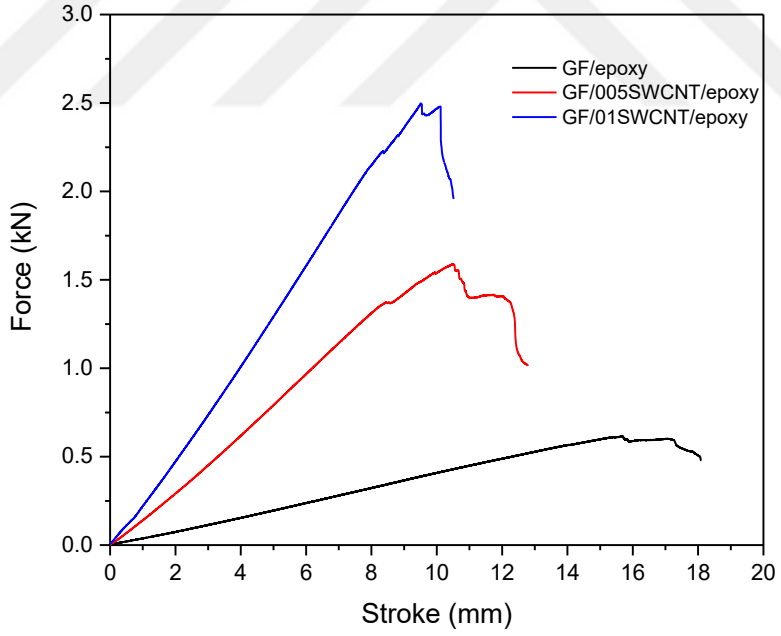

(b)

Figure 5.20 Load vs displacement curves of GF/epoxy, GF/005SWCNT/epoxy, and GF/01SWCNT/epoxy composites with an inner diameter of (a) 60, and (b) 275 mm.

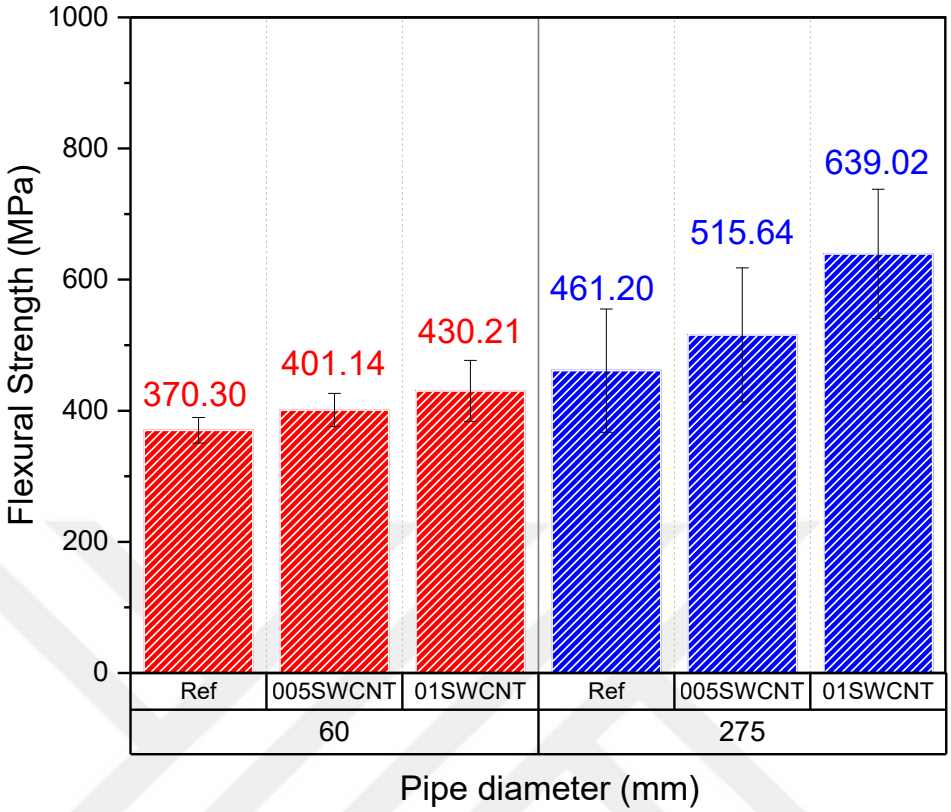

Figure 5.21 The flexural strength of CFRPCs with an inner diameter of 60 and 275mm as a function of SWCNT content

The interlaminar shear failure was observed for the curved GF/epoxy, GF/005SWCNT/epoxy, and GF/01SWCNT/epoxy composite samples with an inner diameter of 60 and 275mm. In addition to the interlaminar shear failure, other damages can be observed during the SBS test. However, ILSS can be calculated correctly when only interlaminar shear failure is obtained. According to Fan et al., pure interlaminar shear failure is obtained when firstly the load is increased due to the linear elastic behavior of composites, and then load dropped dramatically because interlayer delamination occurred at the 1st layer of the composites [155]. The SBS test determines the ability of the fiber-based composites to resist delamination. For the long-term usage of the fiber-based composites improvement of delamination is an important issue. Thus, the results of the SBS test provide valuable information on the response of the composite samples under the Mod-I loading.

According to the three-point bending test, the short beam strength was calculated for GF/epoxy, GF/005SWCNT/epoxy, and GF/01SWCNT/epoxy composites and illustrated in Figure 5.22. When the short beam strength was improved a maximum value of 21% with the incorporation of 0.05 wt.% SWCNT for composite with 60 mm inner diameter, the improvement of strength was 22% with the incorporation of 0.05 wt.% SWCNT for composite with 275 mm inner diameter. The strength was slightly decreased for GF/01SWCNT/epoxy when compared to GF/005SWCNT/epoxy for both types of CFRPCs. However, the reduction of the strength was not exceeded below the value of GF/epoxy composites.

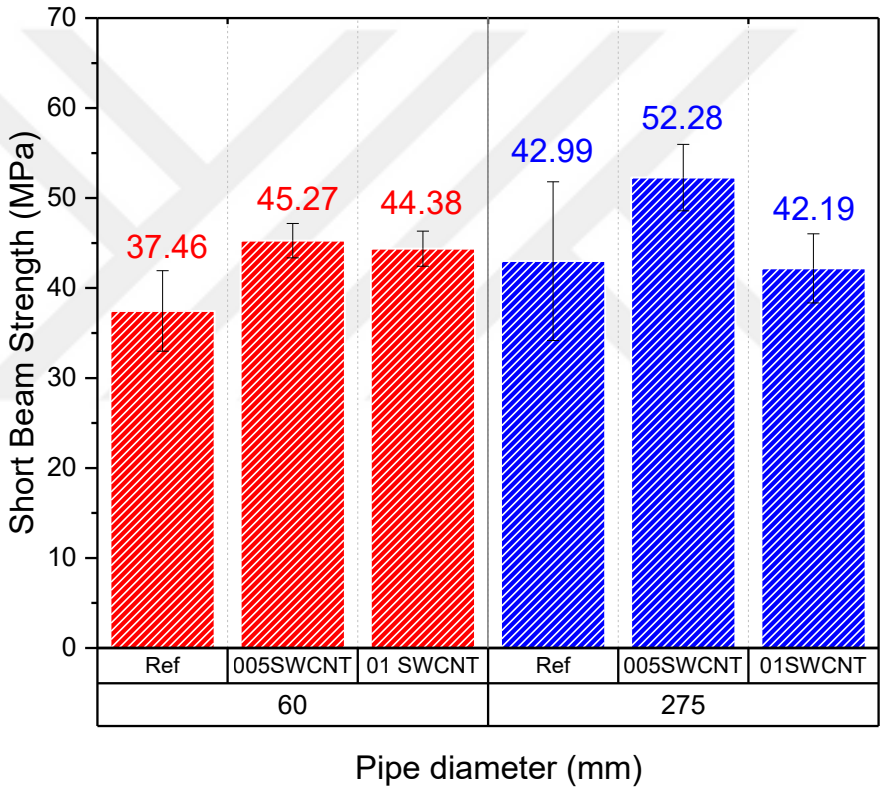

Figure 5.22 Short beam strength of the curved composites with an inner diameter of 60 and 275mm as a function of SWCNT content

Figure 5.23 represents the fractured surfaces of GF/epoxy and GF/005SWCNT/epoxy composites after the SBS test. The interlayer delamination, which occurred during the crack propagation between two layers, was a more predominant mechanism for the GF/epoxy (Figure 5.23 (a)) than for the GF/005SWCNT/epoxy

(Figure 5.23 (c)), the lower short beam strength values were obtained for reference composites. Besides, during the crack propagation, the crack jumped to a neighboring interface with the existence of SWCNT, as shown in Figure 5.23 (b). This is due to the resistance to the interlayer delamination of larger areas that were offered by SWCNT.

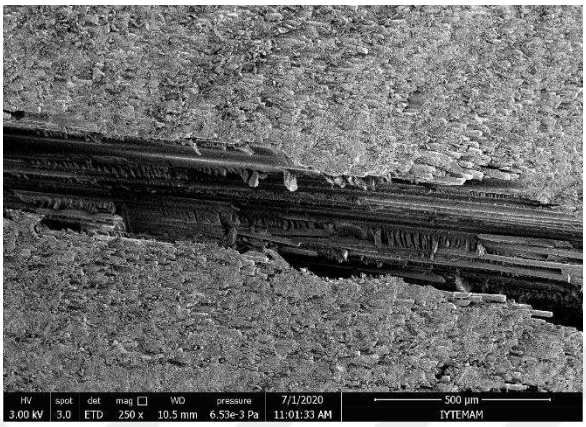

(a)

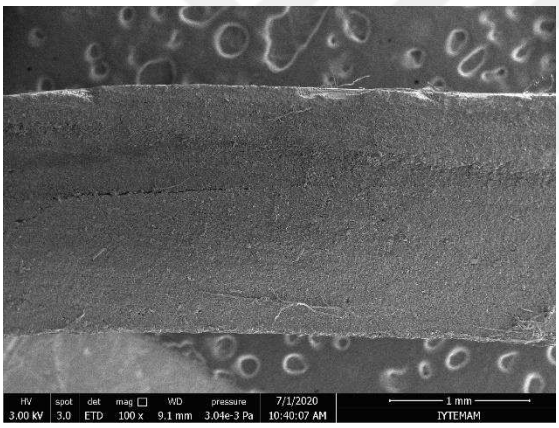

(b)

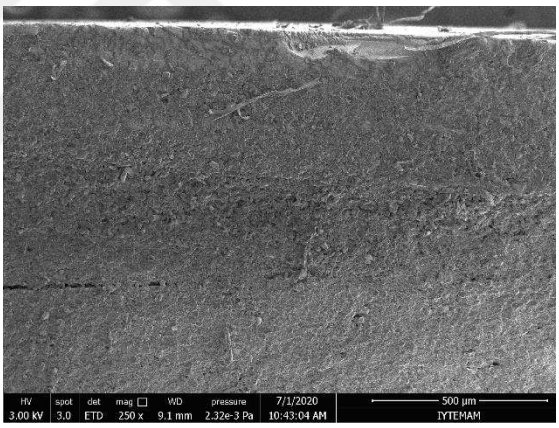

(c)

Figure 5.23 SEM images of (a) GF/epoxy at 250x magnification and GF/005SWCNT/epoxy composites at (b) 100x, and (b) 250x magnification after the SBS test

When the ILSS results achieved from this study compared with the literature studies that used the toughening of the epoxy system with nano-sized filler incorporation for the production of fiber by filament winding technique, the ILSS improvement for this study was higher than the reported in the literature [168,255]. These studies in the literature were used CF as a micro-sized reinforcement, and ILSS properties improvement of GF-

based CFRPCs with CNT incorporation has not been reported yet. However, the study of Zhang et al. obtained a 28% improvement on the ILSS of FW CF-based CFRPCs with the incorporation of 6 wt.% MWCNT-NH_2 [159]. The reason for this higher efficiency reported in literature could be the usage of the large amount of CNT. Nevertheless, in this study, unlike the other studies in the literature, an increase of 22% was obtained by using SWCNT incorporated epoxy resin only in the last layer of CFRPCs.

5.8. Effects of Nano-Sized Fillers on the Thermomechanical Properties of GF-based CFRPCs

The glass transition temperature (T_g,) of the transverse and longitudinal samples cut from cylindrical GF/epoxy, GF/005SWCNT/epoxy, and GF/01SWCNT/epoxy composites with an inner diameter of 275 mm determined according to the temperature at maximum Tanδ value was presented in Table 5.2. While T_g values were slightly increased with the incorporation of SWCNT, T_g is not affected by the fiber direction remarkably.

Table 5.2 Glass transition temperature (T_g,) values of CFRPC specimens

Cutting direction of the sample	Sample name	Glass Transition Temperature (T_g, ^{0}C)
Longitudinal	GF/epoxy	147.94
	GF/005SWCNT/epoxy	150.57
	GF/01SWCNT/epoxy	152.16
Transverse	GF/epoxy	147.76
	GF/005SWCNT/epoxy	150.31
	GF/01SWCNT/epoxy	151.97

Figure 5.24 shows the storage and loss modulus values at T_g of GF/epoxy, GF/005SWCNT/epoxy, and GF/01SWCNT/epoxy composites of both transverse and longitudinal directions. While the storage modulus measures the elastic response of the

composite, the loss modulus measures the viscous response of the composite, which gives the energy dissipated as heat. For both composite samples cut in two different directions (longitudinal and transverse), the storage modulus was increased with the incorporation of 0.05 wt.% SWCNT. However, the storage modulus was decreased with the incorporation of 0.1 wt.% SWCNT. The elastic response was more remarkable for the transverse composite samples than the longitudinal composite samples. Three-point bending tests for the transverse samples were consistent with the storage modulus.

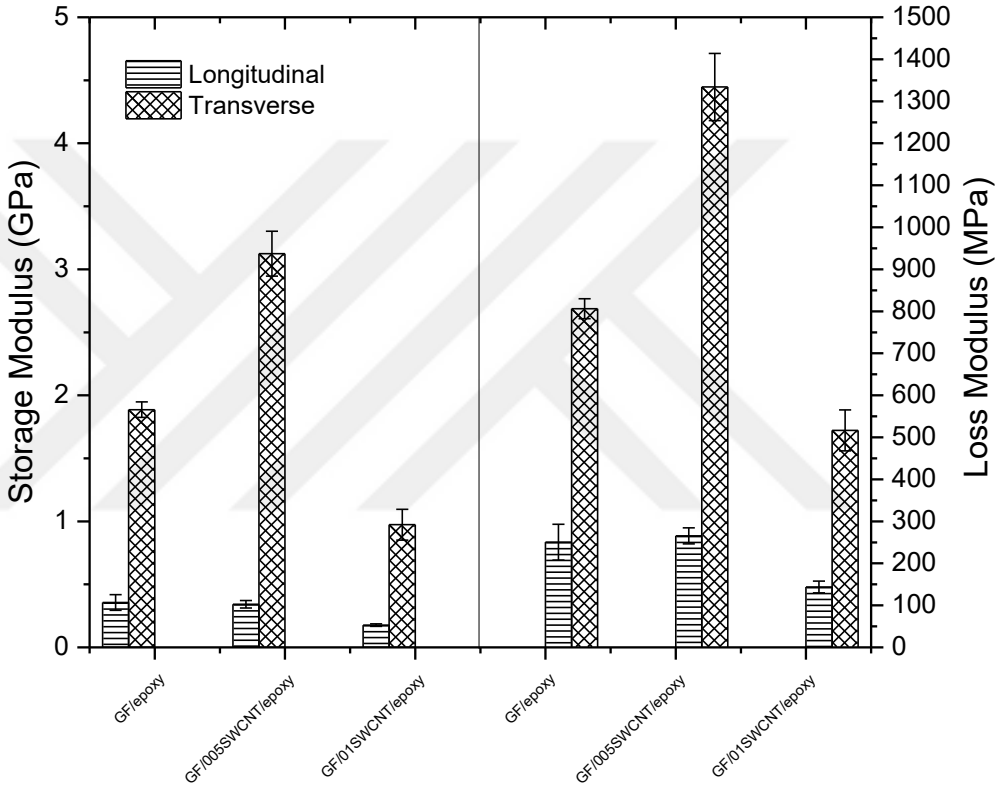

Figure 5.24 Storage and loss modulus of both longitudinal and transverse CFRPC test specimens

Due to the loss modulus measures the vibrational energy, it is sensitive to the mobility of the polymer chain. The addition of nanoparticles within the polymer restricts the motion of the polymer chain by increasing T_g. This trend can be explained by the energy losses caused by the friction between the epoxy and SWCNT through vibrational energy. The incorporation of 0.05 wt.% SWCNT within the matrix increased both flexibility and viscosity of the FRCs for either direction. Accordingly, more energy was needed for the friction between epoxy and SWCNT. However, GF/01SWCNT/epoxy

composites needed less energy for the dispersion of mechanical energy by the frictional forces.

Tanδ peaks were calculated from the ratio of the loss and storage modulus and it represents the damping factor of the composites. Figure 5.25 illustrates the Tanδ values of GF/epoxy, GF/005SWCNT/epoxy, and GF/01SWCNT/epoxy composites in both directions. The mechanical damping efficiency increased with increasing SWCNT content. For reference samples energy dissipation through the GF and epoxy interface was poor, but energy dissipation increased with the addition of 0.5 wt.% SWCNT. During thermal cycling, micro-cracking is initiated and grew at the interface between the fiber and matrix. The flexibility of the polymer influences the microcrack density and T_g of the composites. Due to the restriction of polymer chain motion with the addition of SWCNT, the microcrack density and T_g of GF/epoxy composites decreased and increased, respectively.

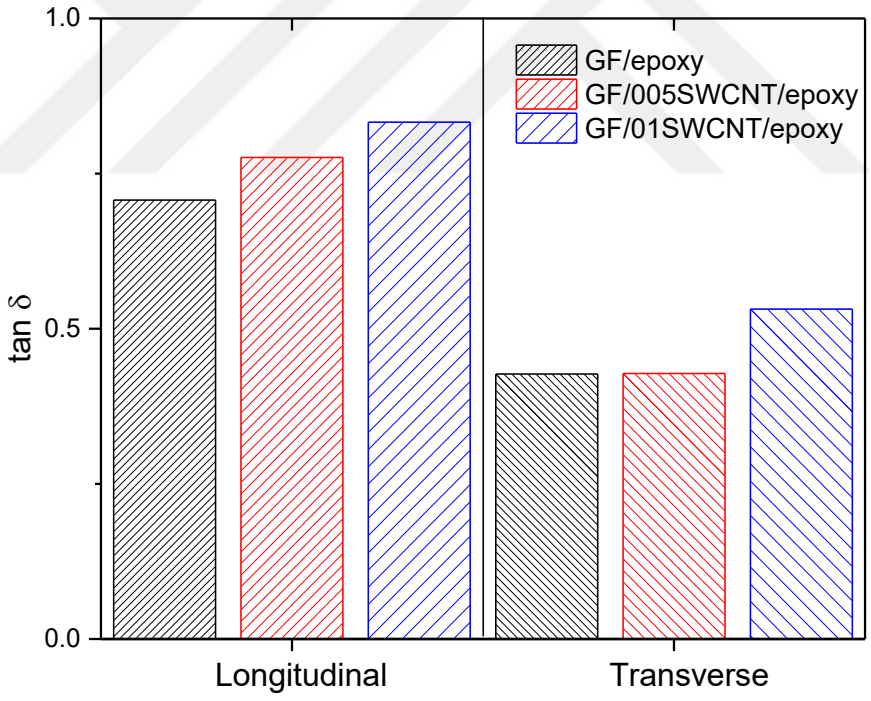

Figure 5.25 Tanδ peak values of both longitudinal and transverse CFRPC samples

5.9. Effects of Nano-Sized Fillers on the Mode-I Interlaminar Fracture Toughness of GF-based CFRPCs

The average load-displacement curves of the longitudinal and transverse DCB test specimens cut from the cylindrical GF/epoxy, GF/005SWCNT/epoxy, and GF/01SWCNT/epoxy with an inner diameter of 275 mm under the Mode I loading are shown in Figure 5.26 and Figure 5.27, respectively. The maximum loads have been achieved for GF/005SWCNT/epoxy composite samples in both transverse and longitudinal directions. The fiber-bridging effect during the Mode I loading of the DCB samples is shown in Figure 5.28 for the transverse and longitudinal specimens. While the crack propagation could be observed between the two adjacent layers properly for transverse specimens (Figure 5.28), the crack did not propagate after the pre-crack for long-GF/xSWCNT/epoxy specimens (Figure 5.29).

As shown in Figure 5.26 and Figure 5.27, there are two stages in the load-displacement curves; in the 1st stage, the load increased linearly with an increasing displacement until the crack progressed and it followed by a decrease in the initial slope, and in the 2nd stage, the load increased non-linearly with an increased displacement with the bridging effects of the fibers. In the 2nd stage, the bridging effects caused stick-slip behavior, which is known as resistance to crack propagation, is slightly observed for GF-based composites.

In the first stage, the load increased nearly linear and the incorporation of SWCNT decreased the initial slope for both transverse and longitudinal CFRPC specimens. In the second stage, the crack propagated while nonlinear behavior was observed, this is where stick-slip behavior was observed. The stick-slip behavior became more dominant with the incorporation of SWCNT, especially at 0.05 wt.% concentration. The fiber-bridging effect based on the stick-slip can be seen in Figure 5.28 (a) and Figure 5.28 (b) for trans- and long- GF/005SWCNT/epoxy composite, respectively. As can be seen in Figure 5.28, while the crack propagated in the middle of the plane for transverse DCB test specimens, the crack tended to move towards one layer from the other by crack jumping for the longitudinal specimens due to the transverse curvature of the sample. It has resulted in a lower effect of fiber-bridging [184].

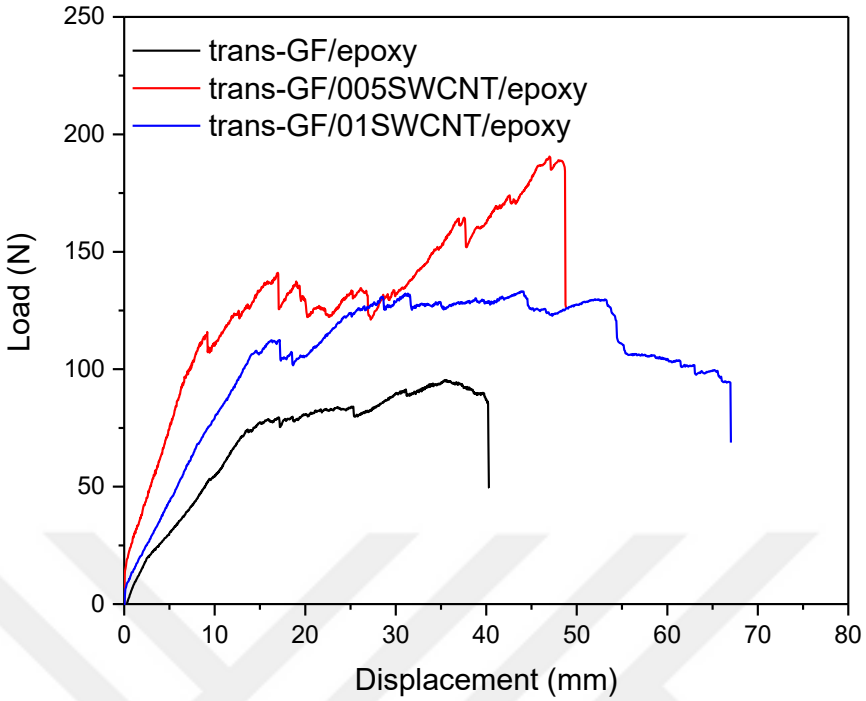

Figure 5.26 Load-displacement curves of transverse GF-based CFRPC DCB specimens under Mode-I loading

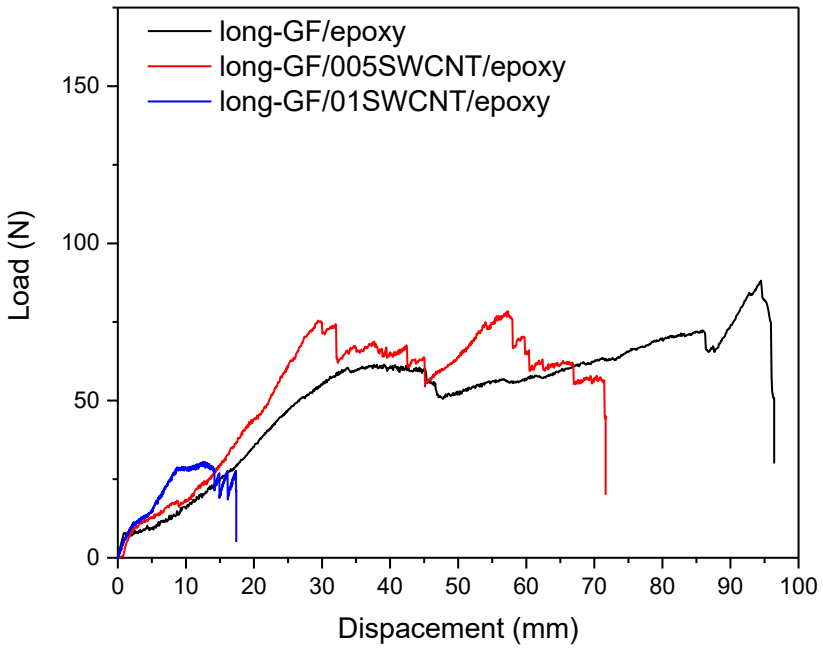

Figure 5.27 Load-displacement curves of longitudinal GF-based CFRPC DCB specimens under Mode-I loading

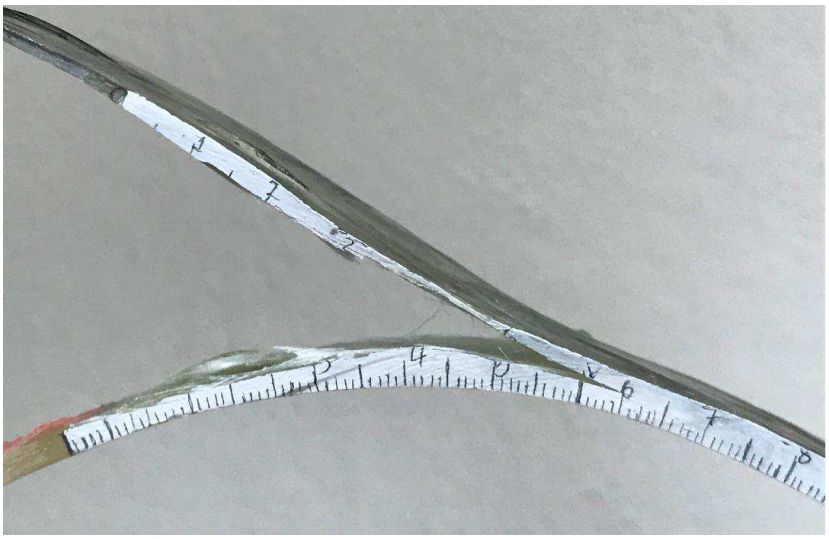

(a)

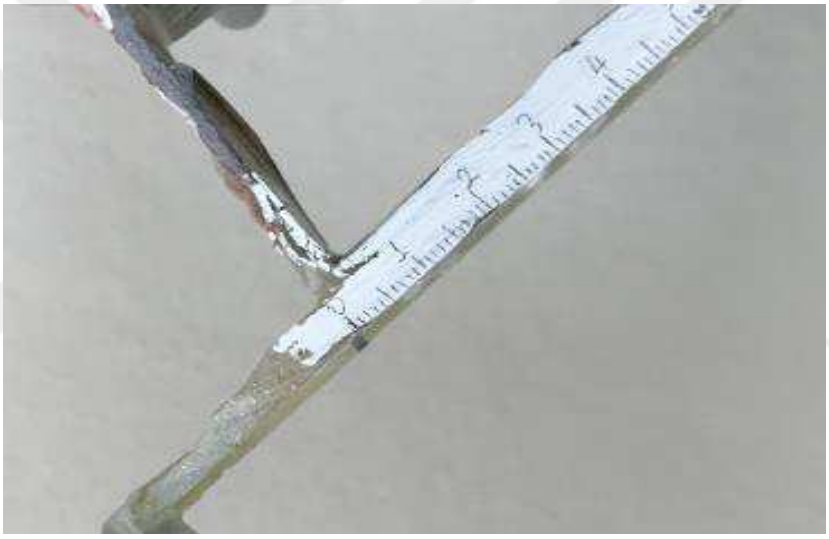

(b)

Figure 5.28 Fiber-bridging effect of (a) Transverse and (b) Longitudinal GF/005SWCNT/epoxy specimens during Mode I loading

Figure 5.29 (a) and (b) show the crack propagation of long-GF/01SWCNT/epoxy DCB specimen during pre-crack formation and after pre-crack formation, respectively. The crack propagation stopped after the pre-crack occurred, and the specimen was broken from the additive layer (Figure 5.29 (b)). This is because the SWCNT additive hardened the GF-based epoxy composite material and the sample was broken from the nonadditive part. Thus, not enough G_{Ic} values were calculated for long-GF/01SWCNT/epoxy (Figure 5.35).

(a)

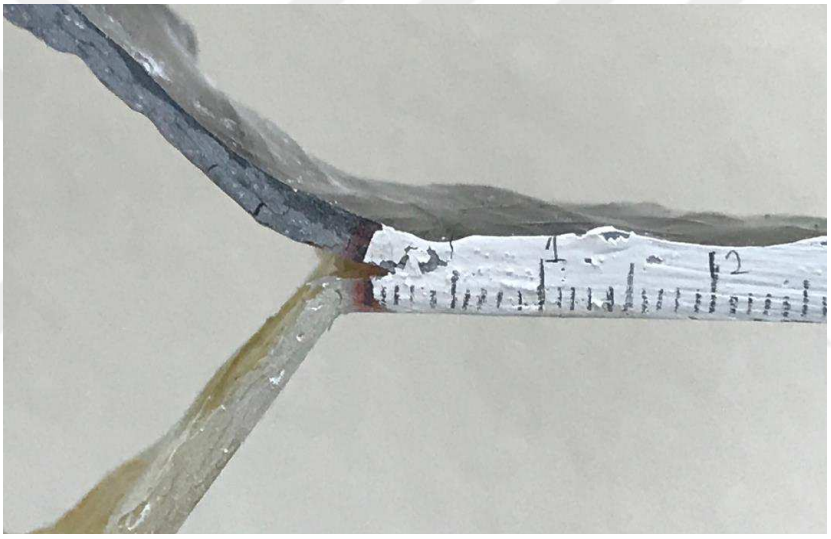

(b)

Figure 5.29 Long-GF/01SWCNT/epoxy during (a) Pre-crack loading and (b) After pre-crack loading

The Mode-I fracture toughness of DCB samples was calculated by using the equation (4.8) and R-curves are illustrated in the following graphics (Figure 5.30, Figure 5.31, Figure 5.32, Figure 5.33, Figure 5.34, and Figure 5.35). The number of data (N), mean, and minimum and maximum G_{Ic} values are shown in R-curves.

Figure 5.30 shows the R-curve of trans-GF/epoxy composite, and the initiation and propagation values were determined as 0.10 and 0.51 kJ/m^2, respectively. After $G_{Ic,ini}$=0.10 kJ/m^2 value, G_{Ic} raised with increasing crack growth, due to the fiber-

bridging toughening mechanism. Figure 5.31 and Figure 5.32 represent the delamination length-dependent G_{Ic} of trans-GF/005SWCNT/epoxy and trans-GF/01SWCNT/epoxy composites, respectively. Since the G_{Ic} value range was higher for trans-GF/005SWCNT/epoxy and trans-GF/01SWCNT/epoxy than for reference composite, incorporation of SWCNT has an extreme effect on the improvement of the Mode-I interlaminar fracture toughness. However, while the initiation of the Mode-I fracture toughness of trans-GF/005SWCNT/epoxy and trans-GF/01SWCNT/epoxy were remained almost the same compared to the reference sample, fracture toughness increased based on the fiber-bridging effect as the crack propagates. After the crack propagation, the G_{Ic} values started to increase and reached the maximum value of 2.13 and 3.35 kJ/m^2 for trans-GF/005SWCNT/epoxy and trans-GF/01SWCNT/epoxy, respectively. While the propagation of Mode I fracture toughness increased by about maximum %200, the maximum Mode I fracture toughness increased by about maximum %216 with the incorporation of 0.1 wt.% SWCNT.

Figure 5.33, Figure 5.34, and Figure 5.35 show the number of data (N), mean, and minimum and maximum G_{Ic} values of the long- GF/epoxy, GF/005SWCNT/epoxy, and GF/01SWCNT/epoxy, respectively. The number of data of composite samples in the transverse direction increased while it decreased for composite samples in the longitudinal direction with increasing SWCNT content. One of the most important reasons for this is the shape of the DCB test samples. The curvature at the transverse samples is in the direction of the crack propagation while for longitudinal samples this is in the vertical direction. Due to the longitudinal DCB test specimens showed non-stable crack growth, not enough G_{Ic} values were calculated. However, when the $G_{Ic,ini}$ value of longitudinal DCB samples compared with transverse DCB samples, it is higher for the longitudinal ones due to exhibiting a lower fiber angle.

The Mode I fracture toughness was obtained with the incorporation of nano-sized filler is much higher than the studies reported in the literature [35,76,192–195,200,146,152,167,169,188–191]. Furthermore, no studies have been reported in the literature that enhancing the Mode I interlaminar fracture toughness of GF-based CFRPCs, which produced by filament winding method with SWCNT toughened epoxy. The remarkable conclusion is that the Mode I fracture toughness of CFRPC DCB samples in the transverse direction was considerably increased in consequence of the usage of SWCNT incorporated epoxy only for the last layer of CFRPCs during the filament winding process.

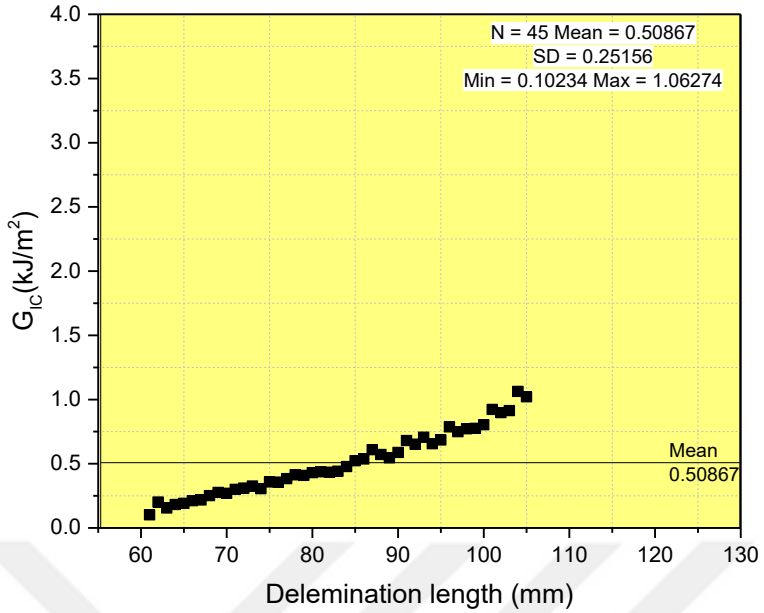

Figure 5.30 G_{Ic} vs. delamination length and average G_{Ic} value of trans-GF/epoxy

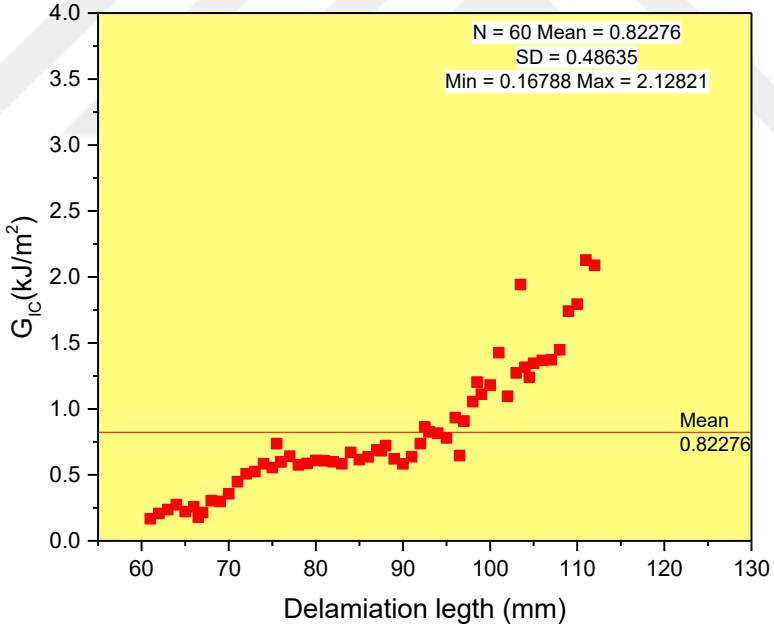

Figure 5.31 G_{Ic} vs. delamination length and average G_{Ic} value of trans-GF/005SWCNT/epoxy

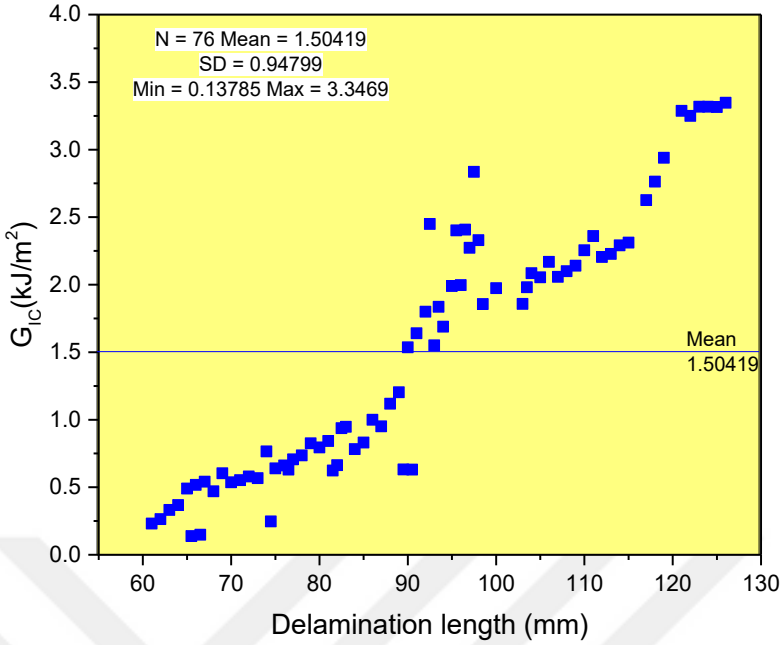

Figure 5.32 G_{Ic} vs. delamination length and average G_{Ic} value of trans-GF/01SWCNT/epoxy

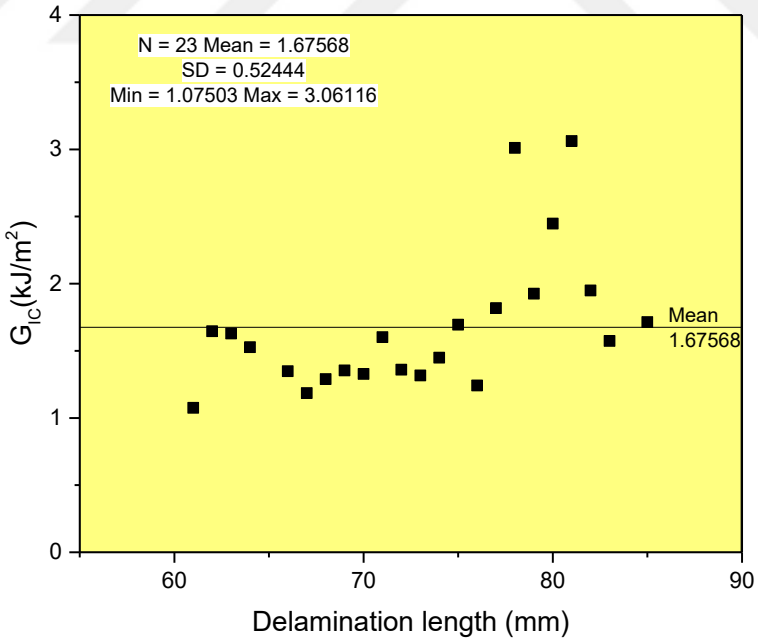

Figure 5.33 G_{Ic} vs. delamination length and average G_{Ic} value of long-GF/epoxy

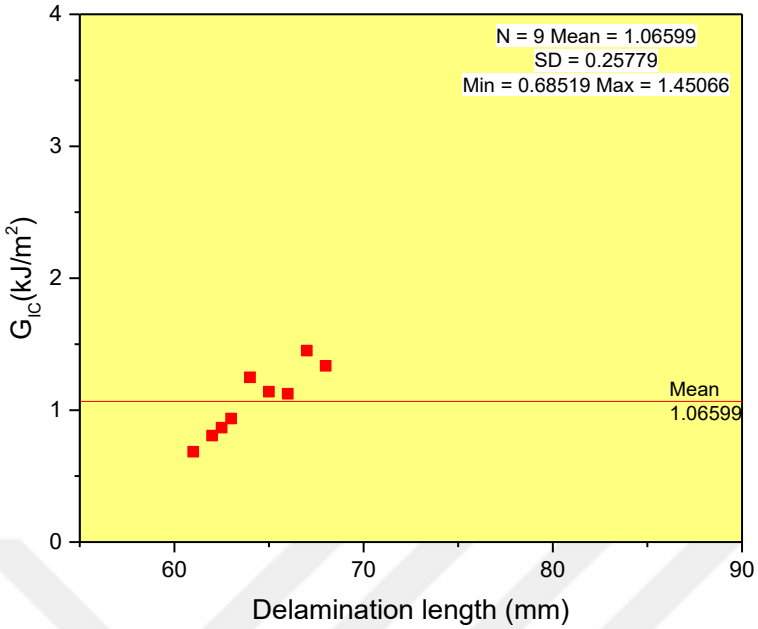

Figure 5.34 G_{Ic} vs. delamination length and average G_{Ic} value of long-GF/005SWCNT/epoxy

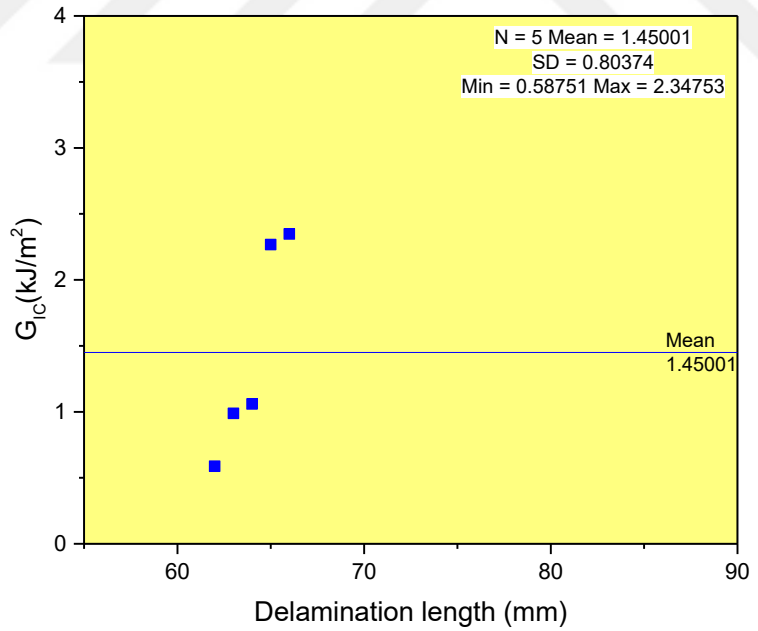

Figure 5.35 G_{Ic} vs. delamination length and average G_{Ic} value of long-GF/01SWCNT/epoxy

The fractured surfaces of the transverse DCB samples were examined under the SEM in different magnifications. The micrographs from the middle of two layers, which

are away from the initial crack, were taken as illustrated in Figure 5.36, Figure 5.37, and Figure 5.38 for trans- GF/epoxy, GF/005SWCNT/epoxy, and GF/01SWCNT/epoxy, respectively. As known, the fiber pull-out and bridging are the main fracture failures during Mode I loading. From the micrographs of the reference samples (GF/epoxy), the regular structure and smooth surface were evidence of easy crack propagation and less plastic deformation during crack propagation (Figure 5.36 (a)). In Figure 5.36 (c) smooth fiber surfaces and fiber prints occurring from the fiber debonding from the matrix of GF/epoxy fractured surfaces indicated the low fracture toughness. When the fractured surfaces of GF/005SWCNT/epoxy and GF/01SWCNT/epoxy were morphologically examined under the SEM, the roughness was increased with increasing SWCNT concentration (Figure 5.37 (b) and, Figure 5.38 (b)). Rough surfaced indicated that

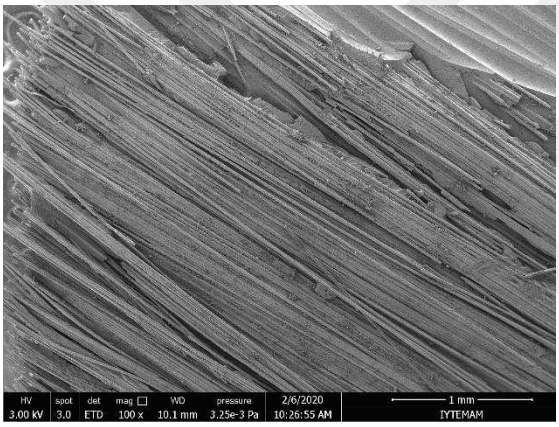

(a)

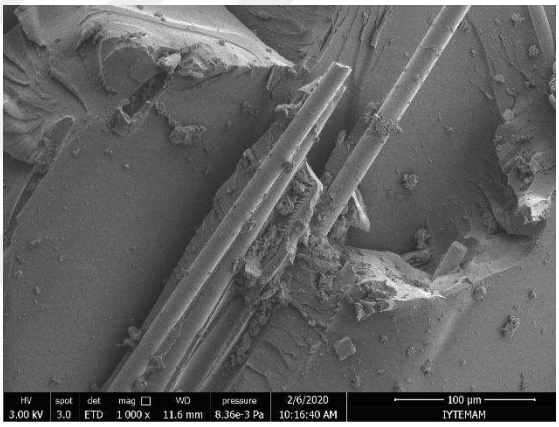

(b)

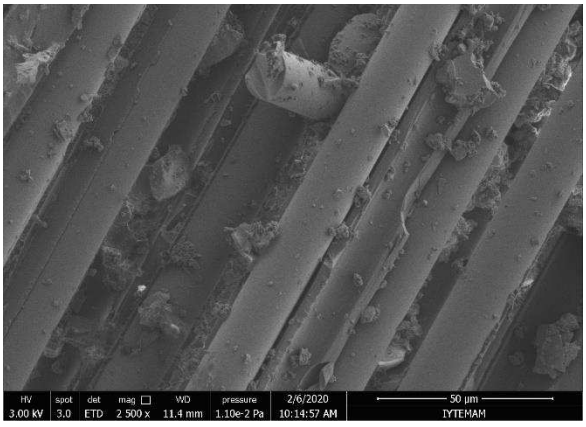

(c)

Figure 5.36 SEM images of GF/epoxy specimen fractured surface at (a)100x, (b) 1000x and (c) 2500x magnifications after DCB test

SWCNT incorporation enhanced the fracture toughness with the plastic deformation. This occurred as a result of the enhancement of the wettability of the fibers according to good interface adhesion between the GF and epoxy with the existence of SWCNT. Furthermore, fiber surfaces from the fractured surfaces of GF/005/SWCNT and GF/01SWCNT/epoxy covered up with epoxy as a result of enhancement of the interfacial adhesion between the fiber and epoxy with the incorporation of SWCNT within the epoxy matrix. Accordingly, the crack propagated not only through the interface between fiber and matrix but also the resin. The crack propagation through the resin was induced by the toughening mechanism at the epoxy resin region, such as fiber-bridging has shown in Figure 5.38 (c). For CFRPCs include SWCNT, both GF and SWCNT contributed to the improvement of the interlaminar Mode I fracture toughness. The microscopic examination

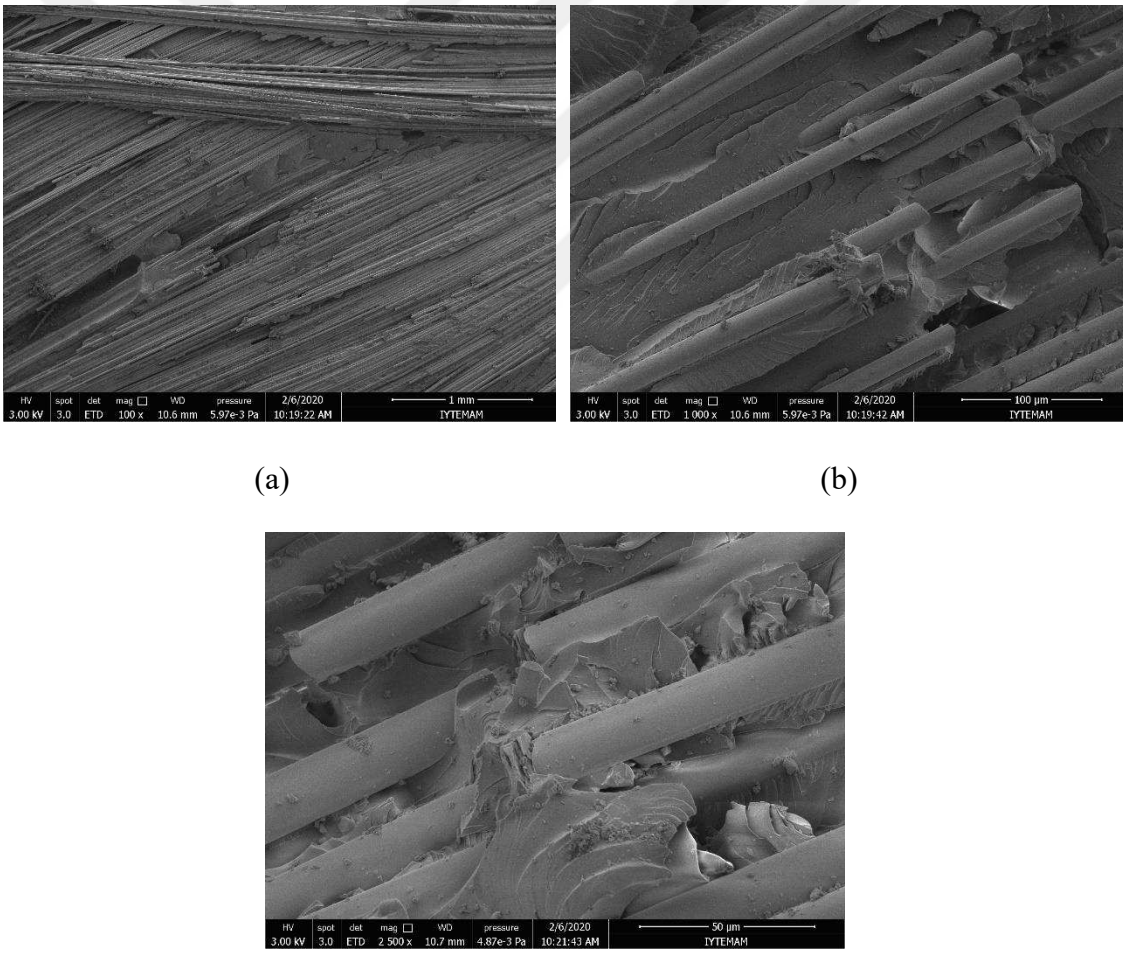

(a) (b)

(c)

Figure 5.37 SEM images of GF/005SWCNT/epoxy specimen fractured surface at (a)100x, (b) 1000x and (c) 2500x magnifications after DCB test

showed that the roles of SWCNT were; (1) enhance the adhesion between the epoxy and GF, and (2) participate in the fracture toughness mechanisms during Mode I loading.

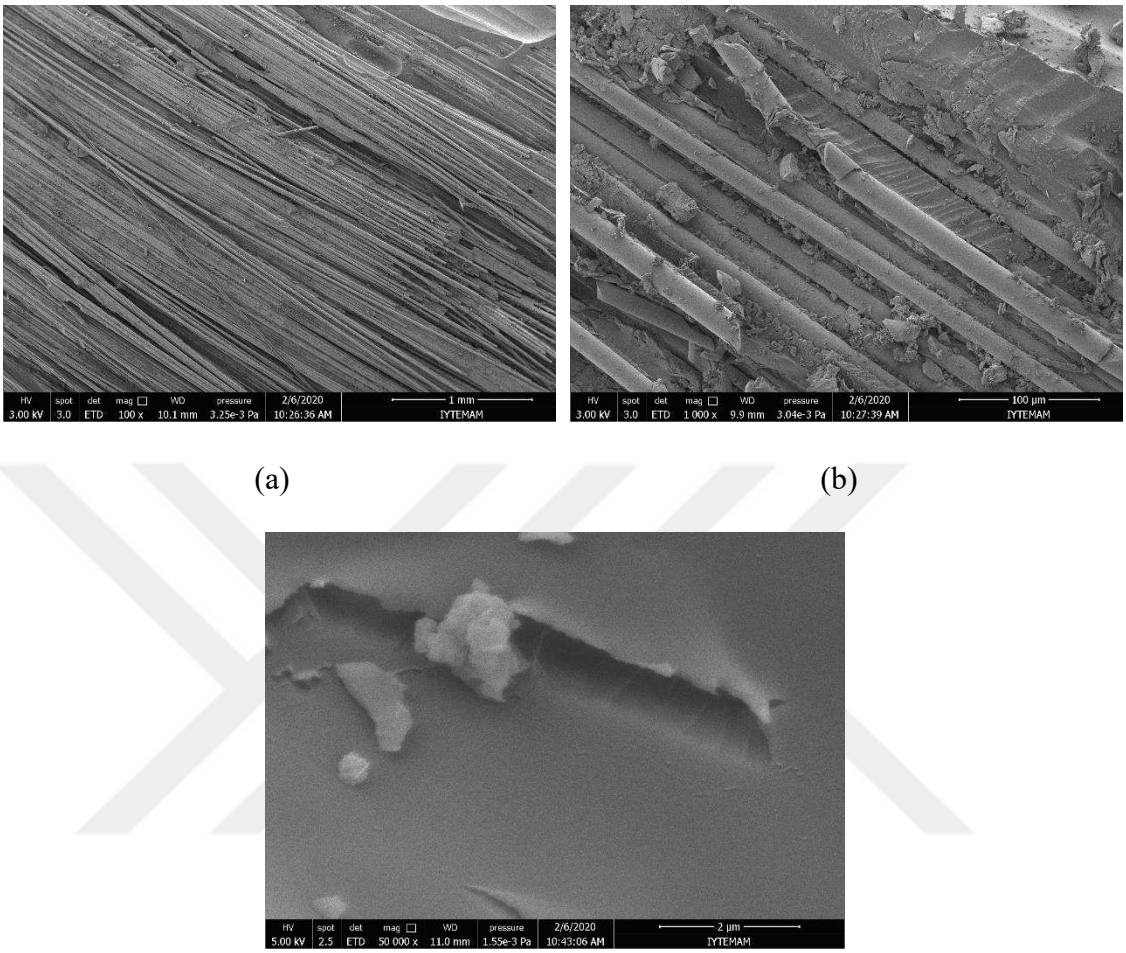

(a) (b)

(c)

Figure 5.38 SEM images of GF/01SWCNT/epoxy specimen fractured surface at (a)100x, (b)1000x, and (c) 2500x magnifications after DCB test

CHAPTER 6

CONCLUDING REMARKS AND FUTURE WORKS

6.1. Conclusions

In recent years application of the high-performance materials in the modern industry- especially transportation, aerospace, and gas, liquid and chemical storage- has been increasing. A wide variety of polymeric composites are used in the terms of compositions and architecture. A typical composite consists of a polymeric matrix and continuous fiber (GF, CF, BF, etc.), and is called FRPC. Pushing further for achieving performance targets and the further integration of structural system has created the concept of multi-functional FRPCs, which are called “multi-scale reinforced composites”. As these composites serve an enhanced performance, safety, and versatility and reduce product size, weight, cost, and power consumption, they have recently drawn the most attention from the researchers, who study composite materials.

In the laminated composite structures, delamination, which is the separation of the adjacent layers, is a common failure mode when the structure is exposed to the impact load. To enhance the delamination of the laminated composite structures, interlaminar properties (interlaminar fracture toughness) should be improved. In the literature recently several methods have been used to enhance delamination resistance, such as three-dimensional (3D) weaving, Z-pinning, and braiding, knitting and stitching, fiber hybridization, and interleaving film, fibers or particles between the composite, and toughening the matrix material with micro/nano-sized fillers (alumina, silica, carbon black, graphene, carbon nanotubes).

Potential impact loading can cause a bending moment in the curved regions, which results in delamination. In other words, the matrix and interface dominated properties, such as shear strength, fracture toughness, and impact damage resistance of CFRPCs should be improved. Toughening the matrix material with micro/nano-sized

fillers could be a promising technique for the production of filament wound cylindrical composite structures.

Nano-sized fillers -especially CNT- modification within the polymeric matrix enhances the mechanical properties, as well as the toughness of FRPCs. Intense efforts have been devoted to understanding the nano-scale and uncovering the capabilities of nano-scale materials offer to structural materials in the last decade. However, as this topic needs more study, the incorporation of nano-scale materials into FRPC for producing multi-scale reinforced composites has been studied widely in the literature.

This study considers to investigate the effect of the type and concentration of the nano-sized fillers on the mechanical, and rheological properties of the epoxy resin, and then evaluate the results for epoxy-based nanocomposites in the performance improvement of FW CFRPCs in terms of delamination, apparent hoop strength, interlaminar shear strength, and thermomechanical properties.

Different types of nano-sized fillers (SWCNT, TEGO, and HNT) in varying concentrations were used to developed epoxy-based nanocomposites. Since based on the literature, the calendaring (3-roll-mill) method is the most promising method for the dispersion of nano-sized fillers within the viscous resin, the calendaring method was used for the dispersion process for this study. Also, because the interfacial adhesion between the filler and matrix highly affects the final product performance with regards to a better dispersion, surface modified nano-sized fillers were used. Once the mechanical performance of the epoxy was improved by the incorporation of nano-sized fillers, the multi-scale CFRPCs were also produced. The used nano-sized filler should not only increase the performance of the epoxy but also not increase viscosity in a way that will affect the production of CFRPCs. Based on the results for the nanocomposites, noncovalently functionalized chemical-vapor-deposition-grown SWCNTs with ethoxylated alcohol was used as a nano-sized filler for the fabrication of filament wound multi-scale CFRPCs. In this context, the reference and SWCNT modified glass fiber (GF)-based CFRPCs with an inner diameter of 60 and 275 mm were manufactured by the filament winding method. The split-disk and three-point bending tests were performed for the reference and SWCNT reinforced GF-based CFRPCs. The double cantilever beam (DCB) test was also carried out on the reference and SWCNT reinforced GF-based composites to investigate the effect of SWCNT existence on the interlaminar fracture toughness of GF-based composites. The fractured surface after the DCB test were

analyzed under SEM to comprehend the toughening mechanisms, and micro-and nano-sized filler morphologies. Comparing the results, toughening the epoxy with SWCNT improved the interlaminar properties of the GF-based composites.

This thesis consists of mainly two parts which were explained in the following paragraphs.

The first stage of the thesis: Three different nano-sized fillers (SWCNT, TEGO, and HNT) were incorporated within Bisphenol-A-based epoxy resin for the production of NCs by the calendaring method. The results obtained from a series of mechanical testing showed that,

- While the addition of SWCNT improved not only the strength but also the strain at lower concentrations (0.0125, 0.025, and even 0.05 wt.% SWCNT), TEGO decreased the stress and the strain frankly, and HNT improved both the strength and strain slightly.
- The Mode I fracture toughness was improved frankly with the incorporation of both SWCNT at 0.025, 0.05, and 0.1 wt.% concentrations, and HNT at 0.5 wt.% concentration. However, Mode I of NCs was not significantly affected by the incorporation of TEGO.
- According to the flexural properties of NCs, the flexural strength of the NCs was increased with the addition of TEGO within the epoxy matrix.
- Viscosity results showed that, viscosity for the reference and 0.0125, 0.025, 0.05, and 0.1 wt.% SWCNT blended suspensions at room temperature (25^0C) and the low shear rate did not exceed 2.0 Pa.s, which is a suitable viscosity value during the filament winding for wetting the continuous filament. Also, during the curing cycle of CFRPCs, the viscosity of the used SWCNT incorporated epoxy suspensions was not significantly affected.
- The pendant drop method showed that the propagation of the epoxy matrix on the GF was not significantly affected by the presence of SWCNT within the epoxy suspension.

The second stage of the thesis: The reference and SWCNT reinforced GF-based CFRPCs with an inner diameter of 60 and 275mm were manufactured by the filament winding method. The produced reference and SWCNT reinforced CFRPCs were tested

with a series of mechanical tests. The mechanical and the thermomechanical results followed as;

- As cylindrical structures are generally used under internal pressure where high hoop stresses are developed, a split-disk test was performed for the unnotched and notched rings cut from CFRPCs with an inner diameter of 60 mm. The apparent hoop strength for the unnotched and notched ring specimens (by about max 16%) and Mode I for the notched ring specimens (by about max %36) were improved with the existence of SWCNT at the last layer of the cylinders.
- Three-point bending tests were performed to determine the flexural and ILSS properties of CFRPCs with an inner diameter of 60 and 275mm. While the flexural strength was increased with increasing SWCNT content, ILSS was increased maximum with the incorporation of 0.05 wt.% SWCNT.
- Regardless of fiber orientation (transverse or longitudinal), the glass transition temperature value slightly increased with the contribution of SWNCT. However, Tanδ values changed depending on the fiber orientation and SWCNT incorporation.
- According to the DCB test results; while SWCNT contribution on the last layer of CFRPCs with an inner diameter of 275 mm improved Mode I interlaminar fracture toughness in the transverse direction by about a maximum of 216%, SWCNT contribution effect on the Mode I interlaminar fracture toughness in the longitudinal direction could not be performed efficiently due to not obtaining sufficient data.

Lastly, if the average cost feasibility of the produced cylindrical composites is made, the price has increased by and an average of 220 dollars, which is caused by the usage of SWCNT. However, an extra 220 dollars investment in the production of these multi-scale cylindrical composites enhances the performance. Also, the usage of SWCNT was lowered in this study by instead of using SWCNT incorporated epoxy in the production of all layers of cylindrical composites, it is used only for the outer layer of the composite.

6.2. Future Works

Toughening the matrix resin with the incorporation of nano-sized fillers offers great potential for the performance enhancement of the multi-scale composites. The result of this thesis study showed that the production of the cylindrical composites with SWCNT incorporated epoxy resin for only the last layer at even low concentrations enhances the interlaminar fracture toughness, hoop strength, flexural strength, and interlaminar shear strength.

In the production of portable tanks used to store the hydrogen gas in consequence of the impact to the outer layer of the structure, and delamination may be occurred due to the bending. External impacts and even internal pressure accelerate the delamination progress. For this reason, improving the fracture toughness, which is a matrix-dominated property, of the composites should be handled and carefully studied for the cylindrical composites. In this thesis, materials used for the production of filament wound pressure vessels were examined and many studies were carried out to enhance their performance. However, as it is a large field of study, there are incompleted and unfinished studies needed a full understanding.

From the research perspective, there many challenging gaps needed to fully understand;

- The behavior of cylindrical composites under the Mode I loading was studied in recent decades both experimentally and numerically. However, how nano-sized filler content affects the behavior of cylindrical composites under Mode I and Mode II remain a question. Also, during fatigue loading of these composites should be clarified due to the difficulty to detect the crack propagation.
- Air conditioning effect on the cylindrical composite pipes needed to be clarified due to the application of composite pipes underground, in-water, etc. The nano-sized filler addition concept can be investigated for this field.
- Although there are a few studies that produced composite pressure vessels with the toughened matrix resin, these studies should be diversified for

completely understanding the nano-sized effects on the performance of CFRPCs.

- For recycling, the materials thermoplastic instead of thermoset resin could be used as a matrix material for the production of CFRPCs. As thermoplastics have fewer mechanical properties than thermosets, the mechanical performance of the thermoplastic can also be improved with the incorporation of nano-sized fillers, which have been studied widely in the literature.
- The production of longer CFRPCs with a 275 mm inner diameter may be a solution for DCB test problems in terms of a stable thickness of the specimens.
- Even toughness mechanism (fiber-bridging) does not occur in Mode II, the calculation of interlaminar fracture toughness under in-plane shear deformation load can provide further information about the interlaminar properties.

REFERENCES

(1) IEA. The Future of Hydrogen https://www.iea.org/reports/the-future-of-hydrogen. https://doi.org/10.1787/1e0514c4-en.

(2) World Energy Technology Outlook 2050–WETO-H2. *Office for Official Publications of the European Communities*. Luxembourg 2006.

(3) Wang, S.; Ge, M. Everything You Need to Know About the Fastest-Growing Source of Global Emissions: Transport https://www.wri.org/blog/2019/10/everything-you-need-know-about-fastest-growing-source-global-emissions-transport#:~:text=Emissions from the transport sector,emissions from burning fossil fuels.

(4) Lynch, F. Hydrogen As A Transportation Fuel. In *An End to Global Warming*; Pergamon: Amsterdam, 2002; pp 127–154.

(5) Basile, A.; Iulianelli, A. *Advances in Hydrogen Production, Storage and Distribution*; Elsevier, 2014.

(6) Grouset, D.; Ridart, C. Lowering Energy Spending Together With Compression, Storage, and Transportation Costs for Hydrogen Distribution in the Early Market. In *Hydrogen Supply Chains*; Academic Press, 2018; pp 201–270.

(7) Stetson, N. T.; McWhorter, S.; Ahn, C. C. Introduction to Hydrogen Storage. In *Compendium of Hydrogen Energy*; Woodhead Publishing, 2016; pp 3–25. https://doi.org/10.1016/b978-1-78242-362-1.00001-8.

(8) Hydrogen Storage https://www.energy.gov/eere/fuelcells/hydrogen-storage.

(9) Laurent, A. ELECTRIC, HYBRID, HYDROGEN: UNDERSTANDING THE DIFFERENCES https://easyelectriclife.groupe.renault.com/en/outlook/technology/electric-hybrid-hydrogen-understanding-the-differences/.

(10) Krishna, R.; Titus, E.; Salimian, M.; Okhay, O.; Rajendran, S.; Rajkumar, A.; G. Sousa, J. M.; C. Ferreira, A. L.; Campos, J.; Gracio, J. Hydrogen Storage for Energy Application. *Hydrog. Storage* **2012**. https://doi.org/10.5772/51238.

(11) U.S. DRIVE Partnership. *Hydrogen Storage Tech Team Roadmap*; 2017.

(12) Demir, I.; Sayman, O.; Dogan, A.; Arikan, V.; Arman, Y. The Effects of Repeated Transverse Impact Load on the Burst Pressure of Composite Pressure Vessel.

Compos. Part B Eng. **2015**, *68*, 121–125. https://doi.org/10.1016/j.compositesb.2014.08.038.

(13) Dorneanu, L. New "Quantum Alloy" Could Improve Hydrogen Storage for Fuel Cells https://news.softpedia.com/news/New-Quantum-Alloy-Could-Improve-Hydrogen-Storage-for-Fuel-Cells-58778.shtml.

(14) Hull, D.; Clyne, T. W. *An Introduction to Composite Materials*, 2nd ed.; Clark, D. R., Suresh, S., Ward FRS, I. M., Eds.; Cambridge University Press, 1996. https://doi.org/10.1017/CBO9781139170130.

(15) Yu, K.; Morozov, E. V.; Ashraf, M. A.; Shankar, K. A Review of the Design and Analysis of Reinforced Thermoplastic Pipes for Offshore Applications. *J. Reinf. Plast. Compos.* **2017**, *36* (20), 1514–1530. https://doi.org/10.1177/0731684417713666.

(16) Thomas, S.; Sinturel, C.; Thomas, R. *Micro and Nanostructured Epoxy/Rubber Blends*; 2014. https://doi.org/10.1002/9783527666874.

(17) Ozdemir, N. G.; Zhang, T.; Aspin, I.; Scarpa, F.; Hadavinia, H.; Song, Y. Toughening of Carbon Fibre Reinforced Polymer Composites with Rubber Nanoparticles for Advanced Industrial Applications. **2016**, *10* (5), 394–407. https://doi.org/10.3144/expresspolymlett.2016.37.

(18) Liu, W.; Hoa, S. V.; Pugh, M. Fracture Toughness and Water Uptake of High-Performance Epoxy/Nanoclay Nanocomposites. *Compos. Sci. Technol.* **2005**, *65* (15–16 SPEC. ISS.), 2364–2373. https://doi.org/10.1016/j.compscitech.2005.06.007.

(19) Manjunath, M.; Renukappa, N. M.; Suresha, B. Influence of Micro and Nanofillers on Mechanical Properties of Pultruded Unidirectional Glass Fiber Reinforced Epoxy Composite Systems. **2015**. https://doi.org/10.1177/0021998315588623.

(20) Rafiee, R. Apparent Hoop Tensile Strength Prediction of Glass Fiber-Reinforced Polyester Pipes. *J. Compos. Mater.* **2013**, *47* (11), 1377–1386. https://doi.org/10.1177/0021998312447209.

(21) Manoj Prabhakar, M.; Rajini, N.; Ayrilmis, N.; Mayandi, K.; Siengchin, S.; Senthilkumar, K.; Karthikeyan, S.; Ismail, S. O. An Overview of Burst, Buckling, Durability and Corrosion Analysis of Lightweight FRP Composite Pipes and Their Applicability. *Compos. Struct.* **2019**, *230* (January), 111419. https://doi.org/10.1016/j.compstruct.2019.111419.

(22) Water, A.; Association, W. *Fiberglass Pipe Design*; 1999.

(23) Hu, G.; Bai, J.; Demianouchko, E.; Bompard, P. Mechanical Behaviour of ±55° Filament-Wound Glass-Fibre/Epoxy-Resin Tubes - III. Macromechanical Model of the Macroscopic Behaviour of Tubular Structures with Damage and Failure Envelope Prediction. *Compos. Sci. Technol.* **1998**, *58* (1), 19–29. https://doi.org/10.1016/S0266-3538(97)00078-X.

(24) Bai, J.; Hu, G.; Bompard, P. Mechanical Behaviour of ±55° Filament-Wound Glass-Fibre/Epoxy-Resin Tubes: II. Micromechanical Model of Damage Initiation and the Competition between Different Mechanisms. *Compos. Sci. Technol.* **1997**, *57* (2), 155–164. https://doi.org/10.1016/S0266-3538(96)00125-X.

(25) Bai, J.; Seeleuthner, P.; Bompard, P. Mechanical Behaviour of ±55° Filament-Wound Glass-Fibre/Epoxy-Resin Tubes: I. Microstructural Analyses, Mechanical Behaviour and Damage Mechanisms of Composite Tubes under Pure Tensile Loading, Pure Internal Pressure, and Combined Loading. *Compos. Sci. Technol.* **1997**, *57* (2), 141–153. https://doi.org/10.1016/S0266-3538(96)00124-8.

(26) Sulaiman, S.; Borazjani, S.; Tang, S. H. Finite Element Analysis of Filament-Wound Composite Pressure Vessel under Internal Pressure. *IOP Conf. Ser. Mater. Sci. Eng.* **2013**, *50* (1). https://doi.org/10.1088/1757-899X/50/1/012061.

(27) Evans, J. T.; Gibson, A. G. Composite Angle Ply Laminates and Netting Analysis. *Proc. R. Soc. A Math. Phys. Eng. Sci.* **2002**, *458* (2028), 3079–3088. https://doi.org/10.1098/rspa.2002.1066.

(28) Li, Y.; Huang, X.; Zeng, L.; Li, R.; Tian, H.; Fu, X.; Wang, Y.; Zhong, W. H. A Review of the Electrical and Mechanical Properties of Carbon Nanofiller-Reinforced Polymer Composites. *J. Mater. Sci.* **2019**, *54* (2), 1036–1076. https://doi.org/10.1007/s10853-018-3006-9.

(29) Domun, N.; Hadavinia, H.; Zhang, T.; Sainsbury, T.; Liaghat, G. H.; Vahid, S. Improving the Fracture Toughness and the Strength of Epoxy Using Nanomaterials-a Review of the Current Status. *Nanoscale* **2015**, *7* (23), 10294–10329. https://doi.org/10.1039/c5nr01354b.

(30) Ma, P. C.; Siddiqui, N. A.; Marom, G.; Kim, J. K. Composites : Part A Dispersion and Functionalization of Carbon Nanotubes for Polymer-Based Nanocomposites : A Review. *Compos. Part A* **2010**, *41* (10), 1345–1367. https://doi.org/10.1016/j.compositesa.2010.07.003.

(31) Fiedler, B.; Gojny, F. H.; Wichmann, M. H. G.; Nolte, M. C. M.; Schulte, K. Fundamental Aspects of Nano-Reinforced Composites. *Compos. Sci. Technol.* **2006**, *66* (16), 3115–3125. https://doi.org/10.1016/j.compscitech.2005.01.014.

(32) Baltopoulos, A.; Kostopoulos, V. Multifunctional Carbon Nanotube-Based Nano-Composites for Aerospace Applications. In *Multifunctionality of Polymer Composites: Challenges and New Solutions*; 2015; pp 448–490.

(33) Nofar, M.; Hoa, S. V.; Pugh, M. D. Failure Detection and Monitoring in Polymer Matrix Composites Subjected to Static and Dynamic Loads Using Carbon Nanotube Networks. *Compos. Sci. Technol.* **2009**, *69* (10), 1599–1606. https://doi.org/10.1016/j.compscitech.2009.03.010.

(34) Chandrasekaran, S.; Sato, N.; Tölle, F.; Mülhaupt, R.; Fiedler, B.; Schulte, K. Fracture Toughness and Failure Mechanism of Graphene Based Epoxy Composites. *Compos. Sci. Technol.* **2014**, *97*, 90–99. https://doi.org/10.1016/j.compscitech.2014.03.014.

(35) Ye, Y.; Chen, H.; Wu, J.; Ming, C. Interlaminar Properties of Carbon Fiber Composites with Halloysite Nanotube-Toughened Epoxy Matrix. **2011**, *71*, 717–723. https://doi.org/10.1016/j.compscitech.2011.01.018.

(36) Huang, J. C. Carbon Black Filled Conducting Polymers and Polymer Blends. *Adv. Polym. Technol.* **2002**, *21* (4), 299–313. https://doi.org/10.1002/adv.10025.

(37) Gojny, F. H.; Wichmann, M. H. G.; Köpke, U.; Fiedler, B.; Schulte, K. Carbon Nanotube-Reinforced Epoxy-Composites: Enhanced Stiffness and Fracture Toughness at Low Nanotube Content. *Compos. Sci. Technol.* **2004**, *64* (15), 2363–2371. https://doi.org/10.1016/J.COMPSCITECH.2004.04.002.

(38) Abdel-Aal, N.; El-Tantawy, F.; Al-Hajry, A.; Bououdina, M. Epoxy Resin/Plasticized Carbon Black Composites. Part II. Correlation among Network Structure and Mechanical Properties. *Polym. Compos.* **2008**, *29* (7), 804–808.

(39) Mamunya, Y. P.; Davydenko, V. V; Pissis, P.; Lebedev, E. V. Electrical and Thermal Conductivity of Polymers FIlled.Pdf. *Eur. Polym. J.* **2002**, *38*, 1887–1897.

(40) Li, Y.; Wang, S.; Zhang, Y.; Zhang, Y. Carbon Black-Filled Immiscible Polypropylene/Epoxy Blends. *J. Appl. Polym. Sci.* **2006**, *99* (2), 461–471. https://doi.org/10.1002/app.22011.

(41) Alam, M. K.; Islam, M. T.; Mina, M. F.; Gafur, M. A. Structural, Mechanical,

Thermal, and Electrical Properties of Carbon Black Reinforced Polyester Resin Composites. *J. Appl. Polym. Sci.* **2014**, *131* (13), 1–11. https://doi.org/10.1002/app.40421.

(42) Carbas, R. J. C.; da Silva, L. F. M.; Andrés, L. F. S. Effect of Carbon Black Nanoparticles Concentration on the Mechanical Properties of a Structural Epoxy Adhesive. *Proc. Inst. Mech. Eng. Part L J. Mater. Des. Appl.* **2018**, *232* (5), 403–415. https://doi.org/10.1177/1464420716629046.

(43) Vilgis, T. A.; Heinrich, G.; Klüppel, M. *Reinforcement of Polymer Nano-Composites: Theory, Experiments and Applications*; Cambridge University Press, 2009.

(44) Iijima, S. Helical Microtubules of Graphitic Carbon. *Nature* **1991**. https://doi.org/10.1038/354056a0.

(45) Nesterenko, A. M.; Kolesnik, N. F.; Akhmatov, Y. S.; Sukhomlin, V. I.; Prilutski, O. V. Metals 3 UDK 869.173. 23. *News Acad. Sci. USSR* **1982**, *12*, 16.

(46) Oberlin, A.; Endo, M.; Koyama, T. Filamentous Growth of Carbon through Benzene Decomposition. *J. Cryst. Growth* **1976**. https://doi.org/10.1016/0022-0248(76)90115-9.

(47) Kokarneswaran, M.; Selvaraj, P.; Ashokan, T.; Perumal, S.; Sellappan, P.; Murugan, K. D.; Ramalingam, S.; Mohan, N.; Chandrasekaran, V. Discovery of Carbon Nanotubes in Sixth Century BC Potteries from Keeladi, India. *Sci. Rep.* **2020**, *10* (1), 1–6. https://doi.org/10.1038/s41598-020-76720-z.

(48) Dresselhaus, M. S.; Dresselhaus, G.; Saito, R. Physics of Carbon Nanotubes. *Carbon N. Y.* **1995**, *33* (7), 883–891. https://doi.org/10.1016/0008-6223(95)00017-8.

(49) Harris, P. J. F. Carbon Nanotubes and Related Structures: New Materials for the Twenty-First Century. **1999**, 294. https://doi.org/10.1016/S0008-6223(00)00037-3.

(50) Ruoff, R. S.; Qian, D.; Liu, W. K. Mechanical Properties of Carbon Nanotubes: Theoretical Predictions and Experimental Measurements. *Comptes Rendus Phys.* **2003**, *4* (9), 993–1008. https://doi.org/10.1016/j.crhy.2003.08.001.

(51) Gojny, F. H.; Wichmann, M. H. G.; Fiedler, B.; Bauhofer, W.; Schulte, K. Influence of Nano-Modification on the Mechanical and Electrical Properties of Conventional Fibre-Reinforced Composites. *Compos. Part A Appl. Sci. Manuf.*

2005, *36* (11), 1525–1535. https://doi.org/10.1016/J.COMPOSITESA.2005.02.007.

(52) Shtein, M.; Nadiv, R.; Lachman, N.; Daniel Wagner, H.; Regev, O. Fracture Behavior of Nanotube-Polymer Composites: Insights on Surface Roughness and Failure Mechanism. *Compos. Sci. Technol.* **2013**, *87*, 157–163. https://doi.org/10.1016/j.compscitech.2013.07.016.

(53) Schmid, C. F. *Simulations of Flocculation in Flowing Fiber Suspensions*; University of Wisconsin--Madison, 1999.

(54) Paipetis, A. S.; Kostopoulos, V. *Carbon Nanotube Enhanced Aerospace Composite Materials: A New Generation of Multifunctional Hybrid Structural Composites*; 2013. https://doi.org/10.1007/978-94-007-4246-8.

(55) Mittal, V. *Polymer-Graphene Nanocomposites*; Royal Society of Chemistry, 2012; Vol. 26.

(56) Bortz, D. R.; Heras, E. G.; Martin-Gullon, I. Impressive Fatigue Life and Fracture Toughness Improvements in Graphene Oxide/Epoxy Composites. *Macromolecules* **2011**, *45* (1), 238–245.

(57) Okan, B. S.; Alp, Y.; Yuda, Y. Polypyrrole Coated Thermally Exfoliated Graphite Nanoplatelets and the Effect of Oxygen Surface Groups on the Interaction of Platinum Catalysts with Graphene-Based Nanocomposites. *Ind. Eng. Chem. Res.* **2011**, *50* (22), 12562–12571. https://doi.org/10.1021/ie201613f.

(58) Bunch, J. S.; Van Der Zande, A. M.; Verbridge, S. S.; Frank, I. W.; Tanenbaum, D. M.; Parpia, J. M.; Craighead, H. G.; McEuen, P. L. Electromechanical Resonators from Graphene Sheets. *Science (80-.).* **2007**, *315* (5811), 490–493.

(59) Liang, J.; Wang, Y.; Huang, Y.; Ma, Y.; Liu, Z.; Cai, J. Letter to the Editor Electromagnetic Interference Shielding of Graphene / Epoxy Composites. *Carbon N. Y.* **2008**, *47* (3), 922–925. https://doi.org/10.1016/j.carbon.2008.12.038.

(60) Xia, F.; Mueller, T.; Lin, Y.; Valdes-Garcia, A.; Avouris, P. Ultrafast Graphene Photodetector. *Nat. Nanotechnol.* **2009**, *4* (12), 839.

(61) Tang, L.; Wan, Y.; Yan, D.; Pei, Y.; Zhao, L.; Li, Y. The Effect of Graphene Dispersion on the Mechanical Properties of Graphene / Epoxy Composites. *Carbon N. Y.* **2013**, *60*, 16–27. https://doi.org/10.1016/j.carbon.2013.03.050.

(62) Mukhopadhyay, P.; Gupta, R. K. *Graphite, Graphene, and Their Polymer Nanocomposites*; CRC Press, 2012.

(63) Raimond, J. M.; Brune, M.; Computation, Q.; Martini, F. De; Monroe, C. Electric Field Effect in Atomically Thin Carbon Films. *Science (80-.).* **2004**, *306* (5696), 666–669.

(64) Kim, K. S.; Zhao, Y.; Jang, H.; Lee, S. Y.; Kim, J. M.; Kim, K. S.; Ahn, J.-H.; Kim, P.; Choi, J.-Y.; Hong, B. H. Large-Scale Pattern Growth of Graphene Films for Stretchable Transparent Electrodes. *Nature* **2009**, *457*, 706.

(65) Sutter, P. W.; Flege, J.-I.; Sutter, E. A. Epitaxial Graphene on Ruthenium. *Nat. Mater.* **2008**, *7*, 406.

(66) Choucair, M.; Thordarson, P.; Stride, J. A. Gram-Scale Production of Graphene Based on Solvothermal Synthesis and Sonication. *Nat. Nanotechnol.* **2008**, *4*, 30.

(67) McAllister, M. J.; Li, J.-L.; Adamson, D. H.; Schniepp, H. C.; Abdala, A. A.; Liu, J.; Herrera-Alonso, M.; Milius, D. L.; Car, R.; Prud'homme, R. K.; et al. Single Sheet Functionalized Graphene by Oxidation and Thermal Expansion of Graphite. *Chem. Mater.* **2007**, *19* (18), 4396–4404. https://doi.org/10.1021/cm0630800.

(68) Hernández-Pérez, A.; Avilés, F.; May-Pat, A.; Valadez-González, A.; Herrera-Franco, P. J.; Bartolo-Pérez, P. Effective Properties of Multiwalled Carbon Nanotube/Epoxy Composites Using Two Different Tubes. *Compos. Sci. Technol.* **2008**, *68* (6), 1422–1431. https://doi.org/10.1016/j.compscitech.2007.11.001.

(69) Acik, M.; Chabal, Y. J. A Review on Reducing Graphene Oxide for Band Gap Engineering. *J. Mater. Sci. Res.* **2012**, *2* (1). https://doi.org/10.5539/jmsr.v2n1p101.

(70) Potts, J. R.; Dreyer, D. R.; Bielawski, C. W.; Ruoff, R. S. Graphene-Based Polymer Nanocomposites. *Polymer (Guildf).* **2011**, *52* (1), 5–25. https://doi.org/10.1016/j.polymer.2010.11.042.

(71) Aloia, A. G. D.; Proietti, A.; Bidsorkhi, H. C.; Tamburrano, A.; Bellis, G. De; Marra, F.; Bregnocchi, A.; Sarto, M. S. Properties of Graphene-Thermoset Polymer Composites Produced Using Acetone-DMF Solvents. *Polymers (Basel).* **2018**, *10* (1), 82. https://doi.org/10.3390/polym10010082.

(72) Chatterjee, S.; Wang, J. W. W.; Kuo, W. S. S.; Tai, N. H. H.; Salzmann, C.; Li, W. L. L.; Hollertz, R.; Nüesch, F. A. A.; Chu, B. T. T. T. T. T. Mechanical Reinforcement and Thermal Conductivity in Expanded Graphene Nanoplatelets Reinforced Epoxy Composites. *Chem. Phys. Lett.* **2012**, *531*, 6–10. https://doi.org/10.1016/J.CPLETT.2012.02.006.

(73) Ganguli, S.; Roy, A. K.; Anderson, D. P. Improved Thermal Conductivity for Chemically Functionalized Exfoliated Graphite / Epoxy Composites. *Carbon N. Y.* **2008**, *46* (5), 806–817. https://doi.org/10.1016/j.carbon.2008.02.008.

(74) Self-, D.; Nanostructures, C. The Piezoresistive Effect in Graphene- Based Polymeric Composites. **2013**. https://doi.org/10.1088/0957-4484/24/46/465702.

(75) Seyyed Monfared Zanjani, J.; Saner Okan, B.; Menceloglu, Y. Manufacturing of Multilayer Graphene Oxide/Poly(Ethylene Terephthalate) Nanocomposites with Tunable Crystallinity, Chain Orientations and Thermal Transitions. *Mater. Chem. Phys.* **2016**, *176*, 58–67. https://doi.org/10.1016/j.matchemphys.2016.03.020.

(76) Wichmann, M. H. G.; Sumfleth, J.; Gojny, F. H. Glass-Fibre-Reinforced Composites with Enhanced Mechanical and Electrical Properties – Benefits and Limitations of a Nanoparticle Modified Matrix. **2006**, *73*, 2346–2359. https://doi.org/10.1016/j.engfracmech.2006.05.015.

(77) Johnsen, B. B.; Kinloch, A. J.; Mohammed, R. D.; Taylor, A. C.; Sprenger, S. Toughening Mechanisms of Nanoparticle-Modified Epoxy Polymers. *Polymer (Guildf).* **2007**, *48* (2), 530–541. https://doi.org/10.1016/j.polymer.2006.11.038.

(78) Zeng, S.; Reyes, C.; Liu, J.; Rodgers, P. A.; Wentworth, S. H.; Sun, L. Facile Hydroxylation of Halloysite Nanotubes for Epoxy Nanocomposite Applications. *Polymer (Guildf).* **2014**, *55* (25), 6519–6528.

(79) Joussein, E.; Petit, S.; Churchman, J.; Theng, B.; Righi, D.; Delvaux, B. Halloysite Clay Minerals — a Review. *Clay Miner.* **2005**, *40* (4), 383–426. https://doi.org/10.1180/0009855054040180.

(80) Vahedi, V.; Pasbakhsh, P.; Chai, S. P. Toward High Performance Epoxy/Halloysite Nanocomposites: New Insights Based on Rheological, Curing, and Impact Properties. *Mater. Des.* **2015**, *68*, 42–53. https://doi.org/10.1016/j.matdes.2014.12.010.

(81) Braiek, S.; Zitoune, R.; Ben Khalifa, A.; Zidi, M. Experimental and Numerical Study of Adhesively Bonded ±55° Filament Wound Tubular Specimens under Uniaxial Tensile Loading. *Compos. Struct.* **2017**, *172*, 297–310. https://doi.org/10.1016/j.compstruct.2017.03.103.

(82) Bunsell, A. R. Composite Pressure Vessels Supply an Answer to Transport Problems. *Reinf. Plast.* **2006**, *50* (2), 38–41. https://doi.org/10.1016/S0034-3617(06)70914-6.

(83) Balasubramanian, K.; Sultan, M. T. H.; Rajeswari, N. *Manufacturing Techniques of Composites for Aerospace Applications*; Elsevier Ltd, 2018. https://doi.org/10.1016/B978-0-08-102131-6.00004-9.

(84) Demirci, M. T. Low Velocity Impact and Fracture Characterization of SiO2 Nanoparticles Filled Basalt Fiber Reinforced Composite Tubes. *J. Compos. Mater.* **2020**. https://doi.org/10.1177/0021998320915952.

(85) Shen, F. C. A Filament-Wound Structure Technology Overview. *Mater. Chem. Phys.* **1995**, *42* (2), 96–100. https://doi.org/10.1016/0254-0584(95)01554-X.

(86) Kelly, A.; Zweben, C.; Carlsson, L. *Comprehensive Composite Materials*, 2nd ed.; Cambridge University Press, 2000.

(87) Quanjin, M.; Rejab, M. R. M.; Idris, M. S.; Zhang, B.; Merzuki, M. N. M.; Kumar, N. M. Wireless Technology Applied in 3-Axis Filament Winding Machine Control System Using MIT App Inventor. *IOP Conf. Ser. Mater. Sci. Eng.* **2019**, *469* (1). https://doi.org/10.1088/1757-899X/469/1/012030.

(88) Gonzalez Henriquez, R.; Mertiny, P. 3.21 Filament Winding Applications. *Compr. Compos. Mater. II* **2018**, 556–577. https://doi.org/10.1016/B978-0-12-803581-8.10313-3.

(89) Quanjin, M.; Rejab, M. R. M.; Idris, M. S.; Bachtiar, B.; Siregar, J. P.; Harith, M. N. Design and Optimize of 3-Axis Filament Winding Machine. In *IOP Conference Series: Materials Science and Engineering*; 2017; Vol. 257. https://doi.org/10.1088/1757-899X/257/1/012039.

(90) Abdalla, F. H.; Mutasher, S. A.; Khalid, Y. A.; Sapuan, S. M.; Hamouda, A. M. S.; Sahari, B. B.; Hamdan, M. M. Design and Fabrication of Low Cost Filament Winding Machine. *Mater. Des.* **2007**, *28* (1), 234–239. https://doi.org/10.1016/j.matdes.2005.06.015.

(91) Bai, H.; Yang, B.; Hui, H.; Yang, Y.; Yu, Q.; Zhou, Z.; Xian, P. Experimental and Numerical Investigation of the Strain Response of the Filament Wound Pressure Vessels Subjected to Pressurization Test. *Polym. Compos.* **2019**, *40* (11), 4427–4441. https://doi.org/10.1002/pc.25304.

(92) Üstün, T.; Ulus, H.; Karabulut, S. E.; Eskizeybek, V.; Şahin, Ö. S.; Avci, A.; Demir, O. Evaluating the Effectiveness of Nanofillers in Filament Wound Carbon/Epoxy Multiscale Composite Pipes. *Compos. Part B Eng.* **2016**, *96*, 1–6. https://doi.org/10.1016/j.compositesb.2016.04.031.

(93) Nelson, J. M.; Sharma, A.; Goetz, D. P.; Hine, A. M.; Sedgwick, P.; Gorsuch, T.; Knauff, D. Nanosilica-Modified Epoxy Resins for Use in Filament-Wound Drive Shaft Applications. *Compos. Adv. Mater. Expo* **2014**.

(94) Poutrel, Q. A.; Wang, Z.; Wang, D.; Soutis, C.; Gresil, M. Effect of Pre and Post-Dispersion on Electro-Thermo-Mechanical Properties of a Graphene Enhanced Epoxy. *Appl. Compos. Mater.* **2017**, *24* (2), 313–336. https://doi.org/10.1007/s10443-016-9541-0.

(95) Krieg, A. S.; King, J. A.; Jaszczak, D. C.; Miskoglu, I.; Mills, O. P.; Odegard, G. M. Tensile and Conductivity Properties of Epoxy Composites Containing Carbon Black and Graphene Nanoplatelets. *J. Compos. Mater.* **2018**, *52* (28), 3909–3918. https://doi.org/10.1177/0021998318771460.

(96) Carbas, R. J. C.; Da Silva, L. F. M.; Andrés, L. F. S. The Mechanical Response of a Structural Epoxy Adhesive Reinforced with Carbon Black Nanoparticles. *Microsc. Microanal.* **2019**, *25* (1), 187–191. https://doi.org/10.1017/S1431927618015106.

(97) Chatterjee, S.; Nafezarefi, F.; Tai, N. H.; Schlagenhauf, L.; Nüesch, F. A.; Chu, B. T. T. Size and Synergy Effects of Nanofiller Hybrids Including Graphene Nanoplatelets and Carbon Nanotubes in Mechanical Properties of Epoxy Composites. *Carbon N. Y.* **2012**, *50* (15), 5380–5386. https://doi.org/10.1016/J.CARBON.2012.07.021.

(98) Domun, N.; Hadavinia, H.; Zhang, T.; Sainsbury, T.; Liaghat, G. H.; Vahid, S. Improving the Fracture Toughness and the Strength of Epoxy Using Nanomaterials – a Review of the Current Status. *Nanoscale* **2015**, *7* (23), 10294–10329. https://doi.org/10.1039/C5NR01354B.

(99) Qiu, J.; Wang, S. Enhancing Polymer Performance through Graphene Sheets. *J. Appl. Polym. Sci.* **2011**, *119* (6), 3670–3674. https://doi.org/10.1002/app.33068.

(100) Abdullah, S. I.; Ansari, M. N. M. Mechanical Properties of Graphene Oxide (GO)/Epoxy Composites. *HBRC J.* **2015**, *11* (2), 151–156. https://doi.org/10.1016/j.hbrcj.2014.06.001.

(101) Galpaya, D.; Wang, M.; George, G.; Motta, N.; Waclawik, E.; Yan, C. Preparation of Graphene Oxide/Epoxy Nanocomposites with Significantly Improved Mechanical Properties. *J. Appl. Phys.* **2014**, *116* (5). https://doi.org/10.1063/1.4892089.

(102) Martin-Gallego, M.; Bernal, M. M.; Hernandez, M.; Verdejo, R.; Lopez-Manchado, M. A. Comparison of Filler Percolation and Mechanical Properties in Graphene and Carbon Nanotubes Filled Epoxy Nanocomposites. *Eur. Polym. J.* **2013**, *49* (6), 1347–1353. https://doi.org/10.1016/j.eurpolymj.2013.02.033.

(103) Gojny, F. H.; Wichmann, M. H. G.; Fiedler, B.; Schulte, K. Influence of Different Carbon Nanotubes on the Mechanical Properties of Epoxy Matrix Composites - A Comparative Study. *Compos. Sci. Technol.* **2005**, *65* (15–16 SPEC. ISS.), 2300–2313. https://doi.org/10.1016/j.compscitech.2005.04.021.

(104) Ghorabi, S.; Rajabi, L.; Madaeni, S. S.; Zinadini, S.; Derakhshan, A. A. Effects of Three Surfactant Types of Anionic, Cationic and Non-Ionic on Tensile Properties and Fracture Surface Morphology of Epoxy/MWCNT Nanocomposites. *Iran. Polym. J. (English Ed.* **2012**, *21* (2), 121–130. https://doi.org/10.1007/s13726-011-0013-y.

(105) Kadhim, N.; Mei, Y.; Wang, Y.; Li, Y.; Meng, F.; Jiang, M.; Zhou, Z. Remarkable Improvement in the Mechanical Properties of Epoxy Composites Achieved by a Small Amount of Modified Helical Carbon Nanotubes. *Polymers (Basel).* **2018**, *10* (10), 1103. https://doi.org/10.3390/polym10101103.

(106) Majzoobi, G. H.; Nejad, S. H. A.; Sabet, S. A. R. Role of Graphene Oxide and Sonication Time on Mechanical Properties of Epoxy Nanocomposites at High Strain Rate. *Mater. Res. Express* **2019**, *6* (6). https://doi.org/10.1088/2053-1591/ab0fde.

(107) Bari, P.; Khan, S.; Njuguna, J.; Mishra, S. Elaboration of Properties of Graphene Oxide Reinforced Epoxy Nanocomposites. *Int. J. Plast. Technol.* **2017**, *21* (1), 194–208. https://doi.org/10.1007/s12588-017-9180-9.

(108) Cha, J.; Jun, G. H.; Park, J. K.; Kim, J. C.; Ryu, H. J.; Hong, S. H. Improvement of Modulus, Strength and Fracture Toughness of CNT/Epoxy Nanocomposites through the Functionalization of Carbon Nanotubes. *Compos. Part B Eng.* **2017**, *129*, 169–179. https://doi.org/10.1016/j.compositesb.2017.07.070.

(109) Ribeiro, B.; Botelho, E. C.; Costa, M. L.; Bandeira, C. F. Carbon Nanotube Buckypaper Reinforced Polymer Composites : A Review. **2017**, *27* (3), 247–255.

(110) An, Y.; He, X. T.; Yang, W. M.; Ding, Y. M. Effect of Surfactants on the Dispersion of Multi-Walled Carbon Nanotubes in Epoxy Resin. *Adv. Mater. Res.* **2011**, *221*, 1–7. https://doi.org/10.4028/www.scientific.net/AMR.221.1.

(111) Nan, X.; Ma, J.; Liu, J.; Zhao, J.; Zhu, W. Effect of Surfactant Functionalization of Multi-Walled Carbon Nanotubes on Mechanical, Electrical and Thermal Properties of Epoxy Nanocomposites. *Fibers Polym.* **2016**, *17* (11), 1866–1874. https://doi.org/10.1007/s12221-016-6388-9.

(112) Geng, Y.; Liu, M. Y.; Li, J.; Shi, X. M.; Kim, J. K. Effects of Surfactant Treatment on Mechanical and Electrical Properties of CNT/Epoxy Nanocomposites. *Compos. Part A Appl. Sci. Manuf.* **2008**, *39* (12), 1876–1883. https://doi.org/10.1016/j.compositesa.2008.09.009.

(113) Islam, M. F.; Rojas, E.; Bergey, D. M.; Johnson, A. T.; Yodh, A. G. High Weight Fraction Surfactant Solubilization of Single-Wall Carbon Nanotubes in Water. *Nano Lett.* **2003**, *3* (2), 269–273. https://doi.org/10.1021/nl025924u.

(114) Sun, P.; Liu, G.; Lv, D.; Dong, X.; Wu, J.; Wang, D. Simultaneous Improvement in Strength, Toughness, and Thermal Stability of Epoxy/Halloysite Nanotubes Composites by Interfacial Modification. *J. Appl. Polym. Sci.* **2016**, *133* (13).

(115) Tang, Y.; Ye, L.; Deng, S.; Yang, C.; Yuan, W. Influences of Processing Methods and Chemical Treatments on Fracture Toughness of Halloysite–epoxy Composites. *Mater. Des.* **2012**, *42*, 471–477.

(116) Deng, S.; Zhang, J.; Ye, L.; Wu, J. Toughening Epoxies with Halloysite Nanotubes. *Polymer (Guildf).* **2008**, *49* (23), 5119–5127.

(117) Kostopoulos, V.; Masouras, A.; Baltopoulos, A.; Vavouliotis, A.; Sotiriadis, G.; Pambaguian, L. A Critical Review of Nanotechnologies for Composite Aerospace Structures. *CEAS Sp. J.* **2017**, *9* (1), 35–57. https://doi.org/10.1007/s12567-016-0123-7.

(118) Wagner, H. D.; Vaia, R. A. Nanocomposites: Issues at the Interface. *Mater. Today* **2004**, *7* (11), 38–42. https://doi.org/10.1016/S1369-7021(04)00507-3.

(119) Qian, H.; Greenhalgh, E. S.; Shaffer, M. S. P.; Bismarck, A. Carbon Nanotube-Based Hierarchical Composites: A Review. *J. Mater. Chem.* **2010**, *20* (23), 4751–4762. https://doi.org/10.1039/c000041h.

(120) Gao, S.; Mäder, E. Multifunctional Interphases in Polymer Composites. In *Multifunctionality of Polymer Composites: Challenges and New Solutions*; 2015; pp 338–362.

(121) Dirand, X.; Hilaire, B.; Soulier, J. P.; Nardin, M. Interfacial Shear Strength in Glass-Fiber/Vinylester-Resin Composites. *Compos. Sci. Technol.* **1996**, *56* (5),

533–539. https://doi.org/10.1016/0266-3538(96)00040-1.

(122) Teng, C. C.; Ma, C. C. M.; Lu, C. H.; Yang, S. Y.; Lee, S. H.; Hsiao, M. C.; Yen, M. Y.; Chiou, K. C.; Lee, T. M. Thermal Conductivity and Structure of Non-Covalent Functionalized Graphene/Epoxy Composites. *Carbon N. Y.* **2011**, *49* (15), 5107–5116. https://doi.org/10.1016/j.carbon.2011.06.095.

(123) Rafiee, M. A. M. A. M. A.; Rafiee, J.; Srivastava, I.; Wang, Z.; Song, H.; Yu, Z.-Z. Z.; Koratkar, N. Fracture and Fatigue in Graphene Nanocomposites. *Small* **2010**, *6* (2), 179–183. https://doi.org/10.1002/smll.200901480.

(124) Wang, X.; Xing, W.; Zhang, P.; Song, L.; Yang, H.; Hu, Y. Covalent Functionalization of Graphene with Organosilane and Its Use as a Reinforcement in Epoxy Composites. *Compos. Sci. Technol.* **2012**, *72* (6), 737–743. https://doi.org/10.1016/j.compscitech.2012.01.027.

(125) Yang, S. Y.; Lin, W. N.; Huang, Y. L.; Tien, H. W.; Wang, J. Y.; Ma, C. C. M.; Li, S. M.; Wang, Y. S. Synergetic Effects of Graphene Platelets and Carbon Nanotubes on the Mechanical and Thermal Properties of Epoxy Composites. *Carbon N. Y.* **2011**, *49* (3), 793–803. https://doi.org/10.1016/j.carbon.2010.10.014.

(126) Lu, K. L.; Lago, R. M.; Chen, Y. K.; Green, M. L. H.; Harris, P. J. F.; Tsang, S. C. Mechanical Damage of Carbon Nanotubes by Ultrasound. *Carbon N. Y.* **1996**, *34* (6), 814–816. https://doi.org/10.1016/0008-6223(96)89470-X.

(127) Shelimov, K. B.; Esenaliev, R. O.; Rinzler, A. G.; Huffman, C. B.; Smalley, R. E. Purification of Single-Wall Carbon Nanotubes by Ultrasonically Assisted Filtration. *Chem. Phys. Lett.* **1998**, *282* (5–6), 429–434. https://doi.org/10.1016/S0009-2614(97)01265-7.

(128) Loos, M. R.; Coelho, L. A. F.; Pezzin, S. H.; Amico, S. C. The Effect of Acetone Addition on the Properties of Epoxy. *Polimeros* **2008**, *18* (1), 76–80. https://doi.org/10.1590/S0104-14282008000100015.

(129) Rafiee, M. a; Rafiee, J.; Wang, Z.; Song, H.; Yu, Z.; Koratkar, N. Enhanced Mechanical Properties of Nanocomposites at Low Graphene Content. *ACS Nano* **2009**, *3* (12), 3884–3890. https://doi.org/10.1021/nn9010472.

(130) Gkikas, G.; Barkoula, N.-M. M.; Paipetis, A. S. S. Composites : Part B Effect of Dispersion Conditions on the Thermo-Mechanical and Toughness Properties of Multi Walled Carbon Nanotubes-Reinforced Epoxy. *Compos. Part B* **2012**, *43* (6), 2697–2705. https://doi.org/10.1016/j.compositesb.2012.01.070.

(131) Sandler, J.; Shaffer, M. S. P.; Prasse, T.; Bauhofer, W.; Schulte, K.; Windle, A. H. Development of a Dispersion Process for Carbon Nanotubes in an Epoxy Matrix and the Resulting Electrical Properties. *Polymer (Guildf).* **1999**, *40* (21), 5967–5971. https://doi.org/10.1016/S0032-3861(99)00166-4.

(132) Zhou, Y. X.; Wu, P. X.; Cheng, Z. Y.; Ingram, J.; Jeelani, S. Improvement in Electrical, Thermal and Mechanical Properties of Epoxy by Filling Carbon Nanotube. *Express Polym. Lett.* **2008**, *2* (1), 40–48.

(133) Niyogi, S.; Hamon, M. A.; Hu, H.; Zhao, B.; Bhowmik, P.; Sen, R.; Itkis, M. E.; Haddon, R. C. Chemistry of Single-Walled Carbon Nanotubes. *Acc. Chem. Res.* **2002**, *35* (12), 1105–1113. https://doi.org/10.1021/ar010155r.

(134) Fu, S. Y.; Chen, Z. K.; Hong, S.; Han, C. C. The Reduction of Carbon Nanotube (CNT) Length during the Manufacture of CNT/Polymer Composites and a Method to Simultaneously Determine the Resulting CNT and Interfacial Strengths. *Carbon N. Y.* **2009**, *47* (14), 3192–3200. https://doi.org/10.1016/j.carbon.2009.07.028.

(135) Jiménez-Suárez, A.; Campo, M.; Gaztelumendi, I.; Markaide, N.; Sánchez, M.; Ureña, A. The Influence of Mechanical Dispersion of MWCNT in Epoxy Matrix by Calendering Method: Batch Method versus Time Controlled. *Compos. Part B Eng.* **2013**, *48*, 88–94. https://doi.org/10.1016/j.compositesb.2012.12.011.

(136) Thostenson, E. T.; Chou, T.-W. W. Processing-Structure-Multi-Functional Property Relationship in Carbon Nanotube/Epoxy Composites. *Carbon N. Y.* **2006**, *44* (14), 3022–3029. https://doi.org/10.1016/j.carbon.2006.05.014.

(137) Bilisik, K. Dimensional Stability of Multiaxis 3D-Woven Carbon Preforms. *J. Text. Inst.* **2010**, *101* (5), 380–388. https://doi.org/10.1080/00405000802440066.

(138) Birman, V.; Byrd, L. W. Effect of Z-Pins on Fracture in Composite Cocured Double Cantilever Beams. *J. Aerosp. Eng.* **2005**, *18* (1), 51–59. https://doi.org/10.1061/(ASCE)0893-1321(2005)18:1(51).

(139) Mouritz, A. P.; Baini, C.; Herszberg, I. Mode I Interlaminar Fracture Toughness Properties of Advanced Textile Fibreglass Composites. *Compos. Part A Appl. Sci. Manuf.* **1999**, *30* (7), 859–870. https://doi.org/10.1016/S1359-835X(98)00197-3.

(140) Jung, H.; Kim, Y. Mode I Fracture Toughness of Carbon-Glass/Epoxy Interply Hybrid Composites. *J. Mech. Sci. Technol.* **2015**, *29* (5), 1955–1962. https://doi.org/10.1007/s12206-015-0416-3.

(141) Beylergil, B.; Tanoğlu, M.; Aktaş, E. Enhancement of Interlaminar Fracture

Toughness of Carbon Fiber–epoxy Composites Using Polyamide-6,6 Electrospun Nanofibers. *J. Appl. Polym. Sci.* **2017**, *134* (35), 1–12. https://doi.org/10.1002/app.45244.

(142) Li, Y.; Wang, D.; Ma, H. Improving Interlaminar Fracture Toughness of Flax Fiber/Epoxy Composites with Chopped Flax Yarn Interleaving. *Sci. China Technol. Sci.* **2015**, *58* (10), 1745–1752. https://doi.org/10.1007/s11431-015-5911-3.

(143) Chen, C.; Li, Y.; Yu, T. Interlaminar Toughening in Flax Fiber-Reinforced Composites Interleaved with Carbon Nanotube Buckypaper. *J. Reinf. Plast. Compos.* **2014**, *33* (20), 1859–1868. https://doi.org/10.1177/0731684414548084.

(144) Tabiei, A.; Zhang, W. Composite Laminate Delamination Simulation and Experiment: A Review of Recent Development. *Appl. Mech. Rev.* **2018**, *70* (3), 1–23. https://doi.org/10.1115/1.4040448.

(145) Ahmadi-Moghadam, B.; Taheri, F. Fracture and Toughening Mechanisms of GNP-Based Nanocomposites in Modes I and II Fracture. *Eng. Fract. Mech.* **2014**, *131*, 329–339. https://doi.org/10.1016/j.engfracmech.2014.08.008.

(146) Srivastava, V. K.; Gries, T.; Veit, D.; Quadflieg, T.; Mohr, B.; Kolloch, M. Effect of Nanomaterial on Mode I and Mode II Interlaminar Fracture Toughness of Woven Carbon Fabric Reinforced Polymer Composites. *Eng. Fract. Mech.* **2017**, *180*, 73–86. https://doi.org/10.1016/j.engfracmech.2017.05.030.

(147) Nayak, R. K.; Dash, A.; Ray, B. C. Effect of Epoxy Modifiers (Al 2 O 3 /SiO 2 /TiO 2) on Mechanical Performance of Epoxy/Glass Fiber Hybrid Composites. *Procedia Mater. Sci.* **2014**, *6* (Icmpc), 1359–1364. https://doi.org/10.1016/j.mspro.2014.07.115.

(148) Walter, T. R.; Subhash, G.; Sankar, B. V.; Song, M. C.; Yen, C. F. A Novel Method for Dynamic Short-Beam Shear Testing of 3D Woven Composites. *Exp. Mech.* **2013**, *53* (3), 493–503. https://doi.org/10.1007/s11340-012-9659-4.

(149) *Mechanics of Composite Materials and Structures*; Carlos A. Mota Soares, Cristóvão M. Mota Soares, M. J. M. F., Ed.; Springer Science & Business Media, 1998; Vol. 100.

(150) Khan, S. U.; Kim, J. K. Impact and Delamination Failure of Multiscale Carbon Nanotube-Fiber Reinforced Polymer Composites: A Review. *Int. J. Aeronaut. Sp. Sci.* **2011**, *12* (2), 115–133. https://doi.org/10.5139/IJASS.2011.12.2.115.

(151) Friedrich, K.; Breuer, U. *Multifunctionality of Polymer Composites: Challenges and New Solutions*; 2015. https://doi.org/10.1016/C2013-0-13006-1.

(152) Tugrul Seyhan, A.; Tanoglu, M.; Schulte, K. Mode I and Mode II Fracture Toughness of E-Glass Non-Crimp Fabric/Carbon Nanotube (CNT) Modified Polymer Based Composites. *Eng. Fract. Mech.* **2008**, *75* (18), 5151–5162. https://doi.org/10.1016/j.engfracmech.2008.08.003.

(153) Qiu, J.; Zhang, C.; Wang, B.; Liang, R. Carbon Nanotube Integrated Multifunctional Multiscale Composites. *Nanotechnology* **2007**, *18* (27). https://doi.org/10.1088/0957-4484/18/27/275708.

(154) Rathore, D. K.; Prusty, R. K.; Kumar, D. S.; Ray, B. C. Mechanical Performance of CNT-Filled Glass Fiber/Epoxy Composite in in-Situ Elevated Temperature Environments Emphasizing the Role of CNT Content. *Compos. Part A Appl. Sci. Manuf.* **2016**, *84*, 364–376. https://doi.org/10.1016/j.compositesa.2016.02.020.

(155) Fan, Z.; Santare, M. H.; Advani, S. G. Interlaminar Shear Strength of Glass Fiber Reinforced Epoxy Composites Enhanced with Multi-Walled Carbon Nanotubes. *Compos. Part A Appl. Sci. Manuf.* **2008**, *39* (3), 540–554. https://doi.org/10.1016/j.compositesa.2007.11.013.

(156) Rahman, M. M.; Zainuddin, S.; Hosur, M. V.; Robertson, C. J.; Kumar, A.; Trovillion, J.; Jeelani, S. Effect of NH 2-MWCNTs on Crosslink Density of Epoxy Matrix and ILSS Properties of e-Glass/Epoxy Composites. *Compos. Struct.* **2013**, *95*, 213–221. https://doi.org/10.1016/j.compstruct.2012.07.019.

(157) Sharma, K.; Shukla, M. Experimental Study of Mechanical Properties of Multiscale Carbon Fiber-Epoxy-CNT Composites. *Adv. Mater. Res.* **2012**, *383–390*, 2723–2727. https://doi.org/10.4028/www.scientific.net/AMR.383-390.2723.

(158) Sánchez, M.; Campo, M.; Jiménez-Suárez, A.; Ureña, A. Effect of the Carbon Nanotube Functionalization on Flexural Properties of Multiscale Carbon Fiber/Epoxy Composites Manufactured by VARIM. *Compos. Part B Eng.* **2013**, *45* (1), 1613–1619. https://doi.org/10.1016/j.compositesb.2012.09.063.

(159) Zhang, Q.; Li, X.; Liang, S.; Zhao, X.; Sui, G.; Yang, X. A Kind of Liquid-like MWCNT Reinforcements for T1000 Carbon Fibre Filament Winding Composites. *Compos. Sci. Technol.* **2016**, *131*, 89–97. https://doi.org/10.1016/j.compscitech.2016.06.004.

(160) Siddiqui, N. A.; Khan, S. U.; Kim, J. K. Experimental Torsional Shear Properties

of Carbon Fiber Reinforced Epoxy Composites Containing Carbon Nanotubes. *Compos. Struct.* **2013**, *104*, 230–238. https://doi.org/10.1016/j.compstruct.2013.04.033.

(161) Jiang, J.; Xu, C.; Su, Y.; Guo, Q.; Liu, F.; Deng, C.; Yao, X.; Zhou, L. Influence of Carbon Nanotube Coatings on Carbon Fiber by Ultrasonically Assisted Electrophoretic Deposition on Its Composite Interfacial Property. *Polymers (Basel).* **2016**, *8* (8). https://doi.org/10.3390/polym8080302.

(162) Zhu, J.; Imam, A.; Crane, R.; Lozano, K.; Khabashesku, V. N.; Barrera, E. V. Processing a Glass Fiber Reinforced Vinyl Ester Composite with Nanotube Enhancement of Interlaminar Shear Strength. *Compos. Sci. Technol.* **2007**, *67* (7–8), 1509–1517. https://doi.org/10.1016/j.compscitech.2006.07.018.

(163) Zhang, X.; Fan, X.; Yan, C.; Li, H.; Zhu, Y.; Li, X.; Yu, L. Interfacial Microstructure and Properties of Carbon Fiber Composites Modified with Graphene Oxide. *ACS Appl. Mater. Interfaces* **2012**, *4* (3), 1543–1552. https://doi.org/10.1021/am201757v.

(164) Zhang, C.; Zhang, X.; Wu, G. Enhancing Interfacial Strength and Hydrothermal Aging Resistance of Silicone Resin Composites by Different Modification of Carbon Fibers with Silica Nanoparticles. *Polym. Compos.* **2019**, *40* (S2), E975–E982. https://doi.org/10.1002/pc.

(165) Rajanish, M.; Nanjundaradhya, N. V.; Sharma, R. S. Influence of Nano-Modification on the Interlaminar Shear Strength of Unidirectional Glass Fiber-Reinforced Epoxy Resin. *J. Miner. Mater. Charact. Eng.* **2014**, *02* (04), 264–269. https://doi.org/10.4236/jmmce.2014.24031.

(166) Han, S.; Chung, D. D. L. Strengthening and Stiffening Carbon Fiber Epoxy Composites by Halloysite Nanotubes, Carbon Nanotubes and Silicon Carbide Whiskers. *Appl. Clay Sci.* **2013**, *83–84*, 375–382. https://doi.org/10.1016/j.clay.2013.08.001.

(167) Tang, Y.; Ye, L.; Zhang, D.; Deng, S. Characterization of Transverse Tensile, Interlaminar Shear and Interlaminate Fracture in CF/EP Laminates with 10 Wt% and 20 Wt% Silica Nanoparticles in Matrix Resins. *Compos. Part A Appl. Sci. Manuf.* **2011**, *42* (12), 1943–1950. https://doi.org/10.1016/j.compositesa.2011.08.019.

(168) Di, C.; Yu, J.; Wang, B.; Lau, A. K. T.; Zhu, B.; Qiao, K. Study of Hybrid

Nanoparticles Modified Epoxy Resin Used in Filament Winding Composite. *Materials (Basel).* **2019**, *12* (23), 1–11. https://doi.org/10.3390/ma122333853.

(169) Abliz, D.; Ziegmann, G. STATIC AND THERMAL DYNAMIC MECHANICAL ANALYSIS OF AlOOH NANOPARTICLE REINFORCED FIBER COMPOSITES. **2017**, No. June, 655–662.

(170) Greenhalgh, E. S. Delamination-Dominated Failures in Polymer Composites. In *Failure Analysis and Fractography of Polymer Composites*; Woodhead Publishing, 2009; pp 164–237. https://doi.org/10.1533/9781845696818.164.

(171) Parker, D. S. Factors Influencing the Mode I Interlaminar Fracture Resistance of Toughened Matrix Composites, University of Michigan, 1989.

(172) Mohammed, O.; Suleiman, E. A Review Study of Delamination in Composite Laminated Plates. **2019**, No. April. https://doi.org/10.13140/RG.2.2.12740.07041.

(173) Manjunatha, C. M.; Anil Chandra, A. R.; Jagannathan, N. Fracture and Fatigue Behavior of Polymer Nanocomposites - A Review. *J. Indian Inst. Sci.* **2015**, *95* (3), 249–266.

(174) Zhao, W. Mode I Delamination Fracture Characterization of Polymeric Composites under Elevated Temperature. *Mech. Aerosp. Eng. - Diss.* **2011**, *Paper 59*, 228.

(175) Z. Suo, G. Bao, B. F. Delamination R-Curve Phenomena Due to Damage. *J. Mech. Phys. Solids* **1992**, *40* (I), 1–16.

(176) Ghadirdokht, A. Delamination R-Curve Behavior of Curved Composite Laminates. *Compos. Part B* **2019**, *175* (July), 107139. https://doi.org/10.1016/j.compositesb.2019.107139.

(177) Carrillo-Escalante, H. J.; Álvarez-Castillo, A.; Valadez-González, A.; Herrera-Franco, P. J. Effect of Fiber-Matrix Adhesion on the Fracture Behavior of a Carbon Fiber Reinforced Thermoplastic-Modified Epoxy Matrix. *Carbon Lett.* **2016**, *19* (1), 47–56. https://doi.org/10.5714/CL.2016.19.047.

(178) Rikards, R.; Buchholz, F. G.; Bledzki, A. K.; Wacker, G.; Korjakin, A. Mode I, Mode II, and Mixed-Mode I/II Interlaminar Fracture Toughness of GFRP Influenced by Fiber Surface Treatment. *Mech. Compos. Mater.* **1996**, *32* (5), 439–462. https://doi.org/10.1007/BF02313863.

(179) Manshadi, B. D.; Vassilopoulos, A. P.; Botsis, J. A Combined Experimental/Numerical Study of the Scaling Effects on Mode I Delamination of

GFRP. *Compos. Sci. Technol.* **2013**, *83*, 32–39. https://doi.org/10.1016/j.compscitech.2013.04.016.

(180) Albertsen, H.; Ivens, J.; Peters, P.; Wevers, M.; Verpoest, I. Interlaminar Fracture Toughness of CFRP Influenced by Fibre Surface Treatment: Part 1. Experimental Results. *Compos. Sci. Technol.* **1995**, *54* (2), 133–145. https://doi.org/10.1016/0266-3538(95)00048-8.

(181) Gill, A. F.; Robinson, P.; Pinho, S. Effect of Variation in Fibre Volume Fraction on Modes I and II Delamination Behaviour of 5HS Woven Composites Manufactured by RTM. *Compos. Sci. Technol.* **2009**, *69* (14), 2368–2375. https://doi.org/10.1016/j.compscitech.2009.02.008.

(182) Davidson, B. D.; Krüger, R.; König, M. Effect of Stacking Sequence on Energy Release Rate Distributions in Multidirectional DCB and ENF Specimens. *Eng. Fract. Mech.* **1996**, *55* (4), 557–569. https://doi.org/10.1016/S0013-7944(96)00037-9.

(183) Saghafi, H.; Fotouhi, M.; Minak, G. Improvement of the Impact Properties of Composite Laminates by Means of Nano-Modification of the Matrix-A Review. *Appl. Sci.* **2018**, *8* (12), 1–26. https://doi.org/10.3390/app8122406.

(184) Perillo, G.; Echtermeyer, A. T. Mode I Fracture Toughness Testing of Composite Pipes. **2013**, No. December 2012, 1135–1146. https://doi.org/10.1007/s10443-013-9318-7.

(185) Laid, M.; Hecini, M.; Khechai, A. An Experimental Investogation of Mode-I Interlaminar Fracture of Composite Pipes. **2018**, 1–4.

(186) Alessi, S.; Pitarresi, G.; Spadaro, G. Effect of Hydrothermal Ageing on the Thermal and Delamination Fracture Behaviour of CFRP Composites. *Compos. Part B Eng.* **2014**, *67*, 145–153. https://doi.org/10.1016/j.compositesb.2014.06.006.

(187) Bhanushali, H.; Bradford, P. D. Woven Glass Fiber Composites with Aligned Carbon Nanotube Sheet Interlayers. *J. Nanomater.* **2016**, *2016*. https://doi.org/10.1155/2016/9705257.

(188) Godara, A.; Mezzo, L.; Luizi, F.; Warrier, A.; Lomov, S. V.; van Vuure, A. W.; Gorbatikh, L.; Moldenaers, P.; Verpoest, I. Influence of Carbon Nanotube Reinforcement on the Processing and the Mechanical Behaviour of Carbon Fiber/Epoxy Composites. *Carbon N. Y.* **2009**, *47* (12), 2914–2923.

https://doi.org/10.1016/j.carbon.2009.06.039.

(189) Ashrafi, B.; Guan, J.; Mirjalili, V.; Zhang, Y.; Chun, L.; Hubert, P.; Simard, B.; Kingston, C. T.; Bourne, O.; Johnston, A. Enhancement of Mechanical Performance of Epoxy/Carbon Fiber Laminate Composites Using Single-Walled Carbon Nanotubes. *Compos. Sci. Technol.* **2011**, *71* (13), 1569–1578. https://doi.org/10.1016/j.compscitech.2011.06.015.

(190) Arca, M. A.; Coker, D. Experimental Investigation of CNT Effect on Curved Beam Strength and Interlaminar Fracture Toughness of CFRP Laminates. *J. Phys. Conf. Ser.* **2014**, *524* (1). https://doi.org/10.1088/1742-6596/524/1/012038.

(191) Yokozeki, T.; Iwahori, Y.; Ishiwata, S.; Enomoto, K. Mechanical Properties of CFRP Laminates Manufactured from Unidirectional Prepregs Using CSCNT-Dispersed Epoxy. *Compos. Part A Appl. Sci. Manuf.* **2007**, *38* (10), 2121–2130. https://doi.org/10.1016/j.compositesa.2007.07.002.

(192) Mujika, F.; Vargas, G.; Ibarretxe, J.; De Gracia, J.; Arrese, A. Influence of the Modification with MWCNT on the Interlaminar Fracture Properties of Long Carbon Fiber Composites. *Compos. Part B Eng.* **2012**, *43* (3), 1336–1340. https://doi.org/10.1016/j.compositesb.2011.11.020.

(193) Borowski, E.; Soliman, E.; Kandil, U. F.; Taha, M. R. Interlaminar Fracture Toughness of CFRP Laminates Incorporating Multi-Walled Carbon Nanotubes. *Polymers (Basel).* **2015**, *7* (6), 1020–1045. https://doi.org/10.3390/polym7061020.

(194) Karapappas, P.; Vavouliotis, A.; Tsotra, P.; Kostopoulos, V.; Paipetis, A. Enhanced Fracture Properties of Carbon Reinforced Composites by the Addition of Multi-Wall Carbon Nanotubes. *J. Compos. Mater.* **2009**, *43* (9), 977–985. https://doi.org/10.1177/0021998308097735.

(195) Shan, F. L.; Gu, Y. Z.; Li, M.; Liu, Y. N.; Zhang, Z. G. Effect of Deposited Carbon Nanotubes on Interlaminar Properties of Carbon Fiber-Reinforced Epoxy Composites Using a Developed Spraying Processing. *Polym. Compos.* **2013**, *34* (1), 41–50. https://doi.org/10.1002/pc.

(196) Mohammed, F.; Rekbi, L.; Hecini, M.; Khechai, A. Experimental and Numerical Analysis of Mode - I Interlaminar Fracture of Composite Pipes. *J. Brazilian Soc. Mech. Sci. Eng.* **2018**, *40* (10), 1–11. https://doi.org/10.1007/s40430-018-1423-y.

(197) Liu, C.; Bai, R.; Lei, Z.; Di, J.; Dong, D.; Gao, T.; Jiang, H.; Yan, C. Study on Mode-I Fracture Toughness of Composite Laminates with Curved Plies Applied

by Automated Fiber Placement. *Mater. Des.* **2020**, *195*, 108963. https://doi.org/10.1016/j.matdes.2020.108963.

(198) Ozdil, F.; Carlsson, L. A. Characterization of Mode I Delamination Growth in Glass/Epoxy Composite Cylinders. *J. Compos. Mater.* **2000**, *34* (5), 398–419. https://doi.org/10.1177/002199830003400503.

(199) Guedes, R. M.; Sá, A.; de Moura, M. F. S. F. An Experimental and Numerical Assessment of DCB Tests on Glass/Polyester Curved Beams Cut out from Pipes. *Polym. Test.* **2008**, *27* (8), 985–994. https://doi.org/10.1016/j.polymertesting.2008.08.011.

(200) Sadeghian, R.; Gangireddy, S.; Minaie, B.; Hsiao, K. T. Manufacturing Carbon Nanofibers Toughened Polyester/Glass Fiber Composites Using Vacuum Assisted Resin Transfer Molding for Enhancing the Mode-I Delamination Resistance. *Compos. Part A Appl. Sci. Manuf.* **2006**, *37* (10), 1787–1795. https://doi.org/10.1016/j.compositesa.2005.09.010.

(201) Bashar, M. T.; Sundararaj, U.; Mertiny, P. Mode-I Interlaminar Fracture Behaviour of Nanoparticle Modified Epoxy/Basalt Fibre-Reinforced Laminates. *Polym. Test.* **2013**, *32* (2), 402–412. https://doi.org/10.1016/j.polymertesting.2012.10.012.

(202) Norman, D. A.; Robertson, R. E. Rigid-Particle Toughening of Glassy Polymers. *Polymer (Guildf).* **2003**, *44* (8), 2351–2362. https://doi.org/10.1016/S0032-3861(03)00084-3.

(203) Tang, L. C.; Zhang, H.; Sprenger, S.; Ye, L.; Zhang, Z. Fracture Mechanisms of Epoxy-Based Ternary Composites Filled with Rigid-Soft Particles. *Compos. Sci. Technol.* **2012**, *72* (5), 558–565. https://doi.org/10.1016/j.compscitech.2011.12.015.

(204) Kinloch, A. J.; Maxwell, D.; Young, R. J. Micromechanisms of Crack Propagation in Hybrid-Particulate Composites. *J. Mater. Sci. Lett.* **1985**, *4* (10), 1276–1279. https://doi.org/10.1007/BF00723480.

(205) Sakai, M.; Bradt, R. C. Fracture Toughness Testing of Brittle Materials. *Int. Mater. Rev.* **1993**, *38* (2), 53–78. https://doi.org/10.1179/imr.1993.38.2.53.

(206) Lange, F. F. The Interaction of a Crack Front with a Second-Phase Dispersion. *Philos. Mag.* **1970**, *22* (179), 983–992. https://doi.org/10.1080/14786437008221068.

(207) Evans, A. G. The Strength of Brittle Materials Containing Secon Phase

Dispersions. *Philos. Mag.* **1972**, *26* (6), 1327–1344. https://doi.org/10.1038/155509b0.

(208) Green, D. J.; Nicholson, P. S.; Embury, J. D. Fracture of a Brittle Particulate Composite - Part 2 Theoretical Aspects. *J. Mater. Sci.* **1979**, *14* (7), 1657–1661. https://doi.org/10.1007/BF00569287.

(209) Wetzel, B.; Rosso, P.; Haupert, F.; Friedrich, K. Epoxy Nanocomposites - Fracture and Toughening Mechanisms. *Eng. Fract. Mech.* **2006**, *73* (16), 2375–2398. https://doi.org/10.1016/j.engfracmech.2006.05.018.

(210) Faber, K. T.; Evans, A. G. Crack Deflection Processes-I. Theory. *Acta Metall.* **1983**, *31* (4), 565–576. https://doi.org/10.1016/0001-6160(83)90046-9.

(211) Rafiee, M. A.; Rafiee, J.; Srivastava, I.; Wang, Z.; Song, H.; Yu, Z.-Z.; Koratkar, N. Fracture and Fatigue in Graphene Nanocomposites. *Small* **2010**, *6* (2), 179–183. https://doi.org/10.1002/smll.200901480.

(212) Kinloch, A. J.; Taylor, A. C. The Mechanical Properties and Fracture Behaviour of Epoxy-Inorganic Micro- and Nano-Composites. *J. Mater. Sci.* **2006**, *41* (11), 3271–3297. https://doi.org/10.1007/s10853-005-5472-0.

(213) Zhang, H.; Zhang, Z.; Friedrich, K.; Eger, C. Property Improvements of in Situ Epoxy Nanocomposites with Reduced Interparticle Distance at High Nanosilica Content. *Acta Mater.* **2006**, *54* (7), 1833–1842. https://doi.org/10.1016/j.actamat.2005.12.009.

(214) Odegard, G. M.; Clancy, T. C.; Gates, T. S. Modeling of the Mechanical Properties of Nanoparticle/Polymer Composites. *Charact. Nanocomposites Technol. Ind. Appl.* **2017**, *46* (2), 319–342. https://doi.org/10.1201/b19917.

(215) Demirci, M. T.; Tarakçıoğlu, N.; Avcı, A.; Akdemir, A.; Demirci, İ. Fracture Toughness (Mode I) Characterization of SiO2 Nanoparticle Filled Basalt/Epoxy Filament Wound Composite Ring with Split-Disk Test Method. *Compos. Part B Eng.* **2017**, *119* (Mode I), 114–124. https://doi.org/10.1016/j.compositesb.2017.03.045.

(216) Chen, J. kang; Wang, G. T.; Yu, Z. Z.; Huang, Z.; Mai, Y. W. Critical Particle Size for Interfacial Debonding in Polymer/Nanoparticle Composites. *Compos. Sci. Technol.* **2010**, *70* (5), 861–872. https://doi.org/10.1016/j.compscitech.2010.02.004.

(217) Phillips, D. C.; Tetelman, A. S. The Fracture Toughness of Fibre Composites.

Composites **1972**, *3* (5), 216–223. https://doi.org/10.1016/0010-4361(72)90630-1.

(218) Kelly, A. Interface Effects and the Work of Fracture of a Fibrous Composite. *Proc. R. Soc. London. A. Math. Phys. Sci.* **1970**, *319* (1536), 95–116.

(219) Moloney, A. C.; Kausch, H. H.; Kaiser, T.; Beer, H. R. Parameters Determining the Strength and Toughness of Particulate Filled Epoxide Resins. *J. Mater. Sci.* **1987**, *22* (2), 381–393. https://doi.org/10.1007/BF01160743.

(220) Wichmann, M. H. G.; Schulte, K.; Wagner, H. D. On Nanocomposite Toughness. *Compos. Sci. Technol.* **2008**, *68* (1), 329–331. https://doi.org/10.1016/j.compscitech.2007.06.027.

(221) Sun, L.; Boo, W. J.; Liu, J.; Clearfield, A.; Sue, H. J.; Verghese, N. E.; Pham, H. Q.; Bicerano, J. Effect of Nanoplatelets on the Rheological Behavior of Epoxy Monomers. *Macromol. Mater. Eng.* **2009**, *294* (2), 103–113. https://doi.org/10.1002/mame.200800258.

(222) Kim, J. A.; Seong, D. G.; Kang, T. J.; Youn, J. R. Effects of Surface Modification on Rheological and Mechanical Properties of CNT/Epoxy Composites. *Carbon N. Y.* **2006**, *44* (10), 1898–1905. https://doi.org/10.1016/j.carbon.2006.02.026.

(223) Seyhan, A. T.; Gojny, F. H.; Tanoğlu, M.; Schulte, K. Rheological and Dynamic-Mechanical Behavior of Carbon Nanotube/Vinyl Ester-Polyester Suspensions and Their Nanocomposites. *Eur. Polym. J.* **2007**, *43* (7), 2836–2847. https://doi.org/10.1016/j.eurpolymj.2007.04.022.

(224) Abdalla, M.; Dean, D.; Adibempe, D.; Nyairo, E.; Robinson, P.; Thompson, G. The Effect of Interfacial Chemistry on Molecular Mobility and Morphology of Multiwalled Carbon Nanotubes Epoxy Nanocomposite. *Polymer (Guildf).* **2007**, *48* (19), 5662–5670. https://doi.org/10.1016/j.polymer.2007.06.073.

(225) Naffakh, M.; Dumon, M.; Gérard, J. F. Study of a Reactive Epoxy-Amine Resin Enabling in Situ Dissolution of Thermoplastic Films during Resin Transfer Moulding for Toughening Composites. *Compos. Sci. Technol.* **2006**, *66* (10), 1376–1384. https://doi.org/10.1016/j.compscitech.2005.09.007.

(226) Shibley, A. M. Filament Winding. In *Handbook of composites*; Springer, 1982; pp 449–478.

(227) Bashar, M.; Sundararaj, U.; Mertiny, P. Study of Matrix Micro-Cracking in Nano Clay and Acrylic Tri-Block-Copolymer Modified Epoxy/Basalt Fiber-Reinforced Pressure-Retaining Structures. *Express Polym. Lett.* **2011**, *5* (10), 882–896.

https://doi.org/10.3144/expresspolymlett.2011.87.

(228) Zu, L.; Wang, J.; Li, S. Analysis of Multi-Layered Thick-Walled Filament-Wound Hydrogen Storage Vessels. *Int. J. Hydrogen Energy* **2014**. https://doi.org/10.1016/j.ijhydene.2014.10.075.

(229) Thunhorst, K. L.; Hine, A. M.; Sedgwick, P.; Huehn, M. R.; Goetz, D. P. Nanosilica Concentration Effect on Epoxy Resins and Filament-Wound Composite Overwrapped Pressure Vessels. **2011**.

(230) Szabó, G.; Váradi, K.; Felhős, D. Finite Element Model of a Filament-Wound Composite Tube Subjected to Uniaxial Tension. *Mod. Mech. Eng.* **2017**, *07* (04), 91–112. https://doi.org/10.4236/mme.2017.74007.

(231) Onder, A.; Sayman, O.; Dogan, T.; Tarakcioglu, N. Burst Failure Load of Composite Pressure Vessels. *Compos. Struct.* **2009**, *89* (1), 159–166. https://doi.org/10.1016/j.compstruct.2008.06.021.

(232) Erkal, S.; Sayman, O.; Benli, S.; Dogan, T.; Cinar Yeni, E. Fatigue Damage in Composite Cylinders. *Polym. Polym. Compos.* **2010**, *31* (4), 707–713. https://doi.org/10.1002/pc.

(233) Kaynak, C.; Erdiller, E. S.; Parnas, L.; Senel, F. Use of Split-Disk Tests for the Process Parameters of Filament Wound Epoxy Composite Tubes. *Polym. Test.* **2005**, *24* (5), 648–655. https://doi.org/10.1016/j.polymertesting.2005.03.012.

(234) Pavani, G. J.; Pavani, S. A.; Ferreira, C. A. Application of Polymeric Nanocomposites and Carbon Fiber Composites in the Production of Natural Gas Reservoirs. *J. Nanomater.* **2015**, *2015*. https://doi.org/10.1155/2015/658727.

(235) American, A.; Standard, N. Standard Test Method for Ignition Loss of Cured Reinforced Resins 1. 1–2.

(236) ASTM D 638 Standard Test Method for Tensile Properties of Plastics. *Annu. B. ASTM Stand.* **2003**. https://doi.org/10.1520/D0638-14.1.

(237) ASTM. D 2290 - Standard Test Method for Apparent Hoop Tensile Strength of Plastic or Reinforced Plastic Pipe by Split Disk Method. *An Am. Natl. Stand.* **2003**, *D 2290-00*, 1–5. https://doi.org/10.1520/D2290-08.2.

(238) ASTM. ASTM E399-12e2 Linear-Elastic Plane-Strain Fracture Toughness K Ic of of Metallic Materials. *Astm* **2013**, *399*, 1–33. https://doi.org/10.1520/E0399-12E02.2.

(239) ASTM D 5045 Standard Test Methods for Plane-Strain Fracture Toughness and

Strain Energy Release. *Annu. B. ASTM Stand.* **1999**.

(240) ASTM D790 Standard Test Methods for Flexural Properties of Unreinforced and Reinforced Plastics and Electrical Insulating Materials. *Annu. B. ASTM Stand.* **2017**.

(241) ASTM. ASTM D2344/D2344M: Standard Test Method for Short-Beam Strength of Polymer Matrix Composite Materials and Their Laminates. *Annu. B. ASTM Stand.* **2003**, *3* (2), 136–140. https://doi.org/10.1520/D2344.

(242) ASTM. D5528-01 Mode I Interlaminar Fracture Toughness of Unidirectional Fiber-Reinforced Polymer Matrix Composites. *Am. Soc. Test. Mater.* **2010**, *01* (Reapproved 2007), 1–12.

(243) ASTM D 4065 Standard Practice for Plastics : Dynamic Mechanical Properties : Determination And. *Annu. B. ASTM Stand.* **2001**.

(244) Meng, Q.; Jin, J.; Wang, R.; Kuan, H.; Ma, J. Processable 3-Nm Thick Graphene Platelets of High Electrical Conductivity and Their Epoxy Composites. *Nanotechnology* **2014**, *25* (12), 12707. https://doi.org/10.1088/0957-4484/25/12/125707.

(245) Zaman, I.; Kuan, H. C.; Dai, J.; Kawashima, N.; Michelmore, A.; Sovi, A.; Dong, S.; Luong, L.; Ma, J. From Carbon Nanotubes and Silicate Layers to Graphene Platelets for Polymer Nanocomposites. *Nanoscale* **2012**, *4* (15), 4578–4586. https://doi.org/10.1039/c2nr30837a.

(246) Wichmann, M. H. G.; Sumfleth, J.; Fiedler, B.; Gojny, F. H.; Schulte, K. Multiwall Carbon Nanotube/Epoxy Composites Produced by a Masterbatch Process. *Mech. Compos. Mater.* **2006**, *42* (5), 395–406. https://doi.org/10.1007/s11029-006-0050-3.

(247) Hashim, U. R.; Jumahat, A. Improved Tensile and Fracture Toughness Properties of Graphene Nanoplatelets Filled Epoxy Polymer via Solvent Compounding Shear Milling Method. *Mater. Res. Express* **2019**, *6* (2). https://doi.org/10.1088/2053-1591/aaeaf0.

(248) Zhou, Y.; Jeelani, M. I.; Jeelani, S. Development of Photo Micro-Graph Method to Characterize Dispersion of CNT in Epoxy. *Mater. Sci. Eng. A* **2009**, *506* (1–2), 39–44. https://doi.org/10.1016/j.msea.2008.12.044.

(249) Srivastava, I.; Mehta, R. J.; Yu, Z. Z.; Schadler, L.; Koratkar, N. Raman Study of Interfacial Load Transfer in Graphene Nanocomposites. *Appl. Phys. Lett.* **2011**, *98*

(6), 10–13. https://doi.org/10.1063/1.3552685.

(250) Shen, M.-Y.; Chang, T.-Y.; Hsieh, T.-H.; Li, Y.-L.; Chiang, C.-L.; Yang, H.; Yip, M.-C. Mechanical Properties and Tensile Fatigue of Graphene Nanoplatelets Reinforced Polymer Nanocomposites. *J. Nanomater.* **2013**, *2013*, 1–9. https://doi.org/10.1155/2013/565401.

(251) Rahatekar, S. S.; Koziol, K. K. K.; Butler, S. A.; Elliott, J. A.; Shaffer, M. S. P.; Mackley, M. R.; Windle, A. H. Optical Microstructure and Viscosity Enhancement for an Epoxy Resin Matrix Containing Multiwall Carbon Nanotubes. *J. Rheol. (N. Y. N. Y).* **2006**, *50* (5), 599–610. https://doi.org/10.1122/1.2221699.

(252) Lloyd, B. A.; Bell, P. E. J. United States Patent (19). **1986**, 3–7.

(253) Hameed, N.; Thomas, S. P.; Abraham, R.; Thomas, S. Morphology and Contact Angle Studies of Poly(Styrene-Co-Acrylonitrile) Modified Epoxy Resin Blends and Their Glass Fibre Reinforced Composites. *Express Polym. Lett.* **2007**, *1* (6), 345–355. https://doi.org/10.3144/expresspolymlett.2007.49.

(254) Shin, P. S.; Baek, Y. M.; Kim, J. H.; Park, H. S.; Kwon, D. J.; Lee, J. H.; Kim, M. Y.; DeVries, K. L.; Park, J. M. Interfacial and Wetting Properties between Glass Fiber and Epoxy Resins with Different Pot Lifes. *Colloids Surfaces A Physicochem. Eng. Asp.* **2018**, *544* (2010), 68–77. https://doi.org/10.1016/j.colsurfa.2018.02.017.

(255) Zhang, Q.; Wu, J.; Gao, L.; Liu, T.; Zhong, W.; Sui, G.; Yang, X. Influence of a Liquid-like MWCNT Reinforcement on Interfacial and Mechanical Properties of Carbon Fiber Filament Winding Composites. *Polymer (Guildf).* **2016**, *90*, 193–203. https://doi.org/10.1016/j.polymer.2016.03.013.

(256) Ay, Z.; Tanoğlu, M. The Effect of Single-Walled Carbon Nanotube (SWCNT) Concentration on the Mechanical and Rheological Behavior of Epoxy Matrix. *Mech. Compos. Mater.* **2020**, *56* (4), 523–532. https://doi.org/10.1007/s11029-020-09900-7.

(257) Phua, J. L.; Teh, P. L.; Ghani, S. A.; Yeoh, C. K. Comparison Study of Carbon Black (CB) Used as Conductive Filler in Epoxy and Polymethylmethacrylate (PMMA). *J. Polym. Eng.* **2016**, *36* (4), 391–398. https://doi.org/10.1515/polyeng-2015-0026.

(258) Eqra, R.; Janghorban, K.; Daneshmanesh, H. Mechanical Properties and Toughening Mechanisms of Epoxy/Graphene Nanocomposites. *J. Polym. Eng.*

2015, *35* (3), 257–266. https://doi.org/10.1515/polyeng-2014-0134.

(259) Kumar, A.; Chouhan, D. K.; Alegaonkar, P. S.; Patro, T. U. Graphene-like Nanocarbon: An Effective Nanofiller for Improving the Mechanical and Thermal Properties of Polymer at Low Weight Fractions. *Compos. Sci. Technol.* **2016**, *127*, 79–87. https://doi.org/10.1016/j.compscitech.2016.02.028.

(260) Moniruzzaman, M.; Du, F.; Romero, N.; Winey, K. I. Increased Flexural Modulus and Strength in SWNT/Epoxy Composites by a New Fabrication Method. *Polymer (Guildf).* **2006**, *47* (1), 293–298.

(261) Kumar, A.; Ghosh, P. K.; Yadav, K. L.; Kumar, K. Thermo-Mechanical and Anti-Corrosive Properties of MWCNT/Epoxy Nanocomposite Fabricated by Innovative Dispersion Technique. *Compos. Part B Eng.* **2017**, *113*, 291–299. https://doi.org/10.1016/j.compositesb.2017.01.046.

(262) Ayatollahi, M. R.; Shadlou, S.; Shokrieh, M. M. Fracture Toughness of Epoxy/Multi-Walled Carbon Nanotube Nano-Composites under Bending and Shear Loading Conditions. *Mater. Des.* **2011**, *32* (4), 2115–2124. https://doi.org/10.1016/j.matdes.2010.11.034.

APPENDICES

APPENDIX A

MECHANICAL PROPERTIES OF NANOFILLER-BASED EPOXY NANOCOMPOSITES REPORTED IN THE LITERATURE

Matrix	Method	Filler Type	Filler Concentrations	Mechanical Properties (enhancement ±%)					Reference
				Young's Modulus	Tensile Strength	Fracture Toughness (Mode I)	Flexural Strength	Flexural Modulus	
bisphenol-A diglycidyl ether epoxy	1st Mechanical Stirrer 2nd Three-roll mill	Noncovalent functionalized SWCNT	0.0125 wt.%	-0.2%	+8%	+49%			256
			0.025 wt.%	+22%	+14%	+182%			
			0.05 wt.%	+2%	+3%	+181%			
			0.1 wt.%	+0.6%	-34%	+156%			
			0.3 wt.%	+2.8%	-60%	+119%			
			0.5 wt.%	+4.2%	-63%	+36%			
bisphenol-A diglycidyl ether epoxy	high-speed dissolver	Silica	3 vol.%	+13%	+22%	+48%			203
			6 vol.%	+14%	+29%	+61%			
			9 vol.%	+21%	+34%	+74%			

			12 vol.%	+31%	+45%	+93%			
epoxy	Mechanical mixer	CB	5 vol.%			decreased			257
			10 vol.%						
			15 vol.%						
			20 vol.%			-25%			
epoxy	Speed mixer	CB D:100-140 nm	1 vol.%	increased	SI				96
			5 vol.%	-20%	SD				
			10 vol.%						
			20 vol.%						
		CB D:30-60 nm	1 vol.%	NSI	NSI				
			5 vol.%						
			10 vol.%						
			20 vol.%						
diglycidyl ether of bisphenol F	1st high shear mixer 2nd sonication	GNPs	5 wt.%	+9%	-6%				95
			10 wt.%	+18%	-10%				
			15 wt.%	+24%	-20%				
			20 wt.%	+36%	-36%				
		CB	0.33 wt.%	0%	+5%				
			0.67 wt.%	+1%	+5%				
			1.0 wt.%	+1%	+4%				
		CB/ GNPs	0.33/5 wt.%	+18%	-12%				
			0.67/10 wt.%	+20%	-20%				
Bisphenol-A-based epoxy	1st Ultrasonication with iced bath 2nd Magnetic Stirrer 3rd High-speed shear mixing	SWCNT	0.1 wt.%	+3%					129
		MWCNT	0.1 wt.%		+14%	+20%			
		GO	0.1 wt.%	+31%	+40%	+52%			
Hot cure and low viscous epoxy	1st Mechanical Stirrer 2nd Three-roll mill	GNP	0.5 wt.%			+25%			145
			1 wt.%			+38%			
			2 wt.%			+68%			
			3 wt.%			+90%			

		GNP/ MWCNT	0.5 wt.%			+38%			
			1 wt.%			+62%			
			2 wt.%			+75%			
bisphenol A and epichlorohydrin based epoxy	3-roll mill calendaring	GNP d=5µm	0.1 wt.%			SI		increased	[97]
			0.5 wt.%						
			1.0 wt.%						
			2.0 wt.%			+60%			
		GNP d=25µm	0.1 wt.%			increased		increased	
			0.5 wt.%						
			1.0 wt.%					+9%	
			2.0 wt.%			+82%		increased	
	1st ultrasonication with acetone 2nd high-pressure homogenizer 3rd 3-roll mill calendaring	MWCNT:GNP (d=25µm) (0.5 wt.%)	1:0			+80%		Increased	
			1:3			Increased			
			1:5						
			1:9						
			3:1						
			5:1						
			9:1			+ 77%		+17%	
epoxy	cup-horn ultrasonication with acetone	PG	0.54 vol.%	+17%	-38%	Decreased			[99]
		GO	0.54 vol.%	+24%	+9%	+41%			
Bisphenol-A-based epoxy	1stSonication in ethanol for 2 h at 60^{0}C 2nd Ball milling	RGO	0.05 wt.%	SI	NSI		NSI	SI	[61]
			0.1wt.%						
			0.2 wt.%			+52%			
	1stSonication in ethanol for 2 h at 60^{0}C		0.05 wt.%	SI	DD		DD	SI	
			0.1 wt.%						
			0.2 wt.%			+24%			
Bisphenol	three-roll calendar mill (with a 5µm gap,	GO	0.1 wt.%	+12%	SI	+28-63%	+18%	+9%	[56]
			0.25 wt.%	SI	SI		~+18%	~ +9%	

A/F diglycidyl ether blend	30, 60, 180 rpm rollers speed)		0.5 wt.%	SI	+13%		~+18%	~ +9%	
			1 wt.%	SI	SD		~+23%	~ +12%	
Epoxy	Mixing for 10 min at 25^0C	GO	1.5 vol.%	+45%	+85%				100
			3 vol.%	+54%	+28%				
			4.5 vol.%	+66%	+14%				
			6 vol.%	+79%	+7%				
Bisphenol-F-based epoxy	1st Ultrasonication with iced bath 2nd Magnetic Stirrer	GNS	0.1 wt.%	+32%	+13%		+3%	+0.5%	258
			0.3 wt.%	-	+7%		0	+10%	
			0.5 wt.%	+158%	+4%		-2%	+4%	
			1 wt.%	-	+2%		-3%	+7%	
Diglycidyl Ether of Bisphenol A/F (epoxy)	1st Ultrasonication with iced bath 2nd Magnetic Stirrer	GO	0.1 wt.%	+23%	+5%	+49%			101
			0.3 wt.%	+30%	+2%	+4%			
			0.5 wt.%	+32%	+3%	-2%			
			0.7 wt.%	+24%	+1%	-10%			
Commercial epoxy	1st Mechanical Stirrer with acetone 2nd Three-roll-mill	GNP	0.1 wt.%	+11%	+10%	+28%			247
			0.2 wt.%	+27%	+11%	+56%			
			0.3 wt.%	+32%	+15%	+64%			
Bisphenol A-(epichlorohydrin) epoxy resin	1st Ultrasonication with iced bath 2nd Magnetic Stirrer	GNC	0.005 wt.%	+8%	+2%	+36%	+16%	+15%	259
			0.01 wt.%	+14%	+3%	+51%	+21%	+22%	
			0.05 wt.%	+10%	+2%	+38%	+22%	+23%	
			0.5 wt.%	+10%	+2%	+36%	+23%	+25%	
			1.0 wt.%	+8%	+2%	+19%	+27%	+28%	
			2.0 wt.%	+3%	0%	+18%	+25%	+26%	
Diglycidyl ether of bisphenol-A epoxy resin	1st Mechanical Mixer 2nd Sonication	FGS	0.25 wt.%	+33%	+11%				102
			0.5 wt.%	+41%	+9%				
			0.75 wt.%	+47%	+17%				
			1.5 wt.%	+51%	+16%				
		MWCNT	0.25 wt.%	+20%	+16%				
			0.5 wt.%	+23%	+17%				
			0.75 wt.%	+39%	+22%				

		o-MWCNT	0.5 wt.%	+26%	+28%				
bis-phenol-A-based epoxy resin	three-roll-mill	DWCNT	0.1 wt.%	SI	decreased	+17%			[37]
		DWCNT-NH_2	0.1 wt.%	+6%	NSI	+18%			
			1.0 wt.%	~+6%	SI	+26%			
		CB	0.1 wt.%	NSI	decreased	+18%			
DGEBA-based epoxy	three-roll-mill	CB	0.1 wt.%	+6%	-1%	+17%			[103]
			0.3 wt.%	+8%	-1%	+32%			
			0.5 wt.%	+9%	+2%	+31%			
		SWCNT	0.05 wt.%	+3%	+3%	+11%			
			0.1 wt.%	+4%	+4%	+23%			
			0.3 wt.%	+8%	+5%	+12%			
		DWCNT	0.1 wt.%	+7%	-2%	+17%			
			0.3 wt.%	+11%	+6%	+31%			
			0.5 wt.%	+7%	+6%	+31%			
		DWCNT-NH_2	0.1 wt.%	+1%	-0.2%	+18%			
			0.3 wt.%	+13%	+5%	+41%			
			0.5 wt.%	+15%	+8%	+43%			
		MWCNT	0.1 wt.%	+7%	-1%	+21%			
			0.3 wt.%	+6%	-1%	+23%			
			0.5 wt.%	+0.4%	-4%				
		MWCNT -NH_2	0.1 wt.%	+11%	+1%	+24%			
			0.3 wt.%	+8%	-0.2%	+31%			
			0.5 wt.%	+8%	+0.7%	+29%			
diglycidyl ether of bisphenol F),	1st bath sonication 2nd High shear mixing	SWCNT	0.01				+6%		[260]
			0.05				9%	+15%	
diglycidyl ether of bisphenol A	Ultrasonication with acetone	MWCNT	0.2 wt.%	+3%	-7%				[104]
		MWCNT-X	0.2 wt.%	+12%	-0.2%				
		MWCNT-Y	0.2 wt.%	+34%	+10%				
		MWCNT-Z	0.2 wt.%	+24%	+3%				
	1st sonication	P-HCNTs	0.2 wt.%	increased	SI		SI	~+37%	[105]

Bisphenol A epoxy resin	2nd high shear mixing		0.4 wt.%	increased	SI		SI	~+37%	
			0.6 wt.%	+86%	+13%		SI	~+37%	
			0.8 wt.%	increased	SI		SI	+37%	
		A-HCNTs	0.2 wt.%	increased	SI		SI	SI	
			0.4 wt.%	increased	SI		SI	~+39%	
			0.6 wt.%	+188%	+22%		SI	+39%	
			0.8 wt.%	increased	SI		SI	~+39%	
		K-HCNTs	0.2 wt.%	increased	increased		SI	~+72%	
			0.4 wt.%	+271%	+513%		SI	~+72%	
			0.6 wt.%	increased	increased		Decreased	+72%	
			0.8 wt.%	increased	increased		NSI	~+72%	
Epoxy	Ultrasonication	P-HNT	1 wt.%	+0.4%	-3%	+11%			78
			4.8 wt.%	+11%	-14%	+16%			
		H-HNT	1 wt.%	+11%	+5%	+25%			
			4.8 wt.%	+18%	+2%	+43%			
diglycidyl ether of bisphenol A	Ball milling	HNT	5 wt.%	+1%	+4%	+37%			116
			10 wt.%	+1%	+4%	+47%			
			15 wt.%	+3%	+5%	+38%			
	Mechanical mixing		5wt.%	+5%	+7%	+47%			
			10 wt.%	+22%	-2%	+30%			
	Ball milling	PA-HNT	5 wt.%	+5%	+5%	+40%			
			7 wt.%	+5%	+6%	+45%			
			10 wt.%	+11%	+5%	+51%			
			15 wt.%	+21%	+6%	+34%			
	Mechanical mixing		5 wt.%	+8%	+5%	+40%			
			10 wt.%	+9%	-22%	+33%			
	Ball milling	Silane_HNT	10wt.%	+1%	+5%	+38%			
		CTAC_HNT	10 wt.%	+6%	+6%	51%			
epoxy	1st sonication with acetone	MWCNTs	0.25 wt.%		+11%				261
			0.5 wt.%		+18%				

	2nd mechanical stirrer		0.75 wt.%		+36%				
			1.0 wt.%		+26%				
Bisphenol F	1st mechanical stirrer 2nd sonication	MWCNT	0.1 wt.%	+3%	+5%	+15%			262
			0.5 wt.%	+11%	+8%	+26%			
			1.0 wt.%	+17%	+6%	+19%			
diglycidyl ether of bisphenol A	three-roll-mill	GNP	0.5 wt.%			+24%			34
		TRGO	0.5 wt.%			+40%			
		MWCNT	0.5 wt.%			+8%			

GNP: graphite nano-platelets, TRGO: thermally reduced graphene oxide, MWCNT: multi-wall carbon nanotubes, DWCNT: double walled carbon nanotube, DWCNT-NH_2: amino-functionalized DWCNT, SI: Slightly improved, NSI: no significant improvement, HCNTs: Helical carbon nanotubes, P-HCNTS: pristine HCNTs, A-HCNTs : acid treated HCNTs, K-HCNTs: glycidoxypropyltrimethoxysilane modified HCNTs, -X: treatment with non-ionic surfactant, -Y: treatment with anionic surfactant, -Z: treatment with cationic surfactant, H-HNT: hydroxylated HNTs, CB: Carbon black, GO: Graphene oxide, GNS: graphene nanosheets, GNC: nanocarbon sheets, NSI: no significant improvement, GNC: nanocarbon sheets, BM: ball milling, DD: dramatical decrease, SD: slightly decreased, LI: large increase, FGS: Functionalized graphene sheets, o-MWCNT: oxidized MWCNT, PG: pristine graphene

APPENDIX B

ILSS AND MODE I FRACTURE TOUGHNESS IMPROVEMENT OF MULTI-SCALE FRPCS

Fiber/matrix	The nano-sized filler integration method	Production Method of FRPCs	Type of nano-sized filler	Increase in G_{Ic} (%)	Increase in ILSS (%)	Ref.
Woven-CF/epoxy	Entire epoxy	VARTM	GNP (3 wt.%)	153%	47.5%	[146]
			MWCNT (3 wt.%)	79%	46.7%	
UD CF/epoxy	Entire epoxy	VARIM	Nano-silica (10 wt.%)	23% ($G_{Ic,ini.}$) 1.2% ($G_{Ic,prop.}$)	5%	[167]
			Nano-silica (20 wt.%)	75% ($G_{Ic,ini.}$) 21% ($G_{Ic,prop.}$)	18%	
UD CF prepreg/epoxy	Entire epoxy	Autoclave	MWCNT-modified (0.5 wt.%)	75% ($G_{Ic,ini.}$) 83% ($G_{Ic,prop.}$)	~0	[188]
GF/epoxy [-45°/90°/+45°/0°]s	Entire epoxy	VARTM	MWCNT-NH_2 (0.1 wt.%)	~0	11%	[152]
[0/90] CF prepreg/epoxy	Entire epoxy	Autoclave	SWCNT modified with surfactant (0.1 wt.%)	3% ($G_{Ic,ini.}$) 13% ($G_{Ic,prop.}$)	-	[189]

UD CF prepreg/epoxy	Entire epoxy	VARTM	MWCNT	%25 (3 wt.%)	-	[190]
UD CF prepreg/epoxy	Entire epoxy	Autoclave	cup-stacked carbon nanotubes (CSCNTs)	98% (5 wt.%)	-	[191]
UD CF prepreg/epoxy	Entire epoxy	Hot-press	Functionalized-MWCNT (0.1 wt.%)	22% ($G_{Ic,ini.}$) 14% ($G_{Ic,prop.}$)	-	[192]
UD CF/epoxy	Entire epoxy	VARTM	COOH-MWCNT (0.5 wt.%)	25%	-	[193]
UD CF/ epoxy	Entire epoxy	Autoclave	MWCNT (1 wt.%)	60%	-	[194]
$[(0,-45,90,+45)_2,-45,90,+45,0]_s$ GF/epoxy	Entire epoxy	VARTM	Oxidized-MWCNT (1 wt.%)	-	7.9%	[153]
GF fabric/epoxy	Entire epoxy	Hand lay-up	MWCNT (0.3 wt.%)	-	15%	[154]
GF fabric/epoxy	Entire epoxy	IDVARTM	Oxidized-MWCNT (2 wt.%)	-	33%	[155]
$[(0,+45,90,-45]_s$ GF/epoxy	Entire epoxy	RTM	DWCNT-NH2 (0.3 wt.%)	-	20%	[51]
$[(0,-45,90,+45)_2,-45,90,+45,0]_s$ GF/epoxy	Entire epoxy	RTM	DWCNT (0.3 wt.%)	reduced	16%	[76]
Woven GF fabric/epoxy	Entire epoxy	Hand lay-up	NH_2-MWCNTs (0.3 wt.%)	-	49%	[156]
UD CF/epoxy	Coating on CF	VARTM	CNT	-	58.6%	[161]
Woven GF fabric /epoxy	Coating on GF	VARTM	SWCNT (0.015 wt.%)	-	45%	[162]
CF fabric/epoxy	Entire epoxy	Open mold method	MWCNT-NH_2 (1.5 wt.%)	-	7%	[157]
UD CF/epoxy	Spraying on the fibers	VARIM	MWCNTs-COOH	24% ($G_{av.,prop.}$)	12%	[195]

CF fabric/epoxy	Entire epoxy	VARIM	CNT-NH_2	-	10%	[158]
CF/epoxy	Entire epoxy	FW	MWCNT-NH_2 (6 wt.%)	-	28%	[159]
UD CF/epoxy	Entire epoxy	hot-melt prepregger	Functionalized-MWCNT (0.5 wt.%)	-	12%	[160]
UD CF/epoxy	Coating on CF	Autoclave	GO	-	12.7%	[163]
UD CF/epoxy	Coating on CF	Compression molding method	SiO_2	-	10.92%	[164]
UD GF/epoxy	Entire epoxy	Vacuum bagging	Alumina (0.8 wt.%)	-	2.07%	[165]
CF/epoxy	Entire epoxy	FW	CSR (10 phr) and nano-SiO_2 (2 phr)	-	18.9%	[168]
Woven CF fabric/epoxy	Entire epoxy	hand lay-up	HNT (3 wt.%)	~40% (max)	-	[35]
			HNT (5 wt.%)	-	25% (max)	
UD CF/epoxy	Entire epoxy	RTM	AlOOH nanoparticle (15 wt.%)	32.61%	-	[169]
Random GF mat/PE	Entire PE	VARTM	Surfactant-treated CNF (1 wt.%)	100%	-	[200]
UD CF/epoxy	Entire epoxy	FW	carboxyl-functionalized MWCNTs (3 wt.%)	-	8%	[255]

UD: Unidirectional, CF: Carbon fiber, GF: Glass fiber, VARTM: vacuum-assisted resin transfer molding, IDVARTM: injection double vacuum-assisted resin transfer molding, RTM: Resin transfer molding, FW: Filament winding, HNT: halloysite, CSR: core-shell rubber, PE: polyester, CNF: carbon nanofiber

VITA

Zeynep AY
17.08.1989, İzmir/TURKEY

EDUCATION

- ***Ph.D.*** in English, 2020, Mechanical Engineering, İzmir Institute of Technology.
- ***M.Sc.*** in English, 2013, Nanoscience and Nanoengineering, Dokuz Eylül University.
- ***B.Sc.*** in Turkish, 2008, Department of Chemistry, Dokuz Eylül University.

PUBLICATIONS

SCI-Expanded Publications

Ay, Z. and Tanoglu, M. "The Effect of single-walled carbon nanotube (SWCNT) concentration on the mechanical and rheological behavior of epoxy matrix", Mechanics of Composite Materials, Volume 56, No. 4, September 2020.

Selected International Conference Proceedings

Z. Ay, O. Kartav, M. Tanoğlu, Effect of Nano-Sized Filler Content on The Mechanical Properties of Glass Fiber/Epoxy Filament Wound Composites, International porous and powder materials symposium and exhibition (PPM), October 2019

Z. Ay, O. Kartav, M. Tanoğlu, Effect of Fiber Content on Fatigue Properties of Short Glass Fiber Reinforced Polypropylene Composites, International porous and powder materials symposium and exhibition, September 2017

Z. Ay, O. Kartav, M. Tanoğlu, Effect of Fiber Content on Tensile and Thermo-Mechanical Properties of Short Glass Fiber Reinforced Polypropylene Composites, he 25 th Annual International Conference on Composites/Nano Engineering (ICCE-25), July 2017

- The project that constitutes the main subject of this thesis was selected for the **Composites Challenge at JEC World 2019** and participated in the challenge as one of the finalists in ten doctoral projects.